Calmodulin Disrupts Plasma Membrane Localization of Farnesylated KRAS4b by Sequestering its Lipid Moiety

by

Benjamin Micah Milrod Grant

A thesis submitted in conformity with the requirements
for the degree of Master of Science

Department of Medical Biophysics
University of Toronto

Calmodulin Disrupts Plasma Membrane Localization of Farnesylated KRAS4b by Sequestering its Lipid Moiety

Benjamin Grant

Master of Science

Department of Medical Biophysics
University of Toronto

2019

Abstract

KRAS4b is a small GTPase protein that regulates signal transduction pathways, including MAPK signaling. Recently, there has been considerable interest in the mechanisms underlying interactions between RAS and calcium signaling. KRAS4b function requires farnesylation of its C-terminus and recruitment to the plasma membrane, and some studies have suggested that Ca^{2+}-calmodulin (CaM) modulates this localization. Here, we present a crystal structure, supported by NMR data, revealing that the Ca^{2+}-dependent CaM-KRAS4b interaction is anchored by the sequestration of the KRAS4b farnesyl moiety in the hydrophobic pocket of the CaM C-terminal lobe. We engineered FRET-based probes (CaMeRAS) to monitor this interaction in live cells and demonstrate that, upon stimulation of Ca^{2+} influx by extracellular ligands, KRAS4b reversibly translocates in a Ca^{2+}-CaM dependent manner from the plasma membrane to the cytoplasm in HeLa and HEK293 cells. These results underscore the importance of crosstalk between KRAS4b and Ca^{2+} signaling pathways and reveal one underlying mechanism.

Acknowledgments

I would like to extend my utmost gratitude to Dr. Mitsuhiko Ikura and Dr. Chris Marshall for guiding me on this scientific voyage. You gave me the courage and freedom to explore. The vast support and encouragement I have received from you both over the last five years have been cherished.

Thank you, Danton, for the tough love, the honesty and the belief that I could be and do better. You were a teacher, a mentor and a friend to me, but I have now surpassed you, in foosball and in life. It feels great!

And Safa, thank you for weathering the storms with me. Your love and support have been my guiding light. I see visions of our future, embarking from a near or distant shore, hope and excitement swelling in our hearts. I love you.

Here's to many new adventures.

Dr. Masahiro Enomoto's hard work and expertise was instrumental in the success of this project. He helped design and optimize our *in vivo* FRET system, performed all imaging experiments and managed all statistical and data analysis. Thank you for your dedication, Masa.

X-ray data described in this paper was collected using beamline 08ID-1 at the Canadian Light Source, which is supported by the Canada Foundation for Innovation, Natural Sciences and Engineering Research Council of Canada, the University of Saskatchewan, the Government of Saskatchewan, Western Economic Diversification Canada, the National Research Council Canada, and the Canadian Institutes of Health Research (CIHR).

I thank Dr. Dorus Gadella and Dr. Yu-Zhu Zhang for the generous donations of plasmids, as well as Dominic Esposito at the NCI for donation of and assistance with the KRAS-FMe baculovirus expression system.

I would like to thank the staff at the Advanced Optical Microscopy Facility, University Health Network, for their help with this project. I also thank Genevieve Gasmi-Seabrook for assistance and management of the Princess Margaret NMR facility, funded by the Canada Foundation for Innovation (CFI) and the Princess Margaret Cancer Foundation (PMCF). Lastly, I thank the CIHR (FDN-154284), the Canadian Cancer Society (Grant # 703209), The Heart and Stroke Foundation of Canada (G-16-00014035), CFI, PMCF, and Canada Research Chairs for funding and support.

Table of Contents

List of Tables

List of Figures

List of Appendices

1 Introduction

1.1 RAS Proteins

RAS-family small GTPases are key regulators of signal transduction pathways in cells, controlling proliferation, differentiation, survival and apoptosis [1,2]. RAS proteins act as binary switches in response to external stimuli, cycling between an inactive, GDP-bound, and active, GTP-bound form, catalyzed by guanine nucleotide exchange factors (GEFs) and GTPase activating proteins (GAPs) [3,4]. When localized to the inner leaflet of the plasma membrane, RAS-GTP can bind to and activate several effector proteins, including Raf kinases, PI3K, RalGDS, PLCε and others, which are involved in many diverse cellular response pathways [1,3-5]. GTPase and protein kinase cascades, phospholipid metabolism and calcium signaling are all regulated by RAS proteins [3]. Humans have three *RAS* genes (*HRAS*, *NRAS* and *KRAS*) which encode four unique proteins due to *KRAS* splice variants KRAS4a and KRAS4b, of which the latter is more ubiquitously expressed and more extensively characterized.

RAS proteins share a highly conserved G-domain (the first 85 amino acids, containing nucleotide and effector binding sites, are identical between humans, mice and rats, while the remaining residues show an 85% homology) but are divergent at the C-terminal ~15 amino acids, designated the hypervariable region (HVR) [1,3]. The HVR of each isoform contains a unique combination of membrane localization signals, believed to be largely responsible for differential signaling and oncogenic capacity [4,6-8]. All isoforms contain a C-terminal CaaX box motif (C, cysteine; a, aliphatic; X, any residue), which is a target for irreversible farnesylation of cysteine by farnesyl transferase enzymes, subsequent proteolytic cleavage of the aaX residues by RCE1 and carboxymethylation of the newly exposed C-terminus by ICMT [3,9]. HRAS, NRAS and KRAS4a contain additional cysteines in the HVR that are reversibly palmitoylated, whereas KRAS4b membrane localization is enhanced through electrostatic interactions between the negatively charged membrane surface and a lysine-rich sequence in the HVR called the polybasic region (Figure 1.1) [10-13]. Because KRAS4b lacks palmitoylation sites, its affinity for the plasma membrane is lower than that of the other RAS isoforms [13].

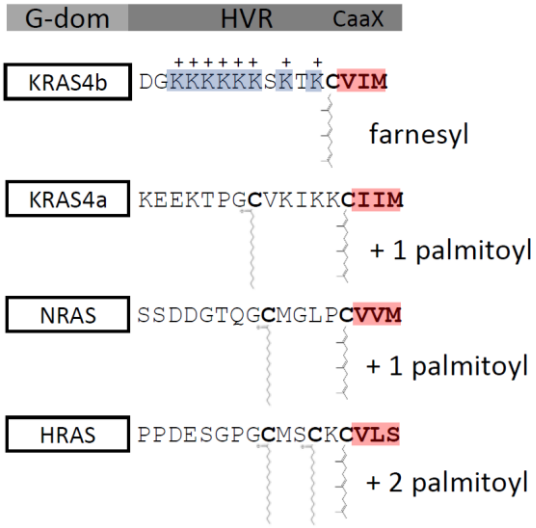

Figure 1.1 RAS isoform-specific hypervariable regions. C-terminal hypervariable regions in RAS proteins encode membrane localization signals that direct unique localization, membrane dynamics and signal output. Terminal residues cleaved during RAS processing are coloured red. Blue highlights residues in the polybasic region of KRAS4b.

1.2 KRAS4b in Cancer

RAS genes are mutated, either in ways that promote constitutive activation or inhibit inactivation, in more than 30% of all human cancers [3,4,6]. *KRAS* is the most frequently mutated isoform (approximately 86% of all *RAS* mutations compared to 11% for *NRAS* and just 3% for *HRAS*), and drives roughly 95% of pancreas, 45% of colon and 31% of lung adenocarcinomas [7,14], three of the four most deadly cancers in Canada today [15]. RAS proteins are well validated targets in oncology, however they lack classic druggable pockets and have thus presented a major challenge to drug discovery efforts. A variety of indirect approaches to restrain RAS signaling have been pursued [16], largely unsuccessfully. One such approach involves disrupting RAS membrane attachment. Recognizing that membrane localization of RAS is required for signaling, inhibitors of farnesyl transferases were developed in the 1990s, however these ultimately failed in the clinic due to alternative prenylation of KRAS and NRAS by geranylgeranyl transferases [17,18]. Farnesyl transferase inhibitors have recently resurfaced in clinical trials to therapeutically target HRAS-driven cancers, with some success, since HRAS is not modified by this alternative prenylation mechanism, although these cancers are rare [7,19]. Inhibition of the mevalonate pathway, which is responsible for the anabolism of farnesyl and geranylgeranyl, has also failed due to the inability to reduce lipid concentrations enough to effectively perturb prenylation in cells [20]. However, new data concerning the regulation of KRAS4b membrane localization by other cellular proteins have reignited research in this field.

KRAS4b association with the membrane is a particularly dynamic process that can be regulated by phosphodiesterase-δ (PDEδ) [21], a noncatalytic subunit of the photoreceptor PDE6. PDEδ binds the farnesylated HVR of cytoplasmic KRAS4b and delivers it to back to the plasma membrane through an active mechanism, regulated by the nucleotide-dependent cargo-displacement factors ARL GTPases, via recycling endosomes [21-24]. Small molecule inhibition of PDEδ causes delocalization of KRAS4b from the plasma membrane and decreases downstream signaling. Furthermore, a series of reports suggest that KRAS4b localization can also be modulated by phosphorylation of Ser181 in the HVR by PKC and PKG [25-29] and by the calcium-sensing protein calmodulin (CaM) [30-34].

1.3 KRAS and Ca^{2+}-signaling Crosstalk

The interaction between KRAS4b and CaM is one of many examples of interplay between the Ca^{2+} and MAPK signaling pathways. Historically, it was observed that inactivation of CaM in serum-starved NIH3T3 cells causes activation of ERK1/2, MEK, C-Raf and RAS, irrespective of tyrosine kinase receptor phosphorylation [35]. Recently, a variety of mechanisms linking these pathways have emerged. For example, the Ca^{2+}-dependent kinase PYK2 promotes recruitment of Grb2 and the GEF SOS to the plasma membrane where it activates RAS. Other RAS GEFs are also regulated by Ca^{2+}: Ras-GRFs contain “IQ” CaM binding motifs and are regulated by Ca^{2+}-CaM, while some of the RAS-GRPs have EF hands, highly conserved calcium-binding helix-turn-helix motifs, and are regulated directly by Ca^{2+} [36,37]. In addition to Ca^{2+}-modulated GEFs, some RAS GAPs are regulated by Ca^{2+} as well: p120 RAS GAP and CAPRI both translocate to the plasma membrane in response to Ca^{2+} signaling, (P120GAP by recruitment to the Ca^{2+}-dependent Annexin A6 and CAPRI through fast C2 domain interactions) [38,39]. Thus, the GTPase cycle and localization of KRAS4b, both of which are required for canonical signaling, are influenced by Ca^{2+} signals. Reciprocally, feedback mechanisms exist by which RAS-MAPK activity modulates Ca^{2+} signaling proteins. Interestingly, Ca^{2+} signaling is dysregulated in many cancer cells, often through over- or under-expression of calcium channels (e.g., STIM/Orai, TRP, IP3R and Cav1) [40]. In some cases, this has been linked to transcriptional control by KRAS4b signaling. For example, deletion of the oncogenic KRAS allele (G13D) or MEK inhibition resulted in enhanced STIM1 expression and store-operated Ca^{2+} entry [41]. The complex interplay between Ca^{2+} and RAS-MAPK signaling pathways requires and merits further study.

1.4 Calmodulin (CaM)

CaM is a ubiquitous calcium-sensing master regulator that controls many important biological pathways. CaM was first discovered as an activator of cyclic AMP phosphodiesterase in the brain by Cheung [42] and Kakiuchi [43] independently. The Ca^{2+} dependence of CaM activity demonstrated by Kakiuchi pioneered the field of calcium-dependent signaling regulators and their cellular pathways.

CaM is a small, 16.7kD protein that is fully conserved among all vertebrates and highly conserved throughout kingdoms animalia and plantae. Humans have three identical copies of the *CALM1* gene, expressing CaM in large quantities (at least 0.1% of cells by weight, and higher in the brain and testes) [44]. The protein is highly acidic, soluble and stable, both in Ca^{2+}-free and -bound states and interacts with binding targets under both conditions [44]. CaM binds Ca^{2+} through motifs called 'EF-hands', first discovered in carp parvalbumin by Kresinger et al [45]. Each of 4 EF-hand motifs in CaM forms 29-amino acid helix-turn-helix structures that coordinate Ca^{2+} through side chains and backbones of five residues in a well-conserved twelve-residue loop; one pair of EF-hands forms an N-terminal lobe and the other pair forms a C-terminal lobe, which are separated by a flexible linker. In the Ca^{2+}-free state, the EF-hand pairs bury large hydrophobic surfaces within each lobe which become exposed following Ca^{2+}-induced structural rearrangements. These methionine-rich hydrophobic pockets in each lobe mediate interactions with Ca^{2+}-dependent binding partners [44]. Mutation of a glutamate at position twelve of each Ca^{2+}-binding loop to glutamine abrogates Ca^{2+}-binding at that site [46,47].

In the Ca^{2+}-free state, CaM interacts primarily with targets containing IQ motifs (consensus sequence: IQxxxRGxxxR). Some proteins, such as neuromodulin, interact with CaM only in the absence of calcium. However, many proteins have multiple CaM binding sites for both Ca^{2+}-free and Ca^{2+}-bound interactions; the Ca^{2+}-free interaction helps pre-localize CaM to increase the efficiency and rate of a Ca^{2+}-response. Some of these hybrid targets include myosin light chain kinase (MLCK), nitrous oxide synthase (NOS) and IQGAPs [44,48,49].

Ca^{2+}-dependent CaM targets are generally highly basic helical peptides that can be classified by the relative position of two hydrophobic residues that "anchor" the two lobes together. Calmodulin kinase II (CaMKII), as well as synapsins and heat shock proteins, exhibit a "1-10" motif, meaning there are eight amino acids between the two hydrophobic anchoring residues.

CaMKIV, MLCK, calcineuin (CN), death associated protein (DAP) kinase and NOS have canonical "1-14" motifs (of which there are several subclasses, including those with internal hydrophobic anchoring residues: "1-8-14" and "1-5-8-14"). However, due to the flexibility of CaM, there are many variations in binding mode. CaMKK is not entirely helical and binds in a non-standard orientation with a "1-16" motif. The ryanodine receptor (RyR) and the plasma membrane ATPase (PMCA) bind with "1-17" and "1-18" respectively [44]. On the other end of the spectrum, the crystal structure of CaM in complex with the MARCKS peptide shows a remarkably compact calmodulin with a "1-3" binding mode [50]. There are also many other non-canonical CaM-binding targets that interact in diverse manners due to the plasticity of CaM (Figure 1.2) [44]. Through binding, CaM can affect protein targets by stabilizing dimers, displacing autoinhibitory domains and allostery.

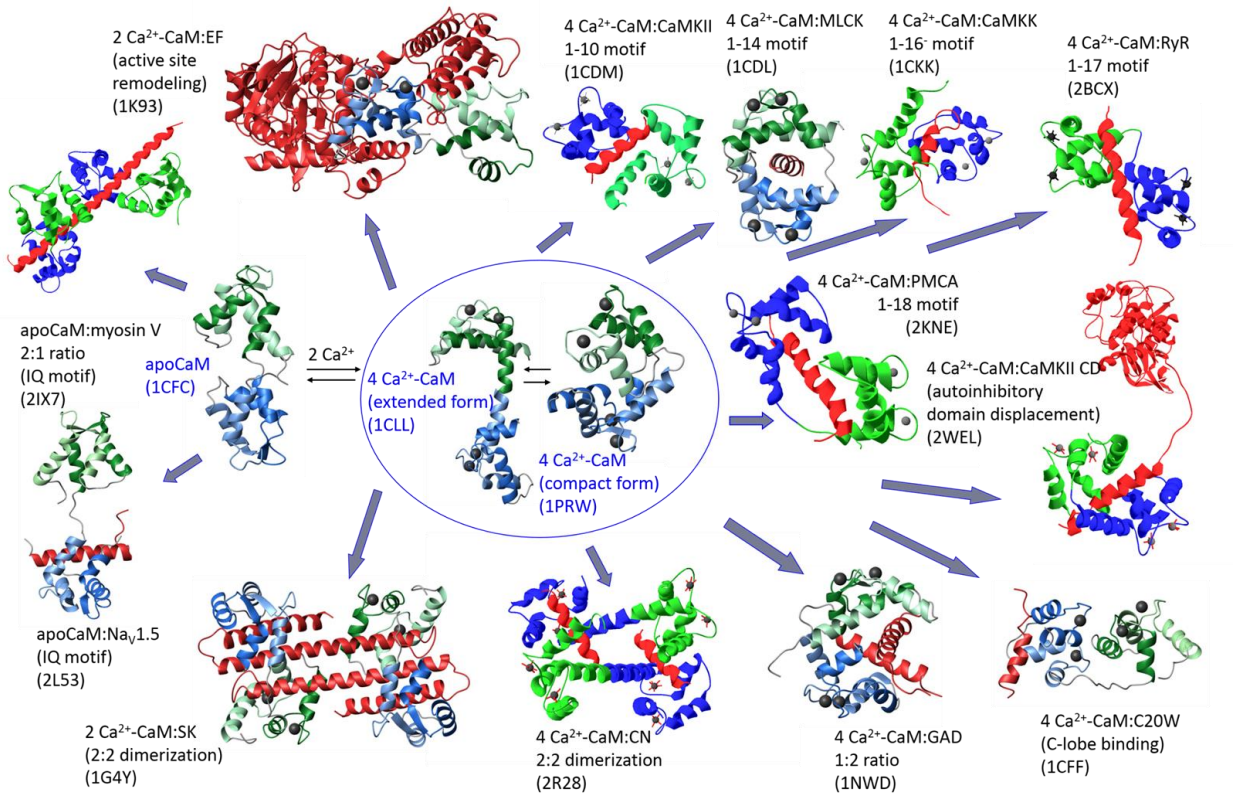

Figure 1.2. Assorted Calmodulin binding modes. A sample of canonical and non-canonical Calmodulin:substrate complexes displaying diverse binding modes. In brackets are the PDB accession codes for each structure visualized. Starting from the top left and proceeding clockwise, protein acronyms are: EF (Edema Factor), CaMKII (Calmdoulin Kinase II), MLCK (Myosin Light Chain Kinase), CaMKK (Calmodulin Kinase Kinase), RyR (Ryanodine Receptor), PMCA (Protein Misfolding Cyclic Amplification), CaMKII CD (CaMKII C-terminal domain), C20W (the C20W peptide from the plasma membrane calcium pump), GAD (Glutamate Decarboxylase), CN (Calcineurin), SK (Small-conductance Ca^{2+}-gated Potassium channel, $Na_V1.5$ (Voltage-gated Sodium channel subunit). This figure is reproduced from the Calmodulin chapter within the Encyclopedia of Metalloproteins [44].

A series of reports since 2001 have shown that CaM interacts with KRAS4b, though the mechanism and impact of this interaction has remained controversial. While the KRAS4b HVR is highly basic and has a propensity to form a helix, at least under some crystallographic conditions [23], it lacks hydrophobic 'anchor' residues characteristic of a canonical CaM target. Little is currently understood about the true nature of this interaction, and whether it may prove useful for the future therapeutic targeting of KRAS4b.

1.5 KRAS4b – Calmodulin Interaction Reports

Several groups have reported that CaM interacts with KRAS4b, but not KRAS4a, HRAS or NRAS, in a Ca^{2+}-dependent manner in cells and *in vitro*, and that this modulates cell signaling [30-34]. It has also been suggested that CaM binding extracts KRAS4b from the plasma membrane and is responsible for relocalizing it in cells, to the cytoplasm and potentially internal membranes, altering signal output [25,31,33]. However, there are contradictions in the literature regarding many of the details of this interaction. Various studies have reported that the KRAS4b-CaM interaction is GTP dependent [30,51-53] and nucleotide independent [31,33,54,55]; farnesylation dependent [31,33,51,53-55] and independent [30,51,52]; that the G-domain is either involved [30,51,53] or not [31,33,52,54,55] (these discrepancies are summarized in Table 1). The effects of the interaction on KRAS4b localization and signaling have also been disputed [31,33,51,54,55]. These inconsistencies have made it difficult for the field to reach a consensus about the nature and role of this interaction. Due to the plasticity of CaM and the lack of canonical CaM binding motifs in KRAS4b, very little is currently understood about the structural and biophysical properties of this complex.

1.6 Summary of Results

In the first part of our study we sought to investigate the structure and biophysical properties of the KRAS4b-CaM interaction *in vitro*. In particular, we examined Ca^{2+}- and nucleotide-dependence, identified interacting elements on both proteins and assessed the ability of CaM to extract KRAS4b from lipid bilayers, using a combination of nuclear magnetic resonance (NMR) and x-ray crystallography. Our NMR data clearly show that CaM binding to KRAS4b is dependent on Ca^{2+} and KRAS4b farnesylation but found no evidence for involvement of the KRAS4b G-domain and no preference for the nucleotide bound to KRAS4b. A crystal structure of Ca^{2+}-CaM in complex with a fragment of the processed HVR, farnesyl cysteine methyl ester

(FCME), shows the farnesyl moiety buried deeply in the C-lobe hydrophobic pocket of CaM, providing a structural rationale for extraction of KRAS4b from the membrane by CaM. In order to validate this model, we employed live cell microscopy using a chimeric CaM-KRAS4b Förster resonance energy transer (FRET) probe, named CaMeRAS, designed on the basis of our structural data. This FRET-based biosensor enabled us to simultaneously monitor the interaction of CaM with KRAS4b as well as intracellular translocation of the complex upon stimulation of a cellular Ca^{2+} signal in both HeLa and HEK293 cells. We demonstrate that intracellular calcium elevation stimulates KRAS4b translocation from the plasma membrane to the cytoplasm, which is spatially and temporally regulated via Ca^{2+}-CaM in mammalian cells.

Chapter 2
Methods

2 Methods

2.1 Products and Preparations

2.1.1 Bacterial Protein Expression and Purification (Calmodulin and KRAS4b 1-185)

2.1.1.1 Isotopically Unlabeled Protein

E. coli BL21 C+ cells were transformed with pET28 plasmids containing CaM or KRAS4b sequences and grown at 37^{O}C to an O.D. of 0.6 - 0.8. Temperature was reduced to 15^{O}C before induction of protein expression with 0.25 mM IPTG. Cells were grown in LB media with 1 mM kanamycin, then lysed by sonication in buffer containing 50 mM Tris-HCl (pH 8), 150 mM NaCl, 0.1% (v/v) NP-40, 10% (v/v) glycerol, 10 mM imidazole, 5 mM $MgCl_2$, 10 mM β-mercaptoethanol, 1 mM PMSF, lysozyme and DNase. CaM and unprocessed KRAS were purified by Ni-NTA His-tag affinity chromatography followed by gel filtration. Detailed expression and purification protocol found in Appendix 1 [56].

2.1.1.2 Uniform ^{15}N Labeled Protein

E. coli BL21 C+ cells were transformed with pET28 plasmids containing CaM or KRAS4b sequences and grown at 37^{O}C to an O.D. of 0.6-0.8. Temperature was reduced to 15^{O}C before

induction of protein expression with 0.25 mM IPTG. Cells were grown in M9 (1 mg/L biotin, 1 mg/L thiamine, 0.3 mM $CaCl_2$, 1 mM kanamycin, 0.2% (w/v) glucose, trace elements [25 µM EDTA, 30.83 µM ferric chloride, 3.67 µM zinc chloride, 0.74 µM cupric chloride, 0.42 µM cobalt chloride, 1.62 µM boric acid, 127.19 µM manganese chloride], and 1 g/L ^{15}N-NH_4Cl) for uniform ^{15}N labeling. Cells were lysed by sonication in buffer containing 50 mM Tris-HCl (pH 8), 150 mM NaCl, 0.1% (v/v) NP-40, 10% (v/v) glycerol, 10 mM imidazole, 5 mM $MgCl_2$, 10 mM β-mercaptoethanol, 1 mM PMSF, lysozyme and DNase. CaM and unprocessed KRAS were purified by Ni-NTA His-tag affinity chromatography followed by gel filtration.

2.1.2 Insect Cell KRAS4b Expression, Labeling and Purification

High Five™ insect cells (Thermo Fisher Scientific) were transfected with bacmids containing farnesyl transferase 1 and 2 and His-MBP-KRAS4b (generous gift from NCI Frederick). Expression and purification of these constructs followed a previously reported protocol (Figure 2.1) [57]. ^{15}N-lysine labeling of KRAS4b was performed in ESF 921 Delta Series media (ΔKRWYFH) (Expession Systems) supplemented with Arg (800 mg/L), Trp (200 mg/L), Tyr (360 mg/L), Phe (1000 mg/L) and His (200 mg/L) (Sigma). ^{15}N-lysine (Cambridge Isotope Laboratory) was added (100 mg/L) 16 hours post infection. ^{13}C-methyl labeling of KRAS4b was performed in ESF 921 Delta Series media (ΔTMILVA) with Ala (400 mg/L) supplemented. ^{13}C-methyl labeled Thr (75 mg/L), Met (100 mg/L), Ile (150 mg/L), Leu (100 mg/L) and Val (50 mg/L) were added 16h post infection, based on a protocol adapted from Gossert et al [58,59].

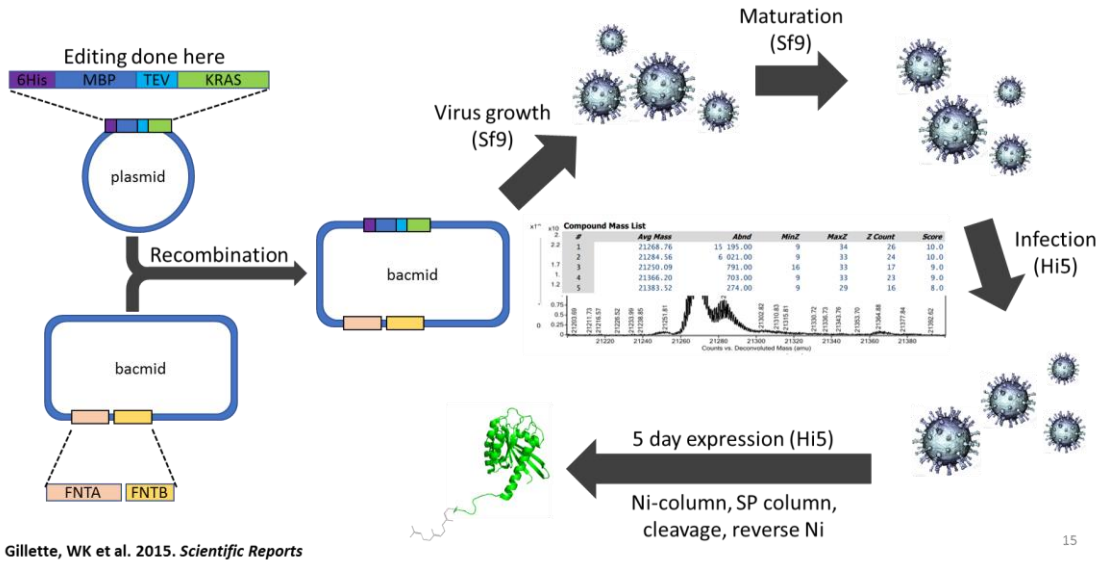

Figure 2.1. Baculovirus expression pipeline for KRAS4b-FMe from insect cells. Details of expression protocol reported by Gillette et al.[57].

2.1.3 Plasmid Construction for FRET Chimeras

The plasmid containing a codon-optimized KRAS4b (KRAS4b-opt) was purchased from Invitrogen GeneArt Gene Synthesis (ThermoFischer Scientific). pmTurquoise2-C1 [60] and pSYFP2-C1 [61] were gifts from Dr. Dorus Gadella (Addgene plasmids # 60560 and 22878, respectively). pEZYmyc-His [62] was a gift from Dr. Yu-Zhu Zhang (Addgene plasmid # 18701). A cDNA encoding KRAS4b-opt amplified by PCR was cloned into pENTR1A (Invitrogen) between BamHI and NotI sites (Plasmid #1). Then, a cDNA encoding CaM amplified by PCR was cloned into BamHI site of Plasmid #1 (Plasmid #2). Further, to insert mTurquoise2 (mTq2) and SYFP2 into Plasmid #2, two short linkers including restriction enzyme site(s) were inserted at the 5'-end of CaM and between CaM and KRAS4b-opt using Q5 site-directed mutagenesis (New England Biolabs Inc.) (Plasmid#3). Then, cDNAs of mTq2 and SYFP2 amplified by PCR using pmTurquoise2-C1 and pSYFP2-C1 as templates were cloned into SphI and KpnI sites and SpeI and BamHI sites of Plasmid#3, respectively, producing mTq2-CaM-SYFP2-KRAS4b, identified as CaMeRAS^{WT}. For making a construct of mTq2-CaM1234Q-SYFP2-KRAS4b, called CaMeRAS^{1234Q}, a cDNA of CaM1234Q [E31Q, E67Q, E104Q, E140Q] amplified by PCR was used to replace wildtype CaM. For mTq2-CaM-SYFP2-KRAS4b-Cys185Astop, or CaMeRAS^{185A}, Cys185 in KRAS4b was mutated to Ala and TAA stop codon was inserted after Ala using Q5 site-directed mutagenesis. To insert a FLAG tag at the N-terminus, a cDNA encoding FLAG-mTurqoise2 was amplified by PCR using a forward primer harboring a FLAG sequence at the 5'-end and replaced with non-tagged mTurquoise2. mTq2-CaM-SYFP2-KRAS4b and mutants made in pENTR1A were transferred into pEZYmyc-His by Gateway LR Clonase II (Invitrogen). All plasmids were confirmed by DNA sequencing. All primers used were listed in Appendix 2.

2.1.4 Expression and Purification of CaMeRAS Construct and Mutants

HeLa cells were transfected with plasmids containing FLAG-mTq2-CaM-SYFP2-KRAS4b and mutants using a transfection reagent, jetPRIME (Polyplus transfection). Cells were harvested at ~48 hours after transfection. For purification, cells were resuspended with lysis buffer (50mM Tris, 300mM NaCl, 2mM DTT, 1mM EDTA, pH 7.4 supplemented with cOmplete, EDTA-free protease inhibitor cocktail (Roche)) and lysed using an EmulsiFlex-C3 (Avestin). Cell lysate was centrifuged at 45,000g for 30 min to remove cell debris. The supernatant was loaded to anti-FLAG M2 agarose (Sigma) and washed with the same buffer for lysis. FLAG-mTq2-CaM-SYFP2-

KRAS4b was eluted with 0.15 mg/mL 3xFLAG peptide (APExBIO) in the buffer (50 mM Tris, 300 mM NaCl, 2mM DTT, pH 7.4).

2.1.5 Nanodisc Preparation

All lipids were purchased from Avanti Polar Lipids, Inc. Nanodiscs were prepared according to previous protocols [63]. 1,2-distearoyl *sn*-glycero-3-phosphoethanolamine-N-diethylenetriaminepentaacetic acid (gadolinium salt) (PE-DTPA(Gd^{3+})) was added to the lipids at a molar ratio of 20 DOPC : 5 DOPS : 1 PE-DTPA (Gd^{3+}). The organic solvents were then removed using gentle nitrogen flow followed by vacuum, and the dried lipid film was solubilized in aqueous buffer containing detergent (20 mM Tris pH 7.4, 100 mM NaCl, and 100 mM sodium cholate). This mixture was subjected to three freeze/thaw cycles, vortexed until clarified, then membrane scaffold protein (MSP1D1, prepared as described previously [64]) was added at a 1:40 molar ratio relative to the lipids. Following 1 h incubation with mild rotation at 20 °C, sodium cholate was removed from the MSP-lipid mixture with Bio-Beads SM-2 Adsorbents (Bio-RAD) using a batch method with 2h incubation at room temperature with mild rotation. The nanodisc particles were then purified via size exclusion chromatography using a 26-60 Superdex 200 column equilibrated with buffer A without TCEP. The particle size was analyzed with dynamic light scattering (DLS) and corresponded with a 10 nm diameter particle (data not shown).

2.2 Experimental Methods

2.2.1 Nuclear Magnetic Resonance (NMR) Experiments

2.2.1.1 ^{1}H – ^{15}N Heteronuclear Single Quantum Correlation (HSQC)

Samples were prepared for NMR by mixing the appropriate labeled proteins and substrates in NMR buffer containing 50 mM HEPES pH 7.4, 100 mM NaCl, 1 mM TCEP and 10% D_2O. Most experiments also included 5 mM $MgCl_2$ and/or 10 mM $CaCl_2$. NMR experiments were primarily conducted on a 600 MHz Bruker Avance magnet with 1.7 mm cryoprobe and 40 µL sample volumes. Experiments conducted on an 800 MHz magnet had 450 µL samples in 5mm tubes.

2.2.1.2 NMR Titrations (HSQCs)

(E,E)-farnesol, (Z,Z)-farnesol and (Z,Z)-farnesyl cysteine methyl ester were solubilized in DMSO to 100 mM, appropriately diluted in NMR buffer, and added directly to separate NMR samples to a final concentration of 2.5% DMSO. Titration HSQCs were collected with 216 μM CaM and 0, 0.35, 0.7, 1, 1.4, 2.9, 5.8, 11.5, 14.3 and 29-fold excess farnesyl compound in an autosampler connected to a 600 MHz Bruker Avance magnet at 25°C. KRAS4b-FMe titrations were collected at 0.1, 0.4, 0.8, 1, 1.3, 2 and 4-fold excess over 0.1 mM CaM, under the same conditions.

2.2.1.3 ^{15}N-Lys KRAS4b – Nanodisc binding

^{15}N-lysine labeled KRAS4b-FMe was purified from insect cells and exchanged into an NMR buffer containing 50 mM HEPES pH 7.3, 100 mM NaCl, 10 mM $CaCl_2$ and 1 mM TCEP. HSQCs were collected at 600 MHz on a Bruker Avance magnet with 128 scans. Four independent NMR samples were prepared with 500 μM ^{15}N-KRAS4b-FMe and the ^{15}-lysine spectrum of KRAS4b-FMe alone was compared to the spectra collected in the presence of either 1:5 Nanodisc (20% DOPS), 1:1 CaM or both. Samples contained 20 μM acetyl glycine as an internal standard for normalization of peak intensities between samples.

2.2.1.4 Paramagnetic Relaxation Enhancement (PRE)

PRE describes the distance-dependent effect of paramagnetic ions, atoms or molecules on the relaxation rate of the nuclear spin of NMR-active nuclei. PRE is caused by dipolar interactions between a nucleus and the unpaired electrons of a paramagnetic center, resulting in increased nuclear relaxation rates [65]. The distance dependence of the PRE effect between the paramagnetic center and nucleus of interest goes like $\langle r^{-6} \rangle$. Two different PRE spin labels are used for this work to probe distinct interactions. To assess CaM-ligand binding, a TEMPO spin label containing a stable aminoxyl radical was conjugated through amine coupling to the exposed amine of FCME. To examine KRAS4b-FMe membrane extraction by CaM, a Gd^{3+} ion was chelated to a lipid headgroup (PE-DTPA - Gd^{3+}, five unpaired electrons) and incorporated into the nanodisc. The lipid diffuses rapidly which conveys a PRE effect to the nanodisc surface, allowing the monitoring of KRAS4b-FMe membrane attachment.

2.2.1.5 KRAS4b – Nanodisc PRE

Baseline ^{1}H-^{13}C HSQC spectra of 200 μM ^{13}C-TILVM KRAS4b-FMe were collected on a 600 MHz Bruker Avance magnet in the presence and absence of unlabeled CaM, with and without Ca^{2+}, at 25^{O}C. PRE experiments were initiated by the addition of 1:20 molar ratio Gd^{3+}-containing nanodisc to similarly prepared NMR samples and collecting corresponding HSQCs. Peak intensity ratios were calculated for nanodisk vs baseline for CaM-containing samples, either in the presence of Ca^{2+} (20 mM HEPES pH 7.3, 100 mM NaCl, 1 mM TCEP, 5 mM Mg^{2+}, 5 mM Ca^{2+}) or absence of Ca^{2+} (20 mM HEPES pH 7.3, 100 mM NaCl, 1 mM TCEP, 0.5 mM Mg^{2+}) by normalizing intensities to a 0.6 mM DSS internal standard.

2.2.2 Calmodulin Crystallization and Structure Determination

1 mM CaM (20 mM HEPES pH 7.4, 10 mM Ca^{2+}) was screened for crystallization with 5mM FCME at room temperature using Protein Complex (Qiagen), Wizard Classic (Rigaku) and Crystal Screen HT (Hampton Research) commercial screening kits. A successful condition from Crystal Screen HT containing 0.2 mM ammonium acetate, 0.1 mM sodium cacodylate pH 6.5 and 30% (w/v) PEG 8000, was further optimized for pH and PEG concentration with 1 mM and 1.25 mM CaM. The diffracted crystal was grown in 5mM FCME, 0.2 mM sodium acetate, 0.1 mM sodium cacodylate pH 6.7 and 28% PEG 8000, with 1.25mM CaM. Glycerol was used as a cryoprotectant. Diffraction data from the Canadian Macromolecular Crystallography Facility 08ID-1 Beamline at the Canadian Light Source was processed with HKL2000 [66] and modeled and refined using COOT [67] and Phenix [68].

2.2.3 In Vitro Fluorescence Resonance Energy Transfer (FRET)-based Calcium Titration

Purified FLAG-mTq2-CaM-SYFP2-KRAS4b was dialyzed with the buffer (50mM Tris, 300mM NaCl, 2mM DTT, pH7.4) in which residual calcium had been chelated with Chelex 100 resin (Bio-Rad). Fluorescence measurement were made on a Shimadzu RF-5301PC fluorimeter (Shimazu Corp.), and Emission spectra of FLAG-mTq2-CaM-SYFP2-KRAS4b excited by 405 nm light in the presence of various concentrations of $CaCl_2$ were scanned from 420 nm to 600 nm at 20°C.

2.2.4 In Vivo Fluorescence Imaging

2.2.4.1 FRET and Calcium Co-imaging and Data Analysis

HeLa or HEK293 cells were transfected with plasmids containing the mTq2-CaM-SYFP2-KRAS4b or its mutants using jetPRIME (Polyplus transfection). The cells were subjected to imaging at 18-24 hours after transfection. HBSS (Gibco) supplemented with 1 mM $CaCl_2$, 0.5 mM $MgCl_2$ and 0.5mM $MgSO_4$ was used as an imaging buffer. After loading the cells with 10 μM Calbryte 630 AM (AAT Bioquest), imaging was performed at room temperature using a Leica SP8 confocal microscope with a 63x/1.4NA oil immersion objective lens and high-sensitivity HyD detectors. For simultaneous visualization of mTq2, SYFP2 and Calbryte 630, a 440 nm solid state laser and a white light laser tuned to 608 nm were used for excitation; and fluorescence emission was collected at 455-490 nm, 525-560 nm and 620-750 nm, respectively. Images were acquired at 3.4 - 4.0 sec/frame and analyzed using Fiji [69].

2.2.4.2 Fluorescence Lifetime Imaging (FLIM) Microscopy and Data Analysis

Fluorescence lifetime images were acquired using a Leica SP8 confocal microscope equipped with a time-correlated single-photon counting module (Picoharp 300, PicoQuant). The donor (mTq2) was excited using a 405 nm solid state laser pulsed at a 40 MHz repetition frequency. Fluorescence signal in the emission range 455-480nm was collected though a 63x/1.4NA oil immersion objective lens using a cooled single-photon counting HyD SMD detector. Fluorescence lifetime traces were analyzed by using SymPhoTime 64 software (PicoQuant). Statistical difference between pre- and post-histamine stimulation was analyzed by using Wilcoxon single-rank test.

Chapter 3
Results

3 Results

3.1 Structural and Biophysical Characterization of the KRAS4b – Calmodulin Interaction

3.1.1 KRAS4b – Calmodulin Interaction is Dependent Upon Farnesylation

Some reports have described an interaction between CaM and unfarnesylated KRAS4b [30,51,52], thus we initiated our study of the interaction using unprocessed KRAS4b expressed in *E. coli* (residues 1-185, representing the full-length protein after -aaX cleavage but lacking farnesylation and carboxy-methylation). We collected ^{1}H-^{15}N heteronuclear single quantum correlation (HSQC) NMR spectra of ^{15}N-labeled KRAS4b or ^{15}N-CaM and analyzed chemical shift perturbations (CSPs) upon the addition of the other, unlabeled protein. These experiments were performed with KRAS4b in both GDP- and GTPγS-loaded states, and in the presence and absence of Ca^{2+}. Even though CSPs are sensitive to weak interactions, no change was detected in the spectrum of either protein when they were mixed in the absence of Ca^{2+} (data not shown). In the presence of Ca^{2+}, minor CSPs were observed in both proteins independent of the nucleotide bound, however no large CSPs that would be indicative of a strong or specific interaction were detected (Figure 3.1). The small CSPs were likely due to non-specific electrostatic interactions between the basic lysine residues in the HVR and the acidic surface of CaM. We do not consider these minor changes relevant in comparison to the large CSPs typically observed upon binding of CaM to canonical targets such as protein kinases and or channels ([70-72]). Hence, we conclude that CaM only makes weak, transient contacts with unfarnesylated KRAS4b in solution.

To determine whether CaM binds to farnesylated KRAS4b, we examined the interaction of CaM with full length, fully-processed KRAS4b expressed in and purified from insect cells using a baculovirus expression protocol developed by NCI Frederick [57] (designated KRAS4b-FMe, which is farnesylated, has the C-terminal tripeptide removed and Cys185 carboxymethylated, as illustrated in Figure 3.2A). In contrast to the unfarnesylated protein, addition of KRAS4b-FMe to ^{15}N-CaM in the presence of Ca^{2+} induced widespread changes in the ^{15}N-CaM spectrum,

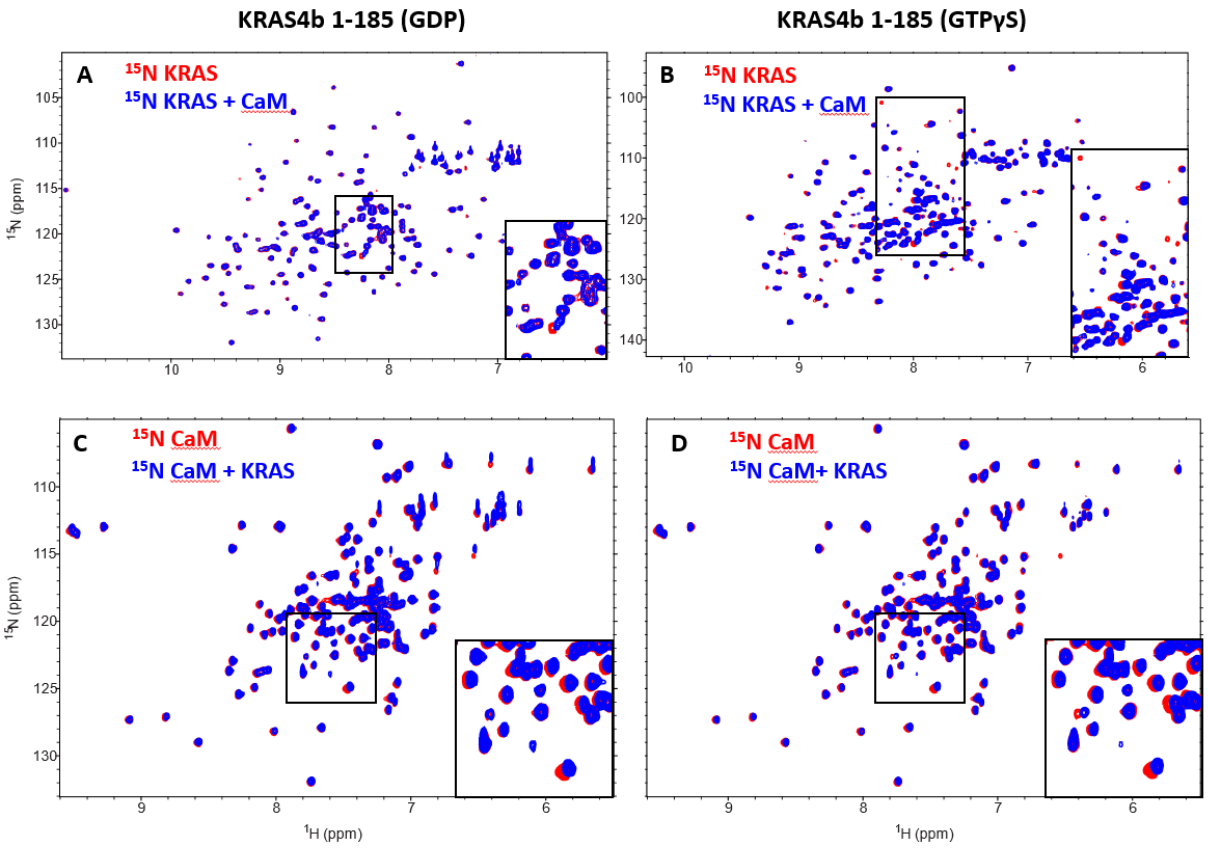

Figure 3.1. There is no major interaction between unfarnesylated KRAS4b (1-185) and calmodulin, independent of bound nucleotide. ^{1}H-^{15}N HSQCs of both 500 µM uniformly^{15}N-labelled KRAS4b and calmodulin show only slight chemical shift perturbations upon addition of the other, unlabeled protein at a 1:1 ratio. All spectra were collected in NMR buffer containing 50 mM HEPES, 100 mM NaCl, 5 mM Mg^{2+}, 1 mM TCEP and 10 mM Ca^{2+}, at 25°C and 600 MHz.

affecting the majority of the crosspeaks (Figure 3.2B). Specifically, KRAS4b-FMe induced severe line broadening of ~80% of the CaM resonances, as well as CSPs in several of the peaks that were not broadened beyond detection, clearly indicating a farnesyl-dependent interaction between KRAS4b-FMe and CaM. The peak broadening is likely caused by several factors, including the increased molecular mass of the complex, transient exchange between bound and unbound states and chemical exchange from non-specific contacts between the G-domain of KRAS4b and CaM. The broadening of NMR signals upon titration of KRAS4b-FMe into CaM was also observed recently by Agamasu et al [55]. Several residues within the C-lobe exhibited chemical shift changes (S81, L116, A128, I130 and A147) indicative of a more stable and specific interaction (arrows, Figure 3.2B). While the CSPs provide probes of the interaction, the extensive signal broadening limited the structural information that could be extracted from these spectra. Therefore, to improve spectral quality and gain insights into the structural mechanism,

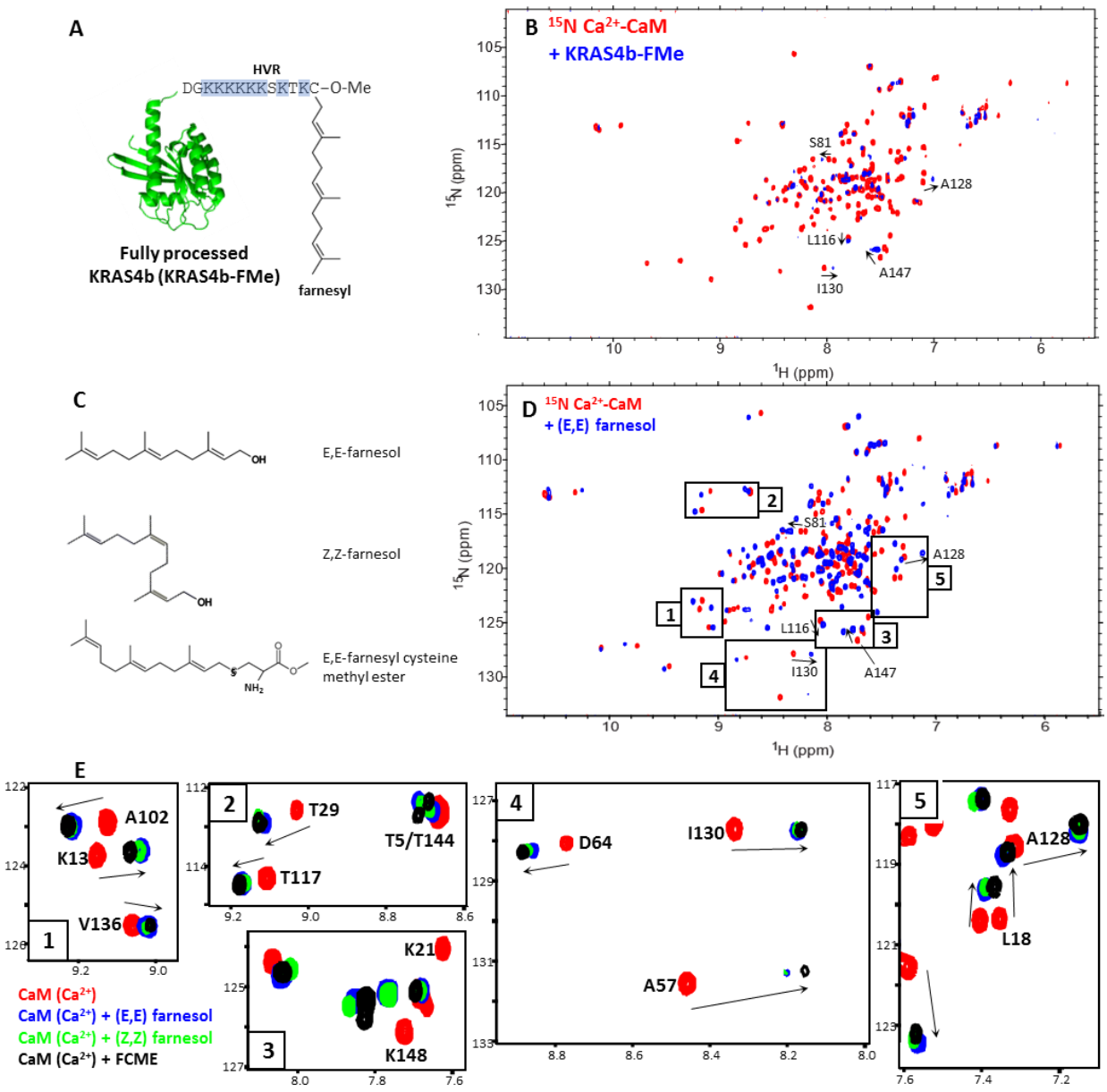

Figure 3.2. Calmodulin interacts strongly with farnesylated KRAS4b and farnesyl compounds. A) Schematic of farnesylated KRAS4b purified from Hi Five insect cells engineered to enhance farnesylation capacity. The aaX (VIM) is cleaved off following farnesylation at C185 and the exposed terminal cysteine is carboxymethylated. The polybasic region of the HVR is highlighted in blue **B)** ^{1}H - ^{15}N HSQC of uniformly ^{15}N-labelled calmodulin alone (red) and in the presence of 4-fold excess KRAS4b-FMe-GDP (blue). The presence of KRAS4b-FMe induces chemical shift perturbations and extensive signal broadening. Unbroadened signals that experience perturbations are highlighted (Arrows) and used as probes for the interaction **C)** Chemical structures of tested farnesyl-derived compounds. **D)** ^{1}H - ^{15}N HSQC of uniformly ^{15}N-labelled Ca^{2+}-bound CaM alone (red) and in the presence of 11-fold excess E,E-farnesol (blue). Titration of farnesol induces global conformational changes. Probe peaks from (B) are marked with arrows **E)** HSQC overlay of all farnesyl-bound spectra at titration endpoints: farnesol stereoisomers – 11-fold excess, FCME – 3-fold excess. Similar chemical shift perturbations are highlighted (Arrows). All spectra were collected in NMR buffer containing 50mM HEPES pH 7.3, 100mM NaCl, 10mM Ca^{2+} and 1mM TCEP at 25°C and 600 MHz

we sought to identify the minimal binding elements that mediate the interaction between KRAS4b-FMe and CaM.

3.1.2 KRAS4b Farnesyl Moiety is Sufficient for Calmodulin Binding

With the knowledge that farnesylation is necessary for the KRAS4b-CaM interaction, we first questioned whether the farnesyl moiety alone is sufficient for CaM binding. Using a series of farnesyl-derived compounds (Figure 3.2C), we assessed CSPs in the ^{1}H-^{15}N HSQC spectra of CaM. First, (E,E)-farnesol, an alcohol derivative of the primary stereoisomer present in mammalian cells, was solubilized in DMSO and titrated into ^{15}N-CaM in the presence of Ca^{2+}. The resulting ^{1}H-^{15}N HSQC spectra exhibited extensive CSPs of almost all cross-peaks indicating that CaM undergoes a substantial structural rearrangement upon addition of (E,E)-farnesol (Figure 3.2D) (but not DMSO). Notably, during titration of farnesol, CaM peaks did not exhibit the broadening caused by KRAS4b-FMe titration, and the five probe peaks identified above (S81, L116, A128, I130 and A147) exhibited similar chemical shift changes in both spectra. This suggests KRAS4b-FMe and farnesol may interact with CaM in a similar manner, however, farnesol titration does not cause peak broadening due to its smaller size and the absence of chemical exchange between CaM and a dynamic G-domain. No CSPs were apparent in the absence of Ca^{2+} indicating that this interaction is fully Ca^{2+}-dependent (Figure 3.3), consistent with every previous report of the KRAS4b-CaM interaction.

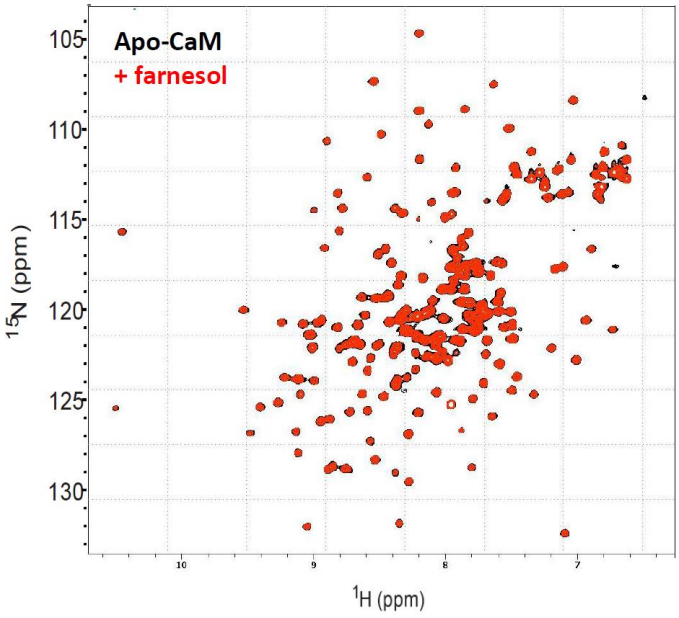

Figure 3.3. Farnesol and CaM do not interact in the absence of Ca^{2+}. ^{1}H-^{15}N HSQC of 500 μM uniformly ^{15}N-CaM (Black) – apo – in the presence of a large excess of (E,E)-farnesol (Red). Samples were prepared in 50 mM HEPES pH 7.4, 100 mM NaCl, 10 mM $CaCl_2$, 1 mM TCEP. Spectra were collected at 25^{o}C and 800 MHz.

To our knowledge, this is the first report that an isolated lipid is sufficient to act as a CaM-binding target, although examples of CaM binding lipopeptides have been published. A structure of myristoylated N-terminal polybasic peptide from CAP23/NAP22 in complex with CaM showed that the myristoyl moiety is directly sequestered [73], but the relative contribution of the peptide versus lipid moieties to CaM binding were not assessed. Agamasu et al. recently performed a titration of CaM with a farnesylated KRAS4b C-terminal 6-mer peptide (KSKTKC-FMe), which produced a CaM spectrum nearly identical to ours in the presence of farnesol alone [55], suggesting the farnesyl moiety may recapitulate the KRAS4b-CaM binding mode. To investigate the stereospecificity of this lipid:CaM interaction, we titrated the natural, rare stereoisomer (Z,Z)-farnesol (Figure 3.2C) into ^{15}N-CaM. The CaM spectra in the presence of the two stereoisomers were very similar (Figure 3.2E), suggesting that structural plasticity of CaM can accommodate either conformation of the lipid by virtue of the flexible linker and malleable methionine-rich hydrophobic pockets [49,74,75]. We titrated ^{15}N-CaM with (E,E)-farnesyl cysteine methyl ester (FCME) (Figure 3.2C), comprising the fully processed C-terminal residue of KRAS4b, which showed that extension of farnesol to include the carboxymethylated cysteine

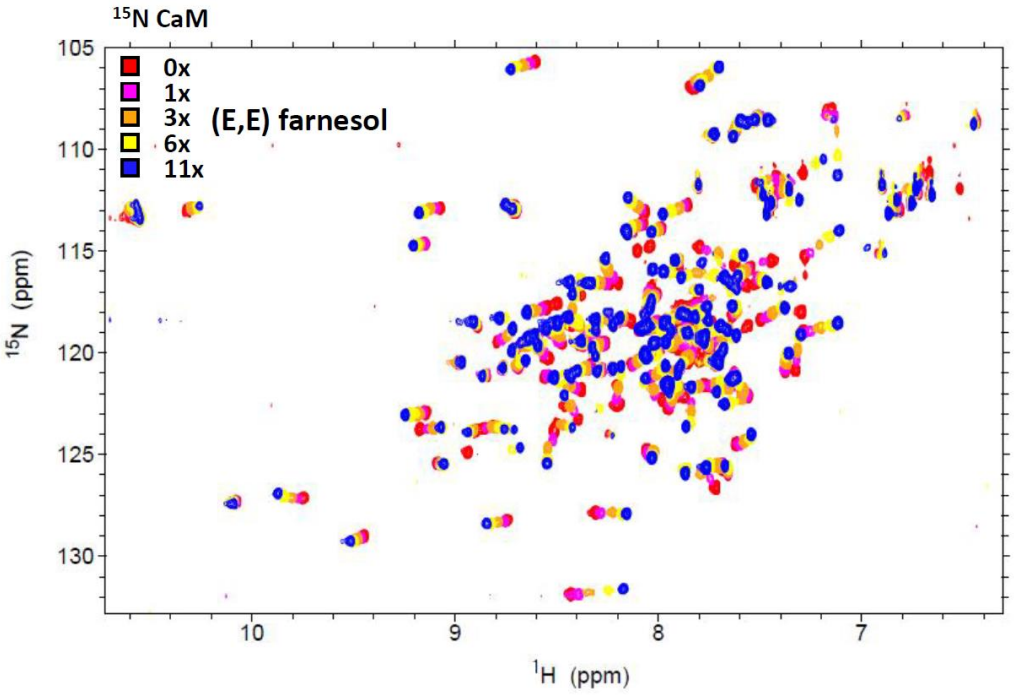

Figure 3.4. Farnesyl compound titrations into CaM. ^{1}H-^{15}N HSQC overlay of 216 μM ^{15}N-CaM (Red) with increasing concentrations of (E,E)-farnesol (similar spectra were produced for (Z,Z)-farnesol and FCME, though saturation was reached at 3x excess FCME compared to 11x excess farnesol). A fast exchange binding mode allowed all peak assignments to be tracked through to saturation (Blue). Titrations points were selected from a larger set to provide even peak separation. Samples were prepared independently, each in 50 mM HEPES pH 7.4, 100 mM NaCl, 10 mM Ca^{2+}, 1 mM TCEP and 2.5% DMSO. Data was collected at 25^{O}C and 600 MHz.

moiety caused minor changes in the pattern of CSPs (Figure 3.2E), and promoted saturation at a lower molar ratio, suggesting that this amino acyl component contributes to binding affinity. Finally, all assigned CaM peaks could be traced to saturation throughout the titrations with farnesyl compounds (Figure 3.4) and were found to overlay with the subset of CaM peaks that remained visible upon titration with KRAS4b-FMe (Figure 3.5), suggesting that CaM interaction with the lipid comprises the core of the KRAS4b-FMe-CaM complex.

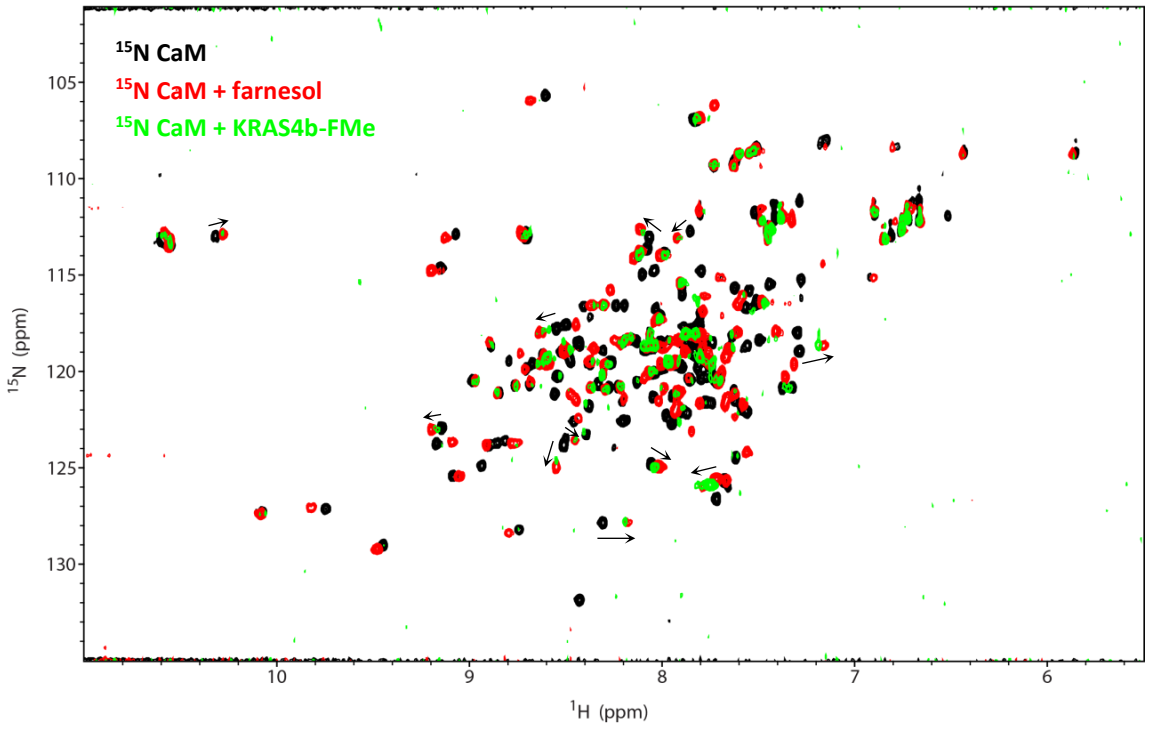

Figure 3.5. KRAS4b-FMe and farnesol perturbations of ^{15}N-CaM share a characteristic pattern. ^{1}H-^{15}N HSQC of 216 µM uniformly ^{15}N-CaM in NMR buffer containing 50 mM HEPES pH 7.4, 100 mM NaCl, 10 mM Ca^{2+}, 1 mM TCEP. **Black** – CaM alone, **Red** – CaM in the presence of 3-fold excess (E,E)-farnesol. **Green** – in the presence of 4-fold excess KRAS4b-FMe. Arrows indicate unbroadened resonances in the KRAS4b-FMe spectrum (green) that share characteristic (similar magnitude and direction) perturbations of ^{15}N-CaM with farnesol (red). Samples were prepared in 50mM HEPES pH 7.4, 100mM NaCl, 10mM Ca^{2+}, 1mM TCEP. Data was collected at 25^{o}C and 600MHz with 8 scans.

3.1.3 Crystal Structure of Calmodulin in Complex with FCME Reveals C-lobe Binding

To obtain an atomic-resolution picture of the interaction, we employed X-ray crystallography. Multiple crystallization trials (~300 conditions) of Ca^{2+}–CaM complexed with (E,E)-farnesol were unsuccessful, however, the FCME complex produced crystals in 66 conditions. After optimization (see Materials and Methods), we obtained a crystal that diffracted to 1.8 Å, and 2.0 Å with anomalous data, using a synchrotron x-ray source. Initially, density maps were generated

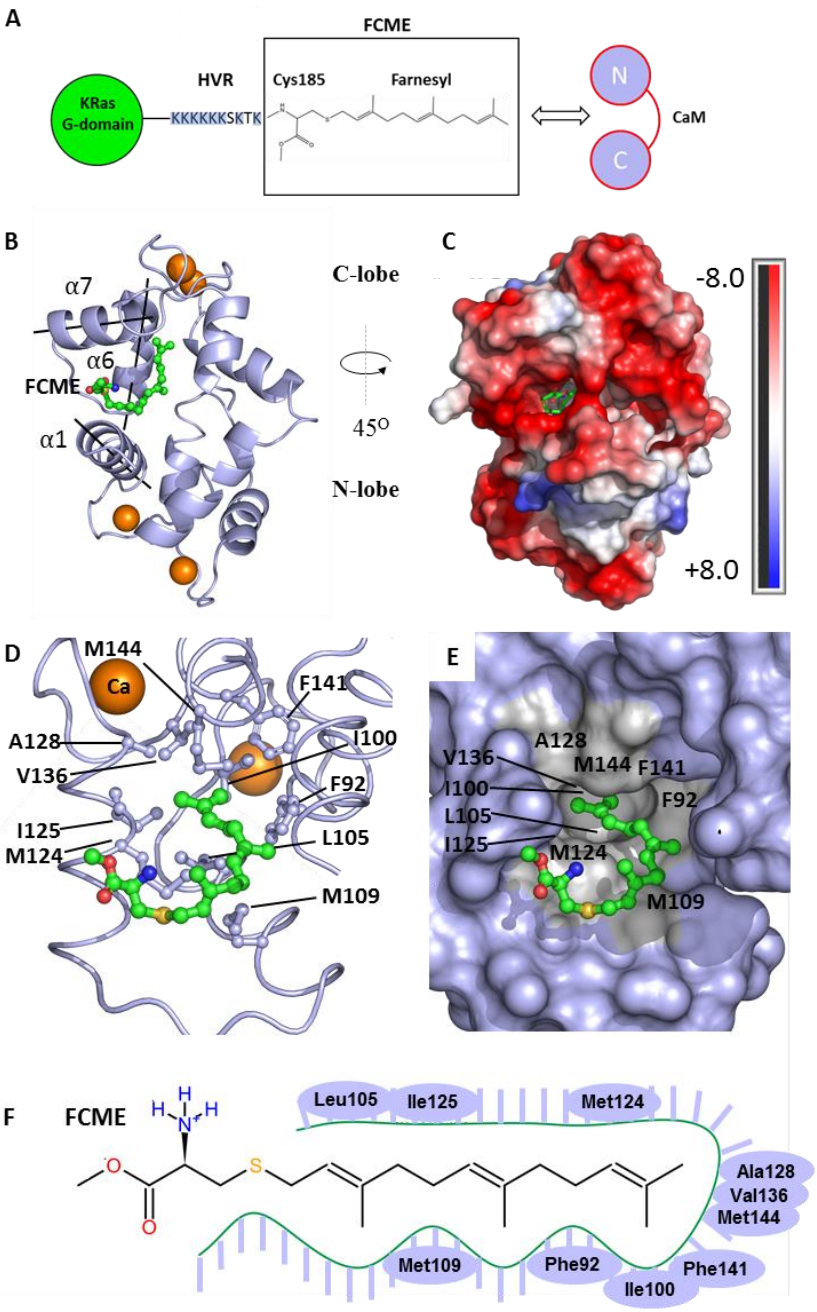

Figure 3.6. Crystal structure of calmodulin in complex with FCME. Structure of Ca^{2+}-CaM bound to farnesyl cysteine methyl ester (FCME), resolved to 1.8Å. **A)** Schematic diagram of the hypothesized CaM-KRAS4b-FMe interaction; the hydrophobic core of CaM sequesters the farnesyl moiety of KRAS4b-FMe **B)** Cartoon diagram of the CaM-FCME structure showing a compact CaM conformation with significant inter-lobe contacts. FCME is buried in the CaM C-lobe hydrophobic pocket with the aminoacyl (C185) group exiting through a gap between α-helices 1, 6 and 7. **C)** Surface electrostatic representation of CaM, showing the channel formed by α-helices 1, 6 and 7 through which the cysteinyl moiety of FCME exits (rotated 45° relative to panel (B), and the highly acidic surface accessible to an adjacent polybasic HVR. Electrostatics were modeled with the APBS Pymol plug-in **D)** A zoomed perspective of FCME in the CaM C-lobe hydrophobic pocket. 10 Residues involved in hydrophobic contacts with the ligand are depicted as sticks and labeled. **E)** A close-up surface representation of FCME in the C-lobe hydrophobic pocket with interacting residues coloured grey. **F)** A ligand interaction map highlighting the hydrophobic interactions between FCME and the CaM C-lobe pocket.

separately by (a) molecular replacement, using a structure of CaM bound to the myristoylated CAP23/NAP22 peptide (PDB: 1L7Z) [73] as a search model, and (b) *a priori* with experimental phasing from anomalous data, primarily scattered by Ca^{2+} ions. Both approaches yielded highly similar structures. The two datasets were combined in HKL2000 and refined in Phenix to yield a high-resolution map of the CaM-FCME complex (crystallographic statistics found in Table 2).

In this structure, the N- and C-lobes of CaM come together to form a compact globular conformation with a hydrophobic core and acidic surface (Figure 3.6B – C), akin to many reported structures of CaM-target complexes [48]. The farnesyl moiety in this complex is bound within the C-lobe hydrophobic pocket of CaM, making hydrophobic contacts with residues F92, I100, L105, M109, M124, I125, A128, V136, F141 and M144 (Figure 3.6D – F). In the major conformation, which exhibits strong, well-defined electron density, the cysteine moiety of FCME protrudes through an opening between α-helices 1, 6, and 7 (Figure 3.6B, Figure 3.7A), however weak additional electron density suggests FCME may exist in an alternate low-occupancy

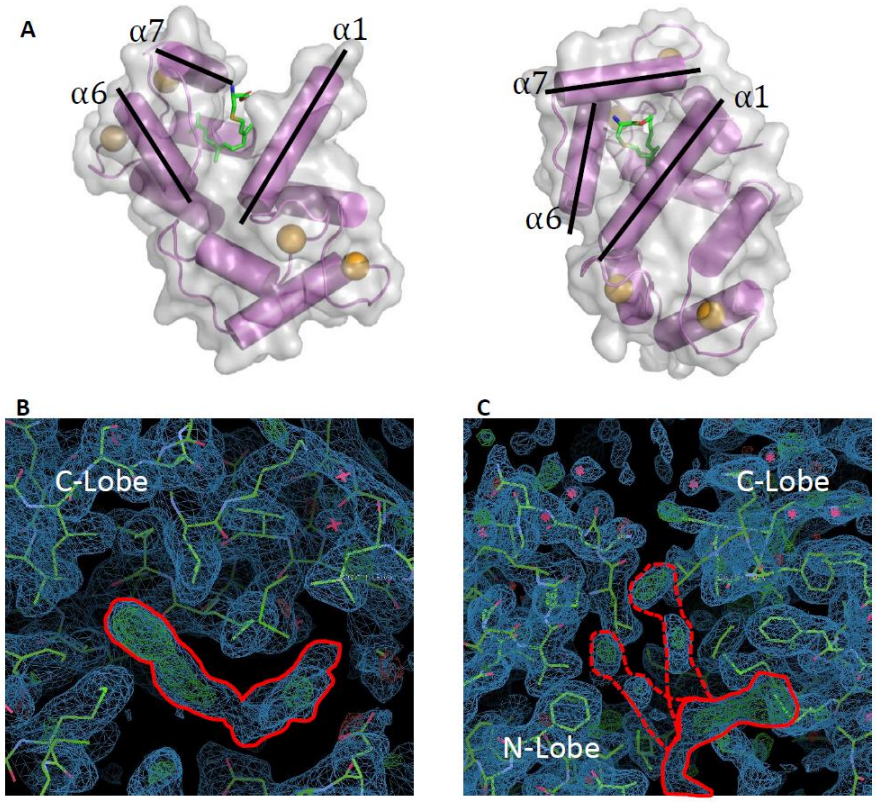

Figure 3.7. Lipid orientation in CaM:FCME complex structure. A) Stick representation of CaM in complex with FCME, showing the principal binding orientation, with FCME cysteine exiting CaM between α1,6,7. **B)** Electron density map generated during CaM:FCME crystal structure refinement in Phenix, showing electron density for FCME in the principle binding orientation, highlighted in solid Red. **C)** Another angle shows less well defined ambiguous electron density potentially representing low-occupancy binding modes, with the FCME cysteine protruding from the opposite side of CaM hydrophobic channel.

conformation in which the aminoacyl end exits the hydrophobic core from the opposite side (Figure 3.7B – C).

Our structure is globally similar to that of CaM in complex with the myristoylated CAP23/NAP22 peptide used for molecular replacement modeling, however, several differences are apparent (Figure 3.8A). In the CAP23/NAP22 structure, the saturated, unbranched myristoyl moiety extends through a hydrophobic channel formed by both lobes, whereas in our structure, the farnesyl moiety of FCME, which is unsaturated and branched, is buried deep within the C-lobe hydrophobic pocket of CaM and the N-lobe pocket is minimally exposed (Figure 3.8B). Interestingly, the C-terminal cysteine residue of FCME occupies a position equivalent to that of the N-terminal myristoylated glycine in CAP23/NAP22 (Figure 3.7B), thus the adjacent polybasic sequences would be tethered in the same region of both complexes, albeit with opposite strand directions.

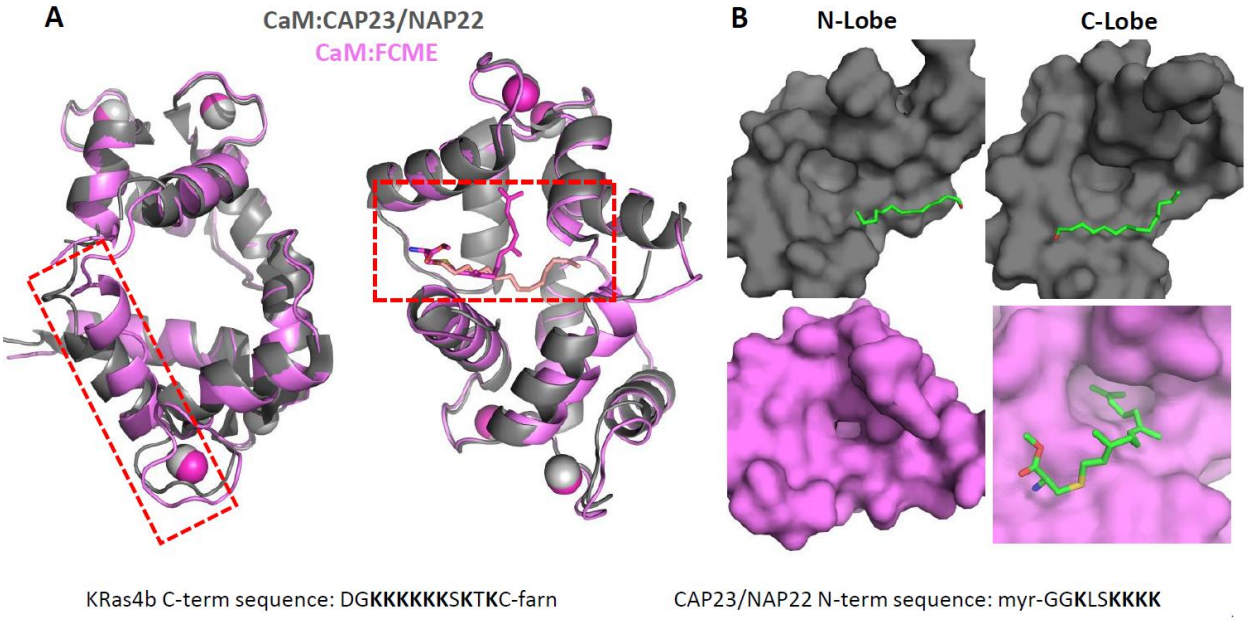

Figure 3.8. Comparison of CaM lipid binding modes for FCME (PDB: 6OS4) and myristoylated CAP23/NAP22 (PDB: 1L7Z). A) Comparison of crystal structures of Ca^{2+}-bound CaM in complex with FCME (**Pink**, PDB: 6SO4) or myristoylated CAP23/NAP22 polybasic peptide (myr-GGKLSKKKK, **Grey**, PFB 1L7Z). The crystal structures are identical but differ in the position of the α4, and orientation of lipid within the hydrophobic core, both highlighted in red. **B)** Myristoyl is saturated and unbranched and is found in a linear orientation, interacting with both hydrophobic pockets. FCME is unsaturated and branched and is bound in the C-lobe pocket only, and the N-lobe is minimally exposed due to the rearrangement of α4.

This structure indicates that CaM sequesters the farnesyl moiety in its hydrophobic core and suggests that electrostatic interactions may form between the acidic surface of CaM (accessible acidic residues include E7, E11, E14, E114, E120, E123 and E127, and the linker, E82/83/84) and the basic HVR of KRAS4b, while this interaction does not directly involve the G-domain. To gain more insight into this structure in solution, we performed NMR experiments using a paramagnetic relaxation enhancement (PRE) probe in which a TEMPO spin labeled molecule was conjugated to the free amine group of FCME [65,76]. TEMPO-FCME was added to ^{15}N-CaM in solution, ^{1}H-^{15}N HSQC spectra were recorded (Figure 3.9A), and the residues associated with PRE-induced peak broadening were mapped onto our crystal structure (Figure 3.9B – C). The

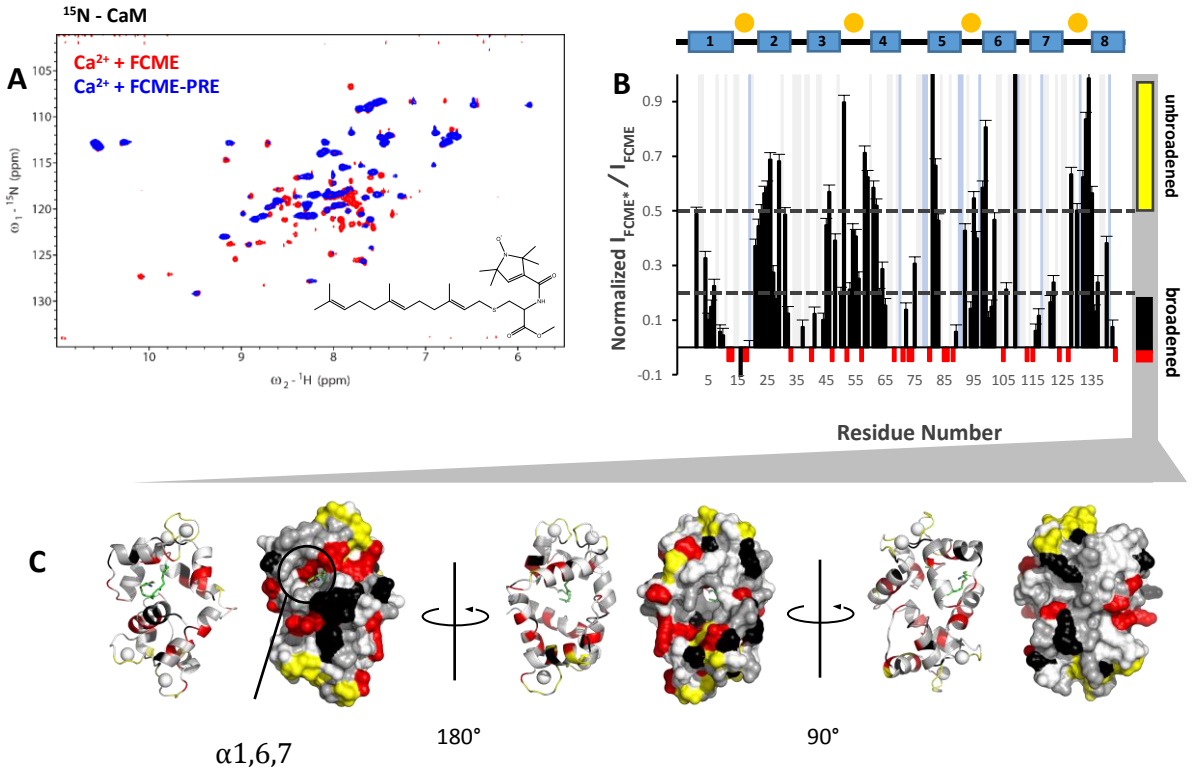

Figure 3.9. Solution NMR PRE validation of CaM-FCME crystal structure A) ^{1}H-^{15}N HSQC of 800µM uniform ^{15}N-CaM with 1x FCME (Red) and with roughly 1x FCME-TEMPO (Blue). Broadening of NMR signals due to PRE effects by FCME-TEMPO was measured, compared to broadening induced by FCME, and plotted as change in intensity by residue in (B). **B)** NMR peaks that retained a relative intensity of 0.5 or greater compared with FCME were considered unbroadened, coloured (Yellow) and mapped onto our crystal structure (C). Peaks that displayed a relative intensity less than 0.2 were considered broadened and coloured (Black) when mapped onto the crystal structure. Peaks present in the FCME-broadened spectrum but undetectable in the FCME-TEMPO spectrum were considered severely broadened and coloured (Red). Residues that are undetectable in the CaM-alone spectrum are shaded grey, residues that are completely broadened following FCME addition are shaded blue and resonances completely relaxed by FCME-TEMPO are shaded red, below the axis. **C)** Broadened and unbroadened residues were mapped by colour onto our crystal structure, showing PRE-free zones on the outsides of the N- and C- lobes, and PRE hotspots near the openings to the hydrophobic channel of CaM. The α1,6,7 exit site shows considerably more broadening, consistent with our crystal structure. NMR was performed in a buffer containing 50mM HEPES pH 7.4, 100mM NaCl, 5mM Mg^{2+}, 10mM Ca^{2+}, 1mM TCEP and 10% DMSO, at 25^{o}C and 600MHz with 8 scans. Error bars represent spectral noise.

largest PRE effect was observed for those residues near the α1,6,7 exit site, and another less intense PRE cluster was observed around the putative alternate exit site. This PRE broadening around α1,6,7 involves both lobes, consistent with our crystal structure and supporting the presence of a compact CaM configuration with inter-lobe contacts in solution (Figure 3.9C).

3.1.4 Membrane and Calmodulin Compete for KRAS4b Binding

Since the farnesyl group and the HVR both contribute to KRAS4b membrane localization and the interaction with CaM, we sought to determine whether KRAS4b binding with CaM and with lipid bilayers is compatible or mutually exclusive. We used ^{15}N-lysine labeled KRAS4b-FMe to probe the HVR, as it contains nine Lys residues in the terminal 15 amino acids. As previously described, we performed NMR experiments to investigate the KRAS4b interaction with membranes using a synthetic lipid bilayer nanodisc (ND) comprised of 80% DOPC and 20% DOPS [77]. Five signals from lysine backbone amides in the KRAS4b-FMe HVR are well-resolved and assignable from previous work [78] (Figure 3.10A). Upon binding to ND (1:5 molar ratio), these signals disappear, presumably due to exchange broadening caused by the interactions between KRAS4b-FMe (farnesyl and the HVR) and the negative surface of the ND (Figure 3.10B). Remarkably, subsequent addition of Ca^{2+}-CaM to this sample restored the intensity of these HVR lysine signals (Figure 3.10C), and the resulting spectrum overlays with that of ^{15}N-lysine KRAS4b-FMe complexed with Ca^{2+}-CaM in the absence of NDs (Figure 3.10D), which is distinct from the spectrum of ^{15}N-lysine KRAS4b-FMe alone in solution (Figure 3.10E).

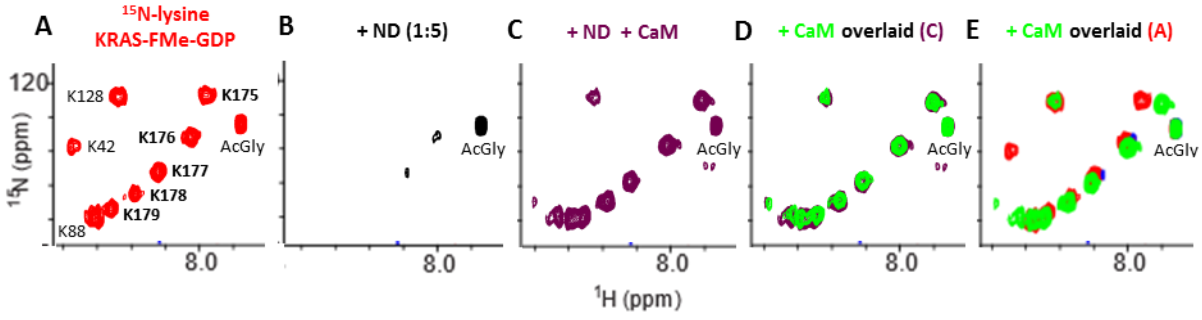

Figure 3.10. Alternative isotopic labeling schemes of KRAS4b-FMe show calmodulin binding is mutually exclusive with membrane association. (A-E) Fully processed KRAS4b-FMe, specifically labeled with ^{15}N-lysine in insect cells, provides 5 NMR probes in the HVR and 11 in the G-domain. The chosen window highlights the lysine residues in the HVR (in bold). Samples contain 20μM acetyl glycine (AcGly) as an internal standard **A) 100μM** KRAS4b-FMe alone **B)** KRAS4b-FMe after addition of nanodiscs (ND) comprised of 80% DOPC and 20% DOPS (5-fold excess KRAS4b-FMe) **C)** KRAS4b-FMe in the presence of NDs and Ca^{2+}-CaM (1:1 KRAS4b-FMe molar ratio) **D)** KRAS4b-FMe and Ca^{2+}-CaM in the absence of nanodiscs, overlaid with (C), showing the same spectrum despite presence of NDs in (C). **E)** KRAS4b-FMe and Ca^{2+}-CaM overlaid with (A), showing chemical shift perturbations in KRAS4b-FMe HVR ^{15}N-lysines after addition of Ca^{2+}-CaM

These data clearly demonstrate direct competition between NDs and CaM for KRAS4b-FMe binding, consistent with the fact that they share the same interacting elements. This is also consistent with the reported affinity of CaM for KRAS4b-FMe (Kd: 0.3-0.4 µM) [55], roughly an order of magnitude higher than the reported KRAS4b-FMe affinity for the lipid bilayer (Kd: 4 µM) [57]. To further validate this observation, we used PRE experiments to directly track KRAS4b-FMe membrane association. As previously described [63,78], we monitored the signals of ^{13}C-methyl labeled KRAS4b-FMe (a total of 92 methyls from Thr/Ile/Leu/Val/Met are labeled) in the presence and absence of NDs containing an embedded Gd^{3+}-chelating lipid, which enabled us to identify, through PRE-induced line broadening, the extent of the interaction of KRAS4b-FMe with the membrane (schematic in Figure 3.11A). Peaks from many residues, especially Ile

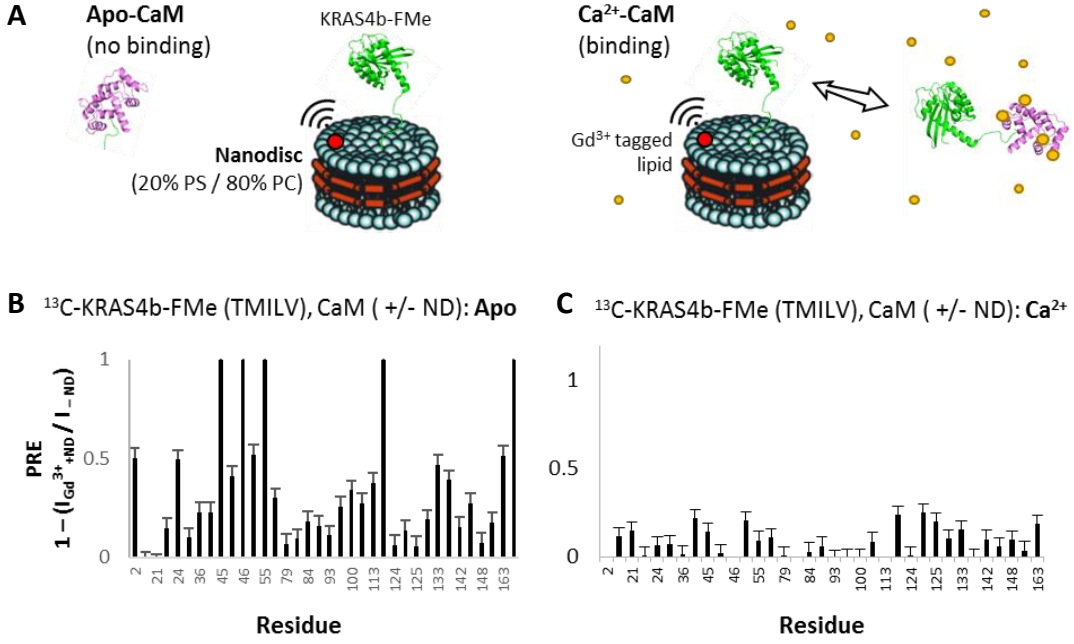

Figure 3.11. Membrane-based PRE probe for KRAS4b-FMe interaction with CaM in solution. KRAS4b-FMe, specifically methyl-labeled with ^{13}C-Thr, Ile, Leu, Val and Met (TMILV) in insect cells, probes interactions with a lipid bilayer using paramagnetic relaxation enhancement (PRE). **A)** Model of the predicted interactions between KRAS4b-FMe, membranes (NDs) and CaM in the presence and absence of Ca^{2+}. Without Ca^{2+}, KRAS4b-FMe is associated with the membrane through HVR electrostatics and farnesyl insertion, thus experiences significant peak broadening by membrane-embedded PRE-active Gd^{3+}. Following addition of Ca^{2+} and activation of CaM, KRAS4b-FMe is extracted from the membrane by CaM and is thus unaffected by PRE-broadening at the membrane. **B)** Ratio of peak intensities by residue of **^{13}**C-TMILV-KRAS4b-FMe-GDP in the presence of apo-CaM (no Ca^{2+}) with Gd^{3+}-conjugated NDs versus no NDs. KRAS4b-FMe experiences significant PRE-induced broadening ($1 - [I_{Gd^{3+}\ ND} / I_{-\ ND}]$). **C)** Ratio of peak intensities of ^{13}C-TMILV-KRAS4b-FMe-GDP in the presence of Ca^{2+}-CaM with Gd^{3+}-conjugated NDs versus no NDs. In the absence of Ca^{2+}, KRAS4b-FMe experiences minimal broadening. A PRE reading of 1 means complete loss of signal while a reading of 0 signifies no change in peak intensity relative to pre-Ca^{2+}. NMR was performed in a buffer containing 50 mM HEPES pH 7.4, 100mM NaCl, 5mM Mg^{2+}, 10mM Ca^{2+}, 1mM TCEP and 10% DMSO, at 25^{o}C and 600MHz with 176 scans per experiment. Error bars represent spectral noise.

24, Val 25, Ile 55 and Leu 113, which are proximal to the membrane surface in the GDP-bound state [63,78], were strongly broadened in the absence of Ca^{2+} (Figure 3.11B). Addition of Ca^{2+} dramatically alleviated the PRE effect on KRAS4b-FMe, significantly restoring peak intensities, consistent with a loss of membrane association of KRAS4b-FMe in the presence of Ca^{2+}-CaM (Figure 3.11C). Taken together, these membrane-based NMR experiments indicate that Ca^{2+}-CaM effectively extracts KRAS4b-FMe from membranes in a Ca^{2+}-dependent manner, due to competition for KRAS4b-FMe farnesyl and HVR.

3.2 In-Cell Fluorescence Studies of KRAS4b – Calmodulin Interaction

To support the structure-based biophysical model of the KRAS4b-CaM interaction that we generated, we wished to translate experiments into a live-cell imaging system for *in vivo* validation. These studies were enabled by the imaging expertise of Dr. Masahiro Enomoto. Masa conducted all live-cell FRET and imaging experiments and processed the data. Masa's student Sung-In Back performed *in vitro* FRET experiments. Their help was invaluable to this project.

3.2.1 Calmodulin-KRAS4b Chimeric Construct (CaMeRAS) Displays Ca^{2+}-Dependent FRET in Vitro

To observe the interaction between KRAS4b-FMe and CaM and monitor the localization of the proteins in cells, we prepared constructs encoding these proteins as fusions with FRET donor/acceptor fluorophores – mTurquoise2 (mTq2) and SYFP2 (i.e., mTq2-CaM and SYFP2-KRAS4b) – and transiently co-expressed them in HeLa and HEK293 cells. To increase the expression of KRAS4b to levels achieved for CaM, it was necessary to optimize the codon usage by removing rare codons [79,80]. Co-expression of KRAS4b and CaM resulted in morphological changes in HeLa cells, including cell rounding, detachment and cell death after 1-2 days post-transfection, which were not observed following transient expression of either protein individually. Interestingly, these effects were mitigated by fusing the proteins into a chimeric construct (i.e., mTq2-CaM-SYFP2-KRAS4b), modeled after the famous CaM FRET-based Ca^{2+}-senor Cameleon [81]. Since both KRAS4b and CaM have multiple interaction partners, linking the two proteins may favour the intramolecular interaction over other binding partners, while also ensuring equimolar expression of KRAS4b and CaM. Our model (Figure 3.12A) predicts that this chimera would localize to the PM through a farnesylated HVR under the resting state,

whereas elevated Ca^{2+} would lead to binding of the CaM domain to the farnesyl moiety. The structural rearrangement from an unbound state on the membrane to a KRAS4b:CaM interaction in the cytosol would perturb the orientation and proximity of the two fluorophores and potentially alter FRET efficiency. We have named this chimeric construct 'CaMeRAS' for its function as a 'camera' to probe the CaM and KRAS4b interaction. To test whether CaMeRAS exhibits a FRET response to Ca^{2+} concentration changes, a FLAG-CaMeRAS construct was expressed in HeLa cells, purified and titrated with Ca^{2+} *in vitro*. CaMeRAS exhibited a small (5.5%) but significant and reliable increase in FRET efficiency in a dose-dependent manner upon addition of Ca^{2+} (Figure 3.12B). (The dose-dependent changes in mTq2 and SYFP2 intensities in

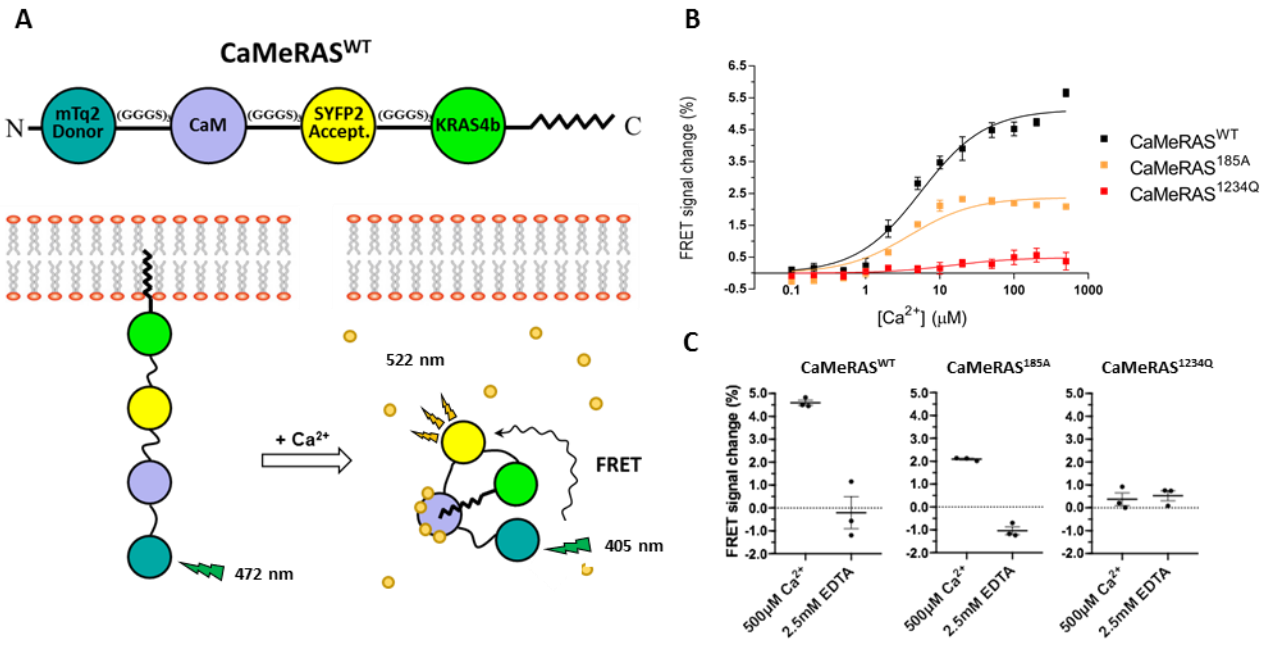

Figure 3.12. CaMeRAS FRET construct demonstrates Ca^{2+}-/farnesyl-dependent FRET signal change *in vitro*. A) Schematic of chimeric construct expressed in HEK293 and HeLa cells, and bimodal use for CaM-KRAS4b binding model validation. When transiently expressed in mammalian cells, the chimeric construct is natively processed at the C-terminal CaaX box, allowing tethering of the construct to the plasma membrane. Upon Ca^{2+} influx, Ca^{2+}-CaM extracts KRAS4b from the membrane, visible with fluorescence imaging, and the structural rearrangement of the chimera leads to detectable FRET. **B)** *In vitro* $Ca^{2=}$ titration into purified CaMeRAS shows FRET signal (SFYP2/mTq2 emission ration) changes for $CaMeRAS^{WT}$ that is disrupted by either removal of KRAS4b farnesyl ($CaMeRAS^{185A}$: FLAG-mTq2-CaM-SYFP2-KRAS4b-C185Astop) or blocking of Ca^{2+} binding ($CaMeRAS^{1234Q}$: FLAG-mTq2-CaM[E31Q, E67Q, E104Q, E140Q]-SYFP2-KRAS4b). Data are mean ± SEM of three independent measurements. FRET signal was calculated by using the peak intensities of mTq2 (at 472 nm) and SYFP2 (at 522 nm) in emission spectra as shown in Figure S9. Data were fit with sigmoidal dose-response equation on Prism8 software (GraphPad). **C)** These *in vitro* Ca^{2+}-dependent FRET changes are reversible by addition of EDTA. For $CaMeRAS^{WT}$ and $CaMeRAS^{185A}$ constructs, FRET after EDTA chelation falls below baseline, likely due to residual ions in the starting buffer, facilitating some interactions. This change is not observable for the Ca^{2+}-deficient mutant $CaMeRAS^{1234Q}$. Data are mean ± SEM of three independent measurements.

response to Ca^{2+}-titration into this construct is shown in Figure 3.13). *In vitro* Ca^{2+} titrations of a farnesylation-deficient CaMeRAS variant, i.e., KRAS4b-C185Astop ($CaMeRAS^{185A}$), elicited a small FRET response, likely induced by compaction of CaM upon Ca^{2+} binding (Figure 3.12B). Consistently, a calcium-binding deficient CaMeRAS mutant with an E to Q mutation at position 12 in each EF hand loop, i.e., CaM E1234Q ($CaMeRAS^{1234Q}$, EF1 – E31Q, EF2 – E67Q, EF3 – E104Q and EF4 – E140Q [46,47]), exhibited no change in FRET in response to Ca^{2+} (Figure 3.12B). These data demonstrate that CaMeRAS senses a Ca^{2+}- and farnesyl-dependent, specific interaction between KRAS4b-FMe and CaM. Importantly, the *in vitro* FRET response to Ca^{2+} titration is reversible with chelation of Ca^{2+} by EDTA (Figure 3.12C). The maximal FRET drops below the Ca^{2+}-free baseline after chelation for both $CaMeRAS^{WT}$ and $CaMeRAS^{185A}$, likely due to residual Ca^{2+} in buffers prior to Ca^{2+} titration. The Ca^{2+}-insensitive $CaMeRAS^{1234Q}$ did not exhibit a change upon addition of Ca^{2+} or EDTA. Having developed and validated this FRET construct in vitro, we sought to validate our binding model *in vivo*.

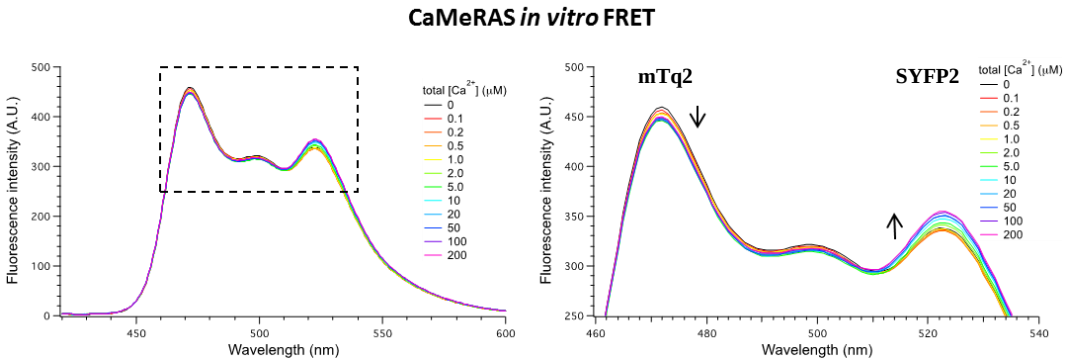

Figure 3.13 Calcium-dependent change in emission spectra of CaMeRAS chimera FRET protein. Emission spectra excited at 405 nm in the presence of various concentrations of $CaCl_2$ are shown in the left panel. 1 μM protein was used. The boxed area is enlarged in the right panel. Addition of Ca^{2+} decreased the 472-nm (mTurquoise2) emission and increased the 522-nm (SYFP2) emission in a dose-dependent manner, indicating calcium-dependent increase in FRET efficiency.

3.2.2 Ca^{2+} Stimulation Induces Reversible KRAS4b-FMe – Calmodulin Interactions and Membrane Extraction in Cells

To fully assess the behaviour of the KRAS4b-CaM interaction in mammalian cells, we employed live cell fluorescence imaging using the CaMeRAS constructs transiently expressed in HeLa cells. $CaMeRAS^{WT}$ was found localized on the plasma membrane in the resting state, in accordance with our model, while an aggressive Ca^{2+} influx stimulated by addition of the Ca^{2+}

ionophore ionomycin caused rapid localization of the complex within the cells (Figure 3.14A). Cellular localization was tracked over time to show translocation (Figure 3.14B). This result is a proof of principle, however, ionomycin provides a potent influx of Ca^{2+} that is not physiologically relevant. We expanded these experiments to include the other

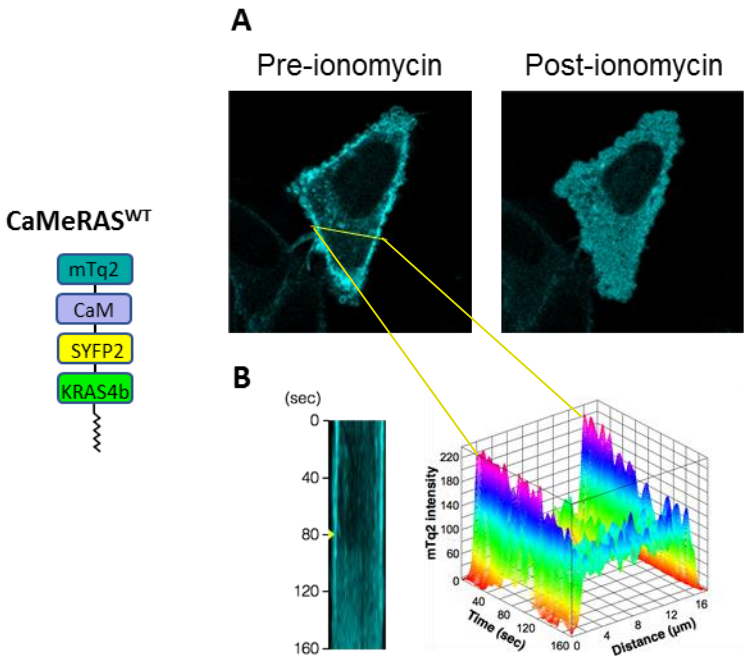

Figure 3.14. Tracking cellular localization of CaMeRAS^{WT} in HeLa cells following ionomycin treatment. A) Cellular localization (mTq2) of the construct before and after 50 μ M ionomycin treatment. **B)** Representative mTq2 intensity distributions over time for cellular cross-sections (yellow line in (A)) show changes in cellular localization following ionomycin treatment at 80 sec (yellow arrowhead) after starting imaging. The construct experiences a marked shift from plasma membrane to cytosol.

CaMeRAS constructs (Figure 3.15A) and employed the physiological Ca^{2+} signal histamine, which initiates store operated calcium entry (SOCE) through STIM, ORAI and the calcium release activated calcium (CRAC) channel [75]. As expected, the farnesyl-containing constructs CaMeRAS^{WT} and CaMeRAS^{1234Q} were concentrated on the PM in resting cells, with a fraction visible in the cytoplasm or on endomembranes, whereas the non-farnesylated CaMeRAS^{185A} exhibited constitutive cytoplasmic localization (Figure 3.15B). Induction of Ca^{2+} influx by addition of histamine caused rapid relocalization of CaMeRAS^{WT} off the plasma membrane, consistent with CaM sequestration of the farnesyl moiety (Figure 3.15C). CaMeRAS^{1234Q}, which is defective for Ca^{2+}-binding, retained plasma membrane localization following Ca^{2+} stimulation, and the cytoplasmic localization of CaMeRAS^{185A} was not affected by Ca^{2+} influx (Figure 3.15C). Representative graphs of CaMeRAS construct localization over time, based on the

fluorescence intensity of mTq2 in line-scan cross-sections of HeLa cells following histamine stimulation, clearly illustrate time-dependent translocation of CaMeRAS^{WT} from the plasma membrane to the cytoplasm in response to histamine (Figure 3.15D), while the other constructs maintain their localization. Stimulation of HEK293 cells with 100µM ATP to elicit a Ca^{2+} signal produced similar results, confirming the robustness of the Ca^{2+}-dependent translocation of CaMeRAS.

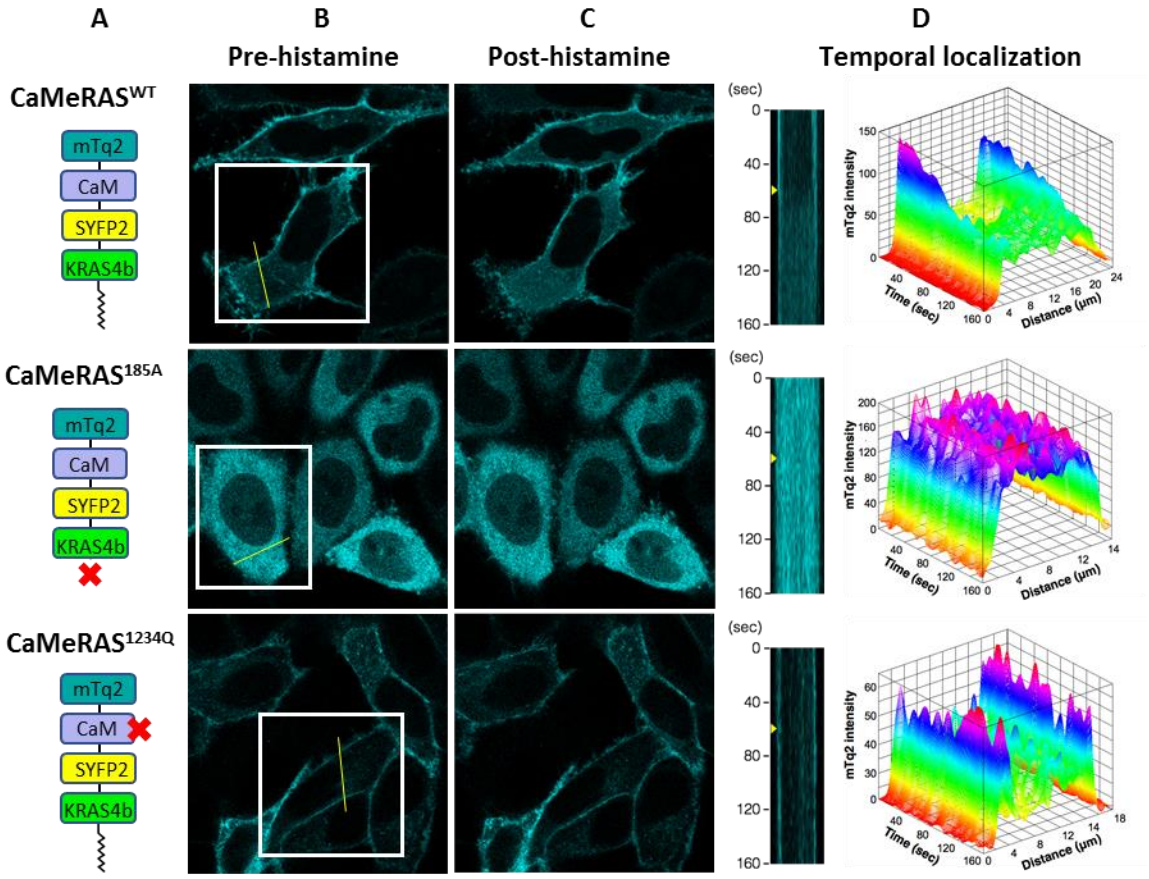

Figure 3.15. Tracking cellular localization of CaMeRAS constructs in HeLa cells following histamine stimulation. A) Schematic of CaMeRAS constructs transiently expressed; CaMeRAS^{WT}, CaMeRAS^{185A}, CaMeRAS^{1234Q}; and where the mutants are deficient. **B)** Cellular localization (mTq2) of constructs before 100 µM histamine stimulation. CaMeRAS^{WT} and CaMeRAS^{1234Q}, farnesylated constructs, are localized on the plasma membrane, while CaMeRAS^{185A} is distributed cytoplasmically. **C)** Cellular localization (mTq2) of constructs at 60 seconds after treatment with 100 µM histamine. The CaMeRAS^{WT} becomes cytoplasmically localized over time while CaMeRAS^{185A} and CaMeRAS^{1234Q} mutants retain their prior localization. **D)** Representative mTq2 intensity distributions over time for cellular cross-sections (yellow lines in **(B)**) show changes in cellular localization following histamine stimulation at 60 sec (yellow arrowheads) after starting imaging. CaMeRAS^{WT} experiences a shift from plasma membrane to cytosol while the membrane and cytosolic localization of CaMeRAS^{185A} and CaMeRAS^{1234Q} remain unperturbed.

Having demonstrated the histamine-induced translocation of CaMeRAS^{WT} in live cells, we sought to further examine whether this phenomenon is indeed synchronized with Ca^{2+} signaling, and how translocation may be coupled to the Ca^{2+}-dependent FRET change observed *in vitro*. Using Calbryte 630, a fluorescent Ca^{2+}-indicator with an absorbance spectrum discrete from mTq2 and SYFP2, we were able to extend our in-cell fluorescence system to simultaneously co-image Ca^{2+}, mTq2 and SYFP2 in response to histamine stimulation. Imaging mTq2 confirmed the CaMeRAS localization and histamine-stimulated translocation described above (Figure 3.16A), while concurrent Ca^{2+} imaging showed a cytosolic increase of Ca^{2+} following histamine stimulation (Figure 3.16B).

In cells expressing CaMeRAS^{WT}, histamine stimulation produced a large and sustained Ca^{2+} signal, possibly amplified by interactions between CaM and ion channels on the membrane, which was reversible with the addition of the cell permeable Ca^{2+} chelator BAPTA-AM. Cells expressing CaMeRAS^{185A} or CaMeRAS^{1234Q} exhibited a more physiological Ca^{2+} response to histamine, possibly due to lack of membrane localization or Ca^{2+} binding, respectively. Segmenting the images into plasma membrane and cytosolic areas to assess localization showed internalization of CaMeRAS^{WT}, which was reversible with the addition of BAPTA-AM, whereas CaMeRAS^{185A} retained cytoplasmic localization and CaMeRAS^{1234Q} remained localized on the membrane (Figure 3.16C), consistent with our previous results. In the same cells, FRET was measured by comparing the ratio of mTq2 to SYFP2 in the relevant cellular locales, before and after histamine stimulation. CaMeRAS^{WT} exhibited a 4.5% reversible FRET increase upon Ca^{2+}-induced translocation from the membrane to the cytoplasm (Figure 3.15D), whereas no detectable FRET change was observed in the cytosol for CaMeRAS^{185A}, or on the plasma membrane for CaMeRAS^{1234Q}.

To further validate the observed *in vivo* FRET, the CaMeRAS constructs were visualized under the same conditions using fluorescence-lifetime imaging (FLIM), a sensitive measure of the rate at which excited fluorophores decay to their ground states, which is affected by changes in structure, dynamics and fluorescent energy transfer. Following histamine stimulation, the cytoplasmic CaMeRAS^{WT} displayed a statistically significant decrease in fluorescence lifetime relative to the membrane localized protein before stimulation while the fluorescence lifetimes of CaMeRAS^{185A} and CaMeRAS^{1234Q} were unchanged (Figure 3.17). The reduction in fluorescence lifetime, indicative of a change in distance and relative orientation between mTq2 and SYFP2,

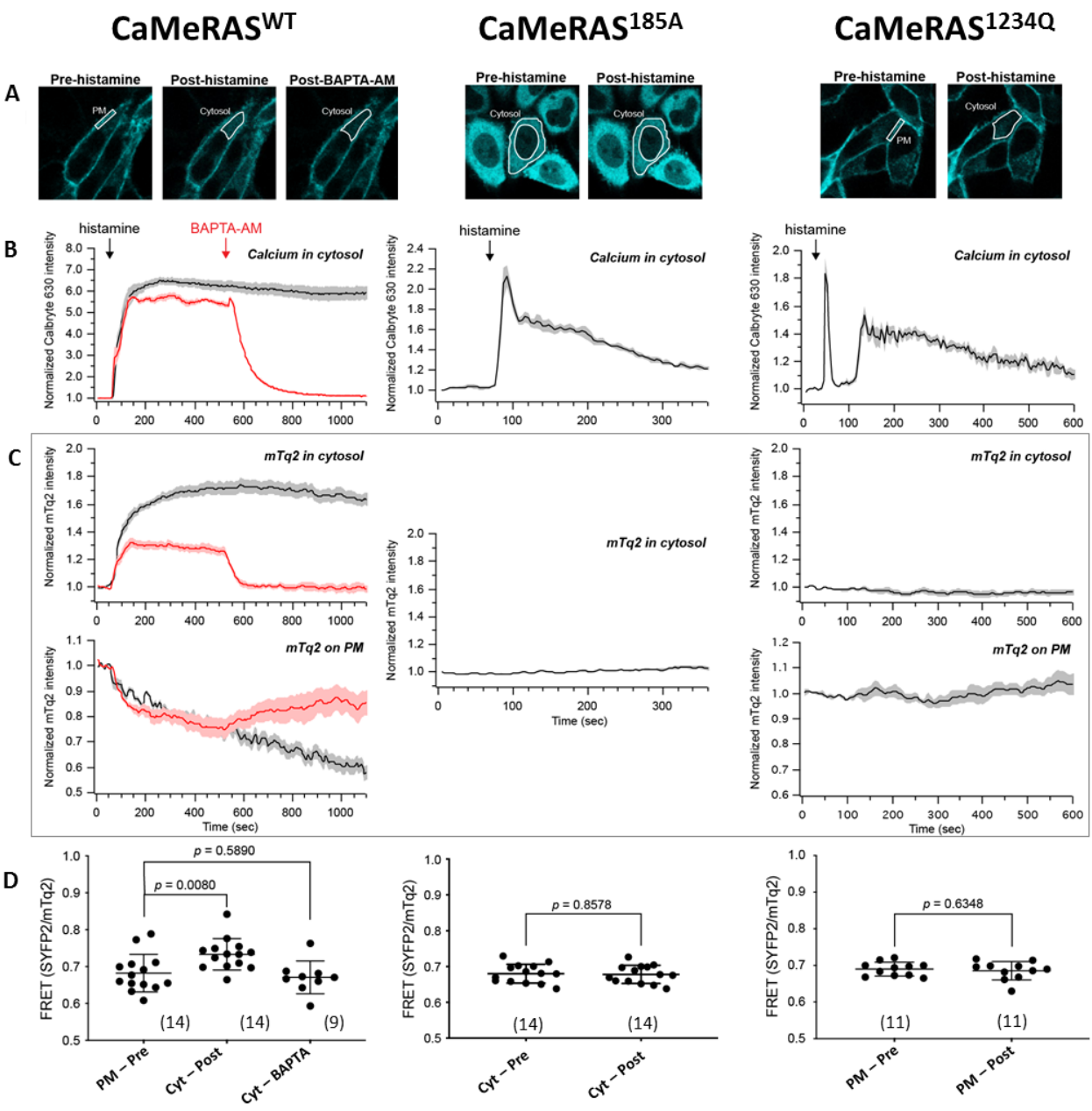

Figure 3.16. CaMeRAS demonstrates reversible Ca^{2+}-/farnesyl-dependent internalization and FRET change i*n vivo*. A) Cellular localization (mTq2) of CaMeRAS constructs in HeLa cells before and after 100 µM histamine stimulation. 10 µM BAPTA-AM treatment was added to HeLa cells expressing $CaMeRAS^{WT}$ in order to examine reversibility. Regions of interest on the plasma membrane or in the cytosol were drawn manually as shown with white outlines. **B)** Normalized Calbryte 630 intensity tracking cytoplasmic Ca^{2+} levels post histamine stimulation. For $CaMeRAS^{WT}$, the red line shows Ca^{2+} levels return to baseline following addition of cell-permeable chelator BAPTA-AM. **C)** mTq2 tracking of cytoplasmic and plasma membrane localization of CaMeRAS constructs over time, post-histamine stimulation, using areas highlighted in (A). $CaMeRAS^{WT}$ shows decreases in plasma membrane localization paired with increase in cytoplasmic localization over time, which return to baseline following BATPA-AM addition (red line). In these traces, the bold lines denote mean while the shadows represent the SEM of five independent cells, respectively. **D)** FRET readout (ratio of SYFP2/mTq2) pre- and post-stimulation in highlighted cellular locales (A). $CaMeRAS^{WT}$ shows a significant change in FRET signal post histamine as it translocates to the cytoplasm. The translocation and FRET change are reserved upon addition of BAPTA-AM. In these beeswarm plots, the number of cells analyzed is shown in parentheses. Bars denote mean ± SD. *P* values were analyzed by unpaired t-test.

combined with the reversible internalization of the CaMeRAS^{WT} sensor, strongly supports our model of Ca^{2+}-dependent sequestration of KRAS4b farnesyl by CaM, which outcompetes PM binding.

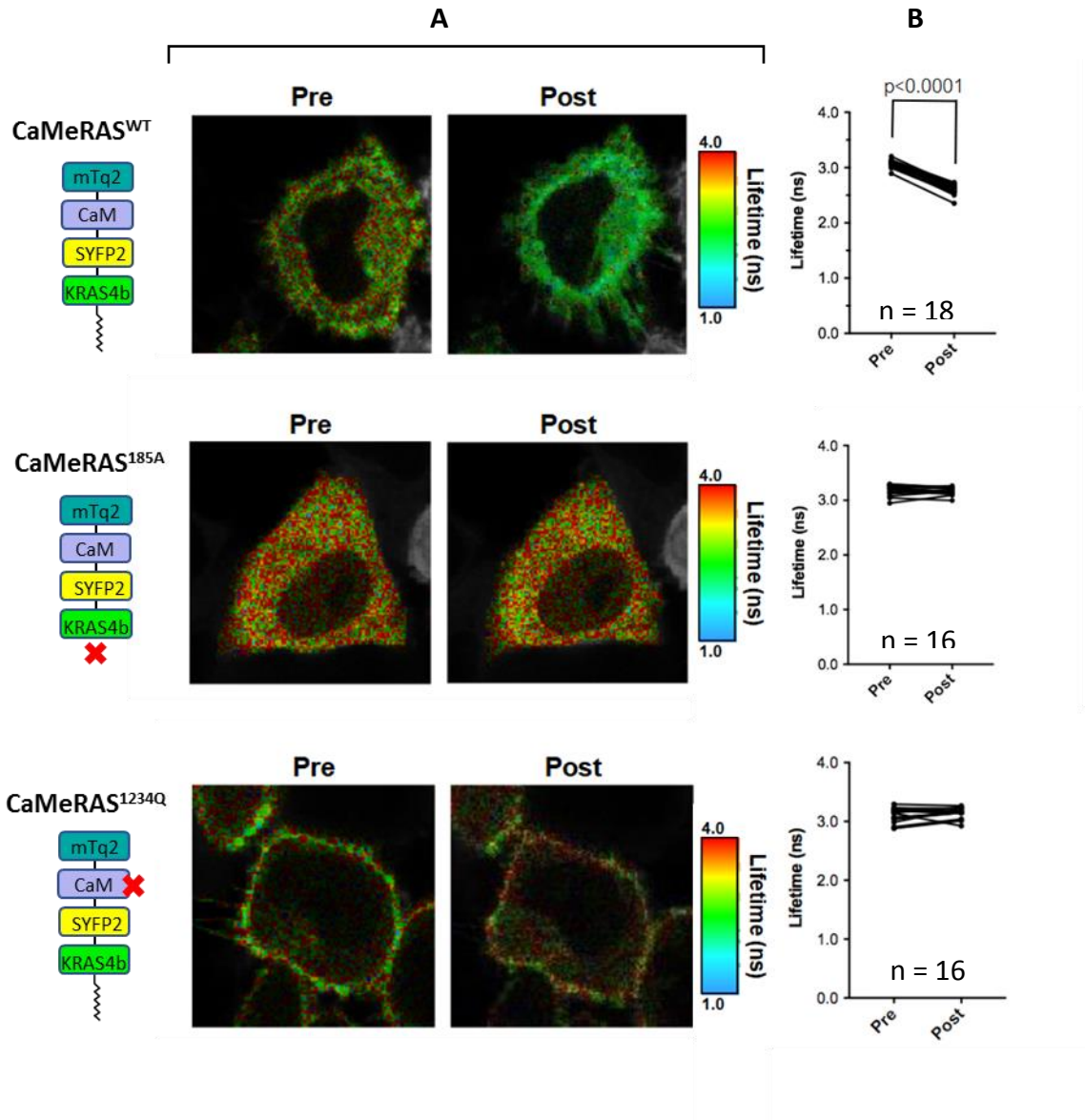

Figure 3.17. Fluorescence lifetime of mTq2 in CaMeRAS^{WT} is reduced by histamine stimulation in HeLa cells. A) Amplitude-averaged fluorescence lifetime (tau_Av_Amp[ns]) pseudo-color map of mTq2 of the CaMeRAS constructs before and at 120 sec after 100 µM histamine stimulation. **B)** Statistical analysis of Amplitude-averaged fluorescence lifetime on the plasma membrane (PM) before histamine stimulation and in cytosol after histamine stimulation. The significantly reduced lifetime of CaMeRAS^{WT} indicates that FRET efficiency is increased in the cytosol after histamine stimulation compared to on the plasma membrane before stimulation. Statistical difference was analyzed by Wilcoxson matched-pairs signed rank test.

Chapter 4
Discussion

4 Discussion

4.1 Previous Studies on the KRAS4b-Calmodulin Interaction

The interaction between KRAS4b and CaM has been observed numerous times over the last two decades, by many different groups and in diverse systems. The first report of an interaction between KRAS4b and CaM surfaced in 2001, following observations that CaM inhibitors in cells perturbed MAPK signaling, increasing levels of pERK. This first paper by Villalonga et al. demonstrated a direct interaction between calmodulin and KRAS4b, but not KRAS4a, HRAS or NRAS, in a Ca^{2+}-dependent manner [30], positioning CaM as an inhibitor of KRAS4b activity in cells. Using a series of pulldown assays, they reported a GTP-dependence for the interaction and observed trace binding of CaM to a recombinant KRAS4b G-domain (1-166). Two years later, this interaction was again reported, in partitioning experiments of endogenous RAS protein from human platelets and MCF-7 breast cancer cells. Sidhu et al. demonstrated that CaM could change the partitioning of KRAS4b, but not KRAS4a, HRAS or NRAS, from membrane fractions to cytosolic fractions of cell lysates in a Ca^{2+}-dependent, GTP-independent manner [82]. This work provides a mechanism by which CaM could inhibit KRAS4b activity in cells. The ability of calmodulin to extract only KRAS4b from membranes indicated that the HVR, both the membrane localization signal and main distinguishing feature between RAS isoforms, may be an important mediator of this interaction.

Researchers in this field all agree that the interaction between KRAS4b and CaM is Ca^{2+}-dependent and isoform specific. However, ever since these initial publications, there have been contradictions in the literature regarding the involvement of the G-domain, the dependence on nucleotide-binding state, the importance of the HVR and the requirement of farnesylation, as well as the implications for KRAS4b membrane extraction and canonical signaling. Summarized below are the major findings from relevant literature on this subject, also visualized in Table 1.

4.1.1 Literature Summaries

(2005) Following up on the reports of membrane extraction by Sidhu et al., Fivaz and Meyer examined Ca^{2+}-CaM dependent translocation of fluorescently tagged KRAS4b off the plasma

membrane in glutamate-stimulated hippocampal neurons [31]. Initially employing only lipidated C-terminal tails, this thorough work demonstrated reversible internalization of KRAS4b and Rap1 (similar HVR) tails by CaM, but no relocalization of the HRAS tail. This behavior was replicated with full length KRAS4b, constitutively active KRAS4b-Q61L, constitutively inactive KRAS4b-S17N, but not full length HRAS. This work clearly argues that the HVR and farnesyl mediates the interaction with CaM, leading to membrane extraction in cells. This model does not require a G-domain interaction or a specific nucleotide state.

(2008) The findings from Lopez-Alcalá et al. were more consistent with the work of Villalonga. They attempted to identify all KRAS4b calmodulin-binding elements by employing pulldown assays with a collection of KRAS4b mutants and truncations expressed in mammalian cells and E. coli [51]. Pulldown assays with purified recombinant protein identified residues in switch II (68-73) and α5 (164) of KRAS4b, as well as lysines in the HVR, that abrogated CaM-sepharose binding. They reported a G-domain interaction, dependent on GTP-loading, which was strengthened by the involvement of the HVR and farnesyl. However, when performing pulldown experiments of KRAS4b from mammalian cell lysates, an intact HVR and farnesyl was required for binding. To our knowledge, no other group has since reported specific interactions with switch II or α5. It is worth noting that pulldown assays are not the gold standard for detecting specific, weak protein-protein interactions.

(2010) Bhagatji et al. also wanted to probe KRAS4b membrane extraction by CaM. They examined membrane transfer dynamics of fluorescently tagged, farnesylated and geranylgeranylated KRAS4b and KRAS4b HVR, expressed and purified from mammalian cells, between synthetic vesicles [83]. They reported a Ca^{2+}-CaM dependent increase in the transfer rate between vesicles for KRAS4b, and KRAS4b-G12V, but not KRAS4b-S17N (dominant negative) or the KRAS4b tail, suggesting membrane extraction occurs but requires a GTP-bound G-domain.

(2011) Wu et al. purified recombinant RAS proteins, processed via *in vitro*, non-native farnesylation, and performed unusual cross-linking experiments and various binding assays to assess the KRAS4b-CaM interaction [52]. By their methods, only GTP-loaded KRAS4b was found cross-linked to CaM, indicative of binding. Dansyl-CaM fluorescence titration and isothermal titration calorimetry (ITC) binding assays were used to calculate binding constants for different

constructs: unprocessed KRAS4b had K_d values around 1 μM by both methods, while KRAS4b-farnesyl had values between 170 and 400 nM. HRAS with a polylysine substitution in the HVR bound CaM with a K_d around 2.5 – 4 μM, while wildtype HRAS did not bind. This work emphasizes the importance of the HVR and farnesyl moiety but shows an interaction in their absence as well.

(2015) Wang et al. built a model using extensive immunoblotting and clonogenic sphere-forming assays to explain differential tumorigenic capacity of KRAS4b compared to other RAS isoforms [32]. They argue that KRAS4b-driven cancers are much more common, aggressive and lethal, despite a lack of elevation in MAPK or PI3K signaling compared to other RAS proteins. Thus, they examined other KRAS4b-specific interactions that may be responsible, namely the interaction with CaM. They claim that the interaction of KRAS4b with CaM sequesters CaM at the membrane, blocking interactions with canonical targets such as CaMK. Preventing CaMK activation suppresses the non-canonical Wnt pathway, promoting stemness and transformation. Nothing more has been published on this subject. The main counterargument to this paradigm is that the binding affinity and cellular concentration of CaMK is several hundred-fold higher than of KRAS4b.

(2016) Sperlich et al. tested the theory of membrane extraction by surface plasmon resonance (SPR) using a membrane mimetic system [33]. Anionic lipid raft monolayers were immobilized and artificially processed KRAS4b (*in* vitro but native) was bound and washed before Ca^{2+}-CaM addition. CaM was able to effectively extract KRAS4b from the lipid rafts in a nucleotide-independent manner.

(2017) For the first time, KRAS4b and CaM were studied via *in silico* methods. Nussinov et al. performed extensive molecular dynamics simulations of farnesylated KRAS4b HVR in complex with CaM [54], in an iterative and unbiased approach. Amongst many models, the two highest-confidence interaction modes involved the farnesyl group buried deeply within either the N-lobe or C-lobe hydrophobic pockets of CaM, with electrostatic interactions between the KRAS4b polybasic region and the surface of CaM. This binding mode is predicted to have no reliance on the G-domain or nucleotide state of KRAS4b.

(2018) Garrido et al. [84] also tried to build an *in silico* model of the KRAS4b-CaM interaction, however it is clear they did not have a thorough understanding of the field before beginning highly restrained and biased simulations. Referencing Villalonga [30], Lopez-Alcalá [51] and Wang [32], they pre-positioned proteins such that CaM binds the G-domain and HVR of KRAS4b, each with one lobe, and refined this model to produce an unusual complex on the membrane.

(2019) Agamasu et al. recently conducted NMR as well as thorough ITC, SPR and analytical ultracentrifugation experiments to build a model of the interaction based on sound biophysical data [55]. They demonstrated by SPR and ITC that both the isolated N- and C-lobes are capable of binding KRAS4b-FMe, with the C-lobe exhibiting 3-8 fold higher affinity. They also reported that intact CaM binds full-length, fully processed KRAS4b with a 2:1 stoichiometry, i.e., one KRAS4b molecule per lobe. This model identifies the farnesyl moiety as the principle anchor, stabilized by the HVR, independent of the G-domain and nucleotide state.

Despite the dearth of consistency in this field, considerable progress has been made over the last 20 years. As techniques and technologies have improved, researchers have come closer to analyzing a native system, more sensitively. The introduction of endogenously processed KRAS4b-FMe from insect cells [57], plasma membrane-mimetics [64], the advent of NMR, ITC and SPR to detect binding and the move towards in-cell imaging, have all improved the reliability of results in this field. As these quantitative methods become more prevalent, results have trended towards similar conclusions. With our contribution to the field of sought-after structural and robust cellular-response data, we have solidified the interaction paradigm of CaM competing for KRAS4b membrane localization signals, leading to membrane extraction.

4.2 Summary of Results and Findings

The interaction between KRAS4b and CaM has been studied for nearly two decades, with increasing intensity and impact in the last several years as researchers recognized the therapeutic potential for manipulating this interaction in cancer. However, as outlined above, many of these reports, using distinctly different methods, came to inconsistent conclusions regarding the nature of this interaction. In this work, we combined well-controlled, *in vitro* biophysical studies of fully processed full-length KRAS4b with observations of an engineered biosensor in live cells, and have demonstrated a Ca^{2+}-dependent, nucleotide-independent interaction mediated by hydrophobic sequestration of the KRAS4b farnesyl moiety within the CaM methionine-rich C-

lobe. This interaction directly competes with membrane association and causes relocalization of KRAS4b within cells.

Our NMR and X-ray crystallographic data show that the KRAS4b-CaM interaction is principally mediated through sequestration of KRAS4b farnesyl in the CaM C-lobe hydrophobic pocket. This interaction is likely further stabilized by electrostatic contacts, presumably between the KRAS4b HVR and the acidic CaM surface. By X-ray crystallography, we revealed for the first time the atomic-resolution structure of Ca^{2+}-CaM complexed with the farnesyl cysteine moiety, which involves intimate interactions between the hydrophobic acyl chain of the fatty acid and many hydrophobic residues of the CaM C-terminal lobe (F92, I100, L105, M109, M124, I125, A128, V136, F141, M144). This finding solidifies the notion that the KRAS4b-CaM interaction is mediated through competition for the hydrophobic KRAS4b membrane localization signal. Interestingly, our NMR binding assays of CaM mutants with N- or C-lobe Ca^{2+}-binding deficiencies (N: E31Q and E67Q, C: E104Q and E140Q) revealed that farnesyl-derived compounds can interact with either the N- or C- lobe of CaM. This dual-lobe binding is not surprising considering the similarity of the N- and C-lobe pockets.

Agamasu et al. recently demonstrated by SPR and ITC that both the isolated N- and C-lobes are capable of binding KRAS4b-FMe, with the C-lobe exhibiting higher affinity. Additionally, they elucidated a 2:1 stoichiometry for the interaction of KRAS4b-FMe with intact CaM, which was reduced to 1:1 with truncated CaM N- or C-lobes [55]. We believe that our crystal structure exhibits exclusive C-lobe binding primarily due to the higher affinity relative to the N-lobe, and the FCME concentration used in crystallization, whereas 2:1 binding becomes feasible under more saturating conditions. This tighter C-lobe binding was also predicted by previous molecular dynamics (MD) studies by Nussinov et al. [54]. The predicted C-lobe binding model from this paper is markedly similar to our crystal structure, and had nearly twice the calculated binding free energy of their predicted N-lobe binding model (-80 kcal/mol vs -45 kcal/mol) [54]. These recent reports reinforce the binding mode observed in our crystal structure and its relevance to the full-length KRAS4b-CaM interaction.

Using this structure, we designed and constructed a biosensor named CaMeRAS, which enabled us to visualize the Ca^{2+}-dependent, reversible translocation of KRAS4b from the plasma membrane to the cytoplasm in HeLa and HEK293 cells. This large chimeric FRET construct

allowed us to simultaneously monitor cellular localization and protein-protein interactions in cells, while also ensuring equimolar expression and limiting off-target interactions. Mutations in this system provided precise and sensitive feedback on dependencies of the interaction: farnesyl deletion caused cytosolic localization but no binding while Ca^{2+}-deficient CaM mutations prevented membrane extraction. These data strongly support the model that canonical KRAS4b signaling, which occurs on the plasma membrane, is down-regulated by Ca^{2+} signals via the multi-functional, ubiquitous calcium sensor protein CaM. Furthermore, the competition for KRAS4b between membrane anchoring and CaM binding only occurs when the cell is stimulated by extracellular ligands that lead to tightly-regulated, elevated cytoplasmic Ca^{2+} concentrations.

4.3 Calmodulin Structural Comparison

An analagous interaction between CaM and another lipid-modified protein was previously reported. An N-terminally myristoylated polybasic peptide (CAP-23/NAP-22) was crystallized in complex with CaM, revealing the myristoyl sequestered within the hydrophobic core (PDB: 1l7Z) [73]. This CaM-myristoyl complex somewhat resembles our CaM-farnesyl structure, but there are two significant differences with respect to (i) the orientation of the lipid within the hydrophobic core and (ii) the position of α4 (Figure 3.8A). Myristoyl is found in a linear orientation, interacting with hydrophobic surfaces of both lobes, but not deeply inserted in the pockets, whereas FCME is bound in the C-lobe pocket only, with the N-lobe pocket minimally exposed due to the rearrangement of α4 (Figure 3.8B). These differences are likely associated with the different properties of the lipids, since the unsaturated and branched farnesyl moiety is bulkier and less flexible than myristoyl. In our CaM:FCME complex, the farnesyl moiety adopts a significantly bent conformation similar to that observed in PEX19 [85] and aristolochene synthase, whereas it binds farnesyltransferase in an extended conformation[86]. Interestingly, the C-terminal cysteine residue of FCME in our structure occupies a position equivalent to that of the N-terminal myristoylated glycine in CAP23/NAP22, thus tethering their adjacent polybasic sequences in the same region, albeit with opposite strand directions. The conformations adopted by CaM bound to the myristoyl and farnesyl moieties are distinct from CaM in complex with any of the canonical peptides but are remarkably similar to CaM in complex with an unusual target peptide derived from the myristoylated alanine-rich protein kinase C substrate (MARCKS, PDB: 1IWQ). This internal MARCKS peptide, which is not myristoylated, assumes an extended

conformation with only a short helical region presenting two hydrophobic residues; a Phe sidechain is buried deeply in the C-lobe of CaM, whereas the N-lobe is closed and its surface makes contact with a Leu two residues away [50].

4.4 Ca^{2+}-Mediated Regulator of Protein Membrane Attachment

CaM interactions with similar myristoylated polybasic peptides, the vSRC N-terminal peptide pp60v and the HIV1 Nef1 peptide, were also previously studied by NMR [87,88]. Additions of these peptides to ^{15}N-CaM induced chemical shift perturbations extremely similar to those induced by FCME (Figure 4.1). The small GTPases Rac1a, Rap1a, RalA and RalB, all of which

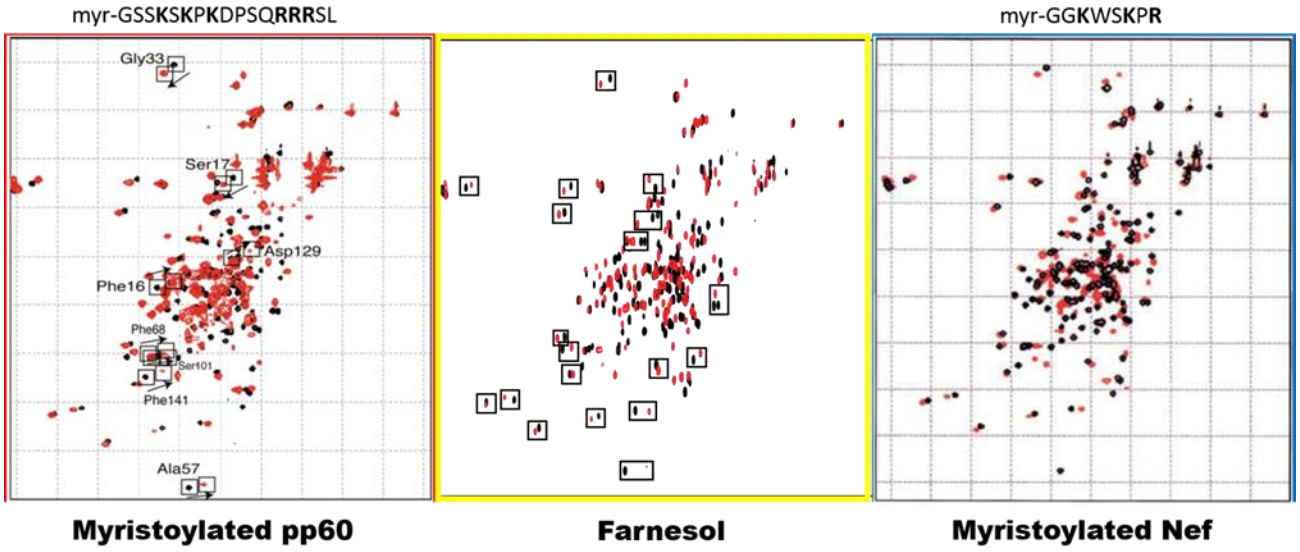

Figure 4.1. New class of non-canonical CaM binding targets: singly lipidated polybasic peptides. Comparison of ^{1}H-^{15}N HSQCs of Ca^{2+}-bound CaM interacting with farnesol and myristoylated polybasic peptides (pp60 – myr-GSSKSKPKDPSQRRRSL, Nef – myr-GGKWSKPR, reported by Hayashi et al. (reproduced with permission from references 87 and 88)). Despite the difference in prenyl moiety and polybasic sequence, all three HSQCs share a pattern of CSPs we believe to be characteristic of lipid binding. In the case of farnesol, this pattern is produced in the absence of an adjacent polybasic region.

have geranylgeranylated C-terminal polybasic sequences, have also been reported to interact with CaM [31,89-95]. Taken together with our structure of FCME-bound CaM and the previous structure of a myristoylated peptide-bound CaM, these proteins embody a general class of non-canonical CaM binding targets defined by a singly lipidated, polybasic sequence. Due to the length of geranylgeranyl (4 prenyl repeats compared to the 3 of farnesyl), it may not fit in the C-lobe pocket alone, as farnesyl does, without becoming solvent exposed. Instead, geranylgeranyl could interact with both lobes, similar to the myristoyl complex from CAP23/NAP22-CaM. The

small GTPases RhoA and RhoH also contain geranylgeranylated polybasic C-termini, however, to date, we are not aware of any reports that they interact with CaM.

Unlike KRAS4b, in addition to irreversible farnesylation, HRAS, NRAS, and KRAS4a are all subject to enzymatic cycles of palmitoylation/depalmitoylation. These modifications help tether them tightly to the membrane and are used to modulate membrane attachment and control signal output [96-98]. The high affinity of these isoforms for the membrane, in combination with their general lack of favourable electrostatics and C-terminal bulkiness likely all contribute to the lack of full compatibility with CaM binding and regulation. In contrast, KRAS4b, and other GTPases with singly lipidated PBRs, have intrinsic membrane localization signals through irreversible prenylation and sequence-mediated electrostatics. It is conceivable that other cellular mechanisms may have evolved to regulate the membrane attachment and signal output of this class of proteins. We believe that CaM serves this vital role in response to Ca^{2+} signaling.

The notion that CaM can bind a membrane-tethering lipid to modulate protein membrane attachment is reinforced by other examples in nature. Unlike in animals, plants often have many homologous CaM proteins with significantly more variation in sequence and function. One such protein, CaM53 from petunias, has an unusual C-terminal extension that includes a polybasic region adjacent to a CaaX box which is farnesylated in cells [99]. This CaM protein cycles between plasma membrane and nuclear localization diurnally. Plants respond to many external stimuli, including exposure to light and temperature, with tightly regulated Ca^{2+} influx [100,101]. Though the authors speculate that the internalization of CaM53 is due to protein turnover and halted farnesyl synthesis, preventing processing, this membrane cycling may also respond to Ca^{2+} signaling that facilitates intramolecular interactions and leads to extraction, similar to our CaMeRAS construct.

4.5 CaMeRAS: Unique Multimodal Imaging Tool

The successful design and construction of CaMeRAS in this study was inspired by the pioneering work of Roger Tsien and co-workers, who first introduced a FRET-based calcium sensor, Cameleon, in 1997 [81]. Since then, numerous FRET-based biosensors have been reported and widely used. Fluorescence proteins have been utilized extensively to elucidate and quantify biological processes in cells [102]. Multi-colour fluorescent proteins fused to target proteins have enabled simultaneous tracking of localization or accumulation [103]. FRET- or bioluminescence resonance energy transfer (BRET)-based biosensors have enabled us to visualize a wide range of

cellular processes such as enzyme activity, protein conformational change, mechanical force and changes in microenvironment and signal transduction [104]. Focusing on RAS and Ca^{2+} signaling, in addition to CaM-based Ca^{2+} biosensors [81,105-107], both FRET- and BRET-based biosensors have been developed to monitor interactions between RAS and its effector proteins in cells [108,109]. To our knowledge, CaMeRAS is one of the first multifunctional FRET biosensors that is targeted to a cell compartment and allows simultaneous monitoring of translocation and protein-protein interactions. However, optimization of linker lengths would help improve the FRET efficiency and reduce noise for a more robust signal. Live-cell imaging with higher spatiotemporal resolution could make it possible to track specific destination(s) of CaMeRAS upon Ca^{2+} elevation, which could advance our understanding of the biological significance of the CaM/KRAS4b interaction.

4.6 Cellular Impact of KRAS4b-CaM Interaction

Internalization of KRAS4b by CaM would abrogate canonical RAS signaling, which requires KRAS4b activation on the membrane and subsequent activation of downstream effector proteins such as RAF kinases. In parallel, another reported consequence of this interaction results from sequestration of Ca^{2+}–bound CaM away from other targets, which reduces activation of CaMKII and suppresses non-canonical Wnt/Ca^{2+} signaling, thereby promoting tumorigenicity [32]. Furthermore, relocalization of KRAS4b to endomembranes may enable interactions with other proteins and modulate other signaling pathways. Such cellular processes have been previously reported as a result of KRAS4b relocalization in response to phosphorylation at S181 by PKC [25-27]. In these studies, phosphorylated KRAS4b is targeted to mitochondria, where it complexes with Bcl-XL and triggers apoptosis. In addition to KRAS4b, nearly all the other singly lipidated polybasic proteins discussed in section 4.4 as putative CaM targets contain Ser/Thr residues within the PBRs, adjacent to site of lipidation. Rap1A, RhoA, RalA and RalB, as well as CAP23/NAP22 and SRC, have well-documented phosphorylation at these sites (curated in PhosphoSitePlus; www.phosphosite.org [110]), which would likely disrupt favourable electrostatic interactions with the membrane, thus regulating membrane attachment, as with KRAS4b. These reports also demonstrate that phosphorylation at S181 and CaM binding are mutually exclusive, hinting at a signal-dependent interplay between multiple regulatory mechanisms [25]. The direct and ill-defined competition between CaM binding, phosphorylation and PDEδ cycling, which returns internalized KRAS4b to the PM from endosomes [21,23], indicates the existence of a

complex and robust regulatory network for these membrane-associated proteins that remains largely undescribed.

4.7 Conclusion

Collectively, our data provides new insights into the regulation of KRAS4b by CaM, supplies tools (i.e., crystal structure of farnesyl-bound CaM and CaMeRAS biosensors) for the further enrichment of this growing field, and solidifies the farnesyl-dependent, membrane extraction and relocalization paradigm for this interaction. Rigorous biophysical studies of Ca^{2+}-CaM regulation of KRAS4b and the cross-talk between MAPK and Ca^{2+} signaling will help bring the field closer to discovering new ways to exploit this interaction for therapeutic gains.

Bibliography

1 Barbacid, M. ras genes. *Annu Rev Biochem* **56**, 779-827, doi:10.1146/annurev.bi.56.070187.004023 (1987).

2 Hancock, J. F. Ras proteins: different signals from different locations. *Nat Rev Mol Cell Biol* **4**, 373-384, doi:10.1038/nrm1105 (2003).

3 Stephen, A. G., Esposito, D., Bagni, R. K. & McCormick, F. Dragging ras back in the ring. *Cancer Cell* **25**, 272-281, doi:10.1016/j.ccr.2014.02.017 (2014).

4 Simanshu, D. K., Nissley, D. V. & McCormick, F. RAS Proteins and Their Regulators in Human Disease. *Cell* **170**, 17-33, doi:10.1016/j.cell.2017.06.009 (2017).

5 Joneson, T. & Bar-Sagi, D. Ras effectors and their role in mitogenesis and oncogenesis. *J Mol Med (Berl)* **75**, 587-593 (1997).

6 Bos, J. L. ras oncogenes in human cancer: a review. *Cancer Res* **49**, 4682-4689 (1989).

7 Prior, I. A., Lewis, P. D. & Mattos, C. A comprehensive survey of Ras mutations in cancer. *Cancer Res* **72**, 2457-2467, doi:10.1158/0008-5472.CAN-11-2612 (2012).

8 Jackson, J. H., Li, J. W., Buss, J. E., Der, C. J. & Cochrane, C. G. Polylysine domain of K-ras 4B protein is crucial for malignant transformation. *Proc Natl Acad Sci U S A* **91**, 12730-12734 (1994).

9 Hancock, J. F., Magee, A. I., Childs, J. E. & Marshall, C. J. All ras proteins are polyisoprenylated but only some are palmitoylated. *Cell* **57**, 1167-1177 (1989).

10 Hancock, J. F., Paterson, H. & Marshall, C. J. A polybasic domain or palmitoylation is required in addition to the CAAX motif to localize p21ras to the plasma membrane. *Cell* **63**, 133-139 (1990).

11 Silvius, J. R. & l'Heureux, F. Fluorimetric evaluation of the affinities of isoprenylated peptides for lipid bilayers. *Biochemistry* **33**, 3014-3022 (1994).

12 Leventis, R. & Silvius, J. R. Lipid-binding characteristics of the polybasic carboxy-terminal sequence of K-ras4B. *Biochemistry* **37**, 7640-7648, doi:10.1021/bi973077h (1998).

13 Silvius, J. R., Bhagatji, P., Leventis, R. & Terrone, D. K-ras4B and prenylated proteins lacking "second signals" associate dynamically with cellular membranes. *Mol Biol Cell* **17**, 192-202, doi:10.1091/mbc.E05-05-0408 (2006).

14 Bryant, K. L., Mancias, J. D., Kimmelman, A. C. & Der, C. J. KRAS: feeding pancreatic cancer proliferation. *Trends Biochem Sci* **39**, 91-100, doi:10.1016/j.tibs.2013.12.004 (2014).

15 Committee, C. C. S. A. Canadian Cancer Statistics 2018. (Canadian Cancer Society, Toronto, ON, 2018).

16 Baines, A. T., Xu, D. & Der, C. J. Inhibition of Ras for cancer treatment: the search continues. *Future Med Chem* **3**, 1787-1808, doi:10.4155/fmc.11.121 (2011).

17 Berndt, N. & Sebti, S. M. Measurement of protein farnesylation and geranylgeranylation in vitro, in cultured cells and in biopsies, and the effects of prenyl transferase inhibitors. *Nat Protoc* **6**, 1775-1791, doi:10.1038/nprot.2011.387 (2011).

18 Cox, A. D., Der, C. J. & Philips, M. R. Targeting RAS Membrane Association: Back to the Future for Anti-RAS Drug Discovery? *Clin Cancer Res* **21**, 1819-1827, doi:10.1158/1078-0432.CCR-14-3214 (2015).

19 Wang, J., Yao, X. & Huang, J. New tricks for human farnesyltransferase inhibitor: cancer and beyond. *Medchemcomm* **8**, 841-854, doi:10.1039/c7md00030h (2017).

20 Sinensky, M., Beck, L. A., Leonard, S. & Evans, R. Differential inhibitory effects of lovastatin on protein isoprenylation and sterol synthesis. *J Biol Chem* **265**, 19937-19941 (1990).

21 Chandra, A. *et al.* The GDI-like solubilizing factor PDEdelta sustains the spatial organization and signalling of Ras family proteins. *Nat Cell Biol* **14**, 148-158, doi:10.1038/ncb2394 (2011).

22 Schmick, M. *et al.* KRas localizes to the plasma membrane by spatial cycles of solubilization, trapping and vesicular transport. *Cell* **157**, 459-471, doi:10.1016/j.cell.2014.02.051 (2014).

23 Dharmaiah, S. *et al.* Structural basis of recognition of farnesylated and methylated KRAS4b by PDEdelta. *Proc Natl Acad Sci U S A* **113**, E6766-E6775, doi:10.1073/pnas.1615316113 (2016).

24 Baehr, W. Membrane protein transport in photoreceptors: the function of PDEdelta: the Proctor lecture. *Invest Ophthalmol Vis Sci* **55**, 8653-8666, doi:10.1167/iovs.14-16066 (2014).

25 Bivona, T. G. *et al.* PKC regulates a farnesyl-electrostatic switch on K-Ras that promotes its association with Bcl-XL on mitochondria and induces apoptosis. *Mol Cell* **21**, 481-493, doi:10.1016/j.molcel.2006.01.012 (2006).

26 Quatela, S. E., Sung, P. J., Ahearn, I. M., Bivona, T. G. & Philips, M. R. Analysis of K-Ras phosphorylation, translocation, and induction of apoptosis. *Methods Enzymol* **439**, 87-102, doi:10.1016/S0076-6879(07)00407-7 (2008).

27 Sung, P. J. *et al.* Phosphorylated K-Ras limits cell survival by blocking Bcl-xL sensitization of inositol trisphosphate receptors. *Proc Natl Acad Sci U S A* **110**, 20593-20598, doi:10.1073/pnas.1306431110 (2013).

28 Cho, K. J. *et al.* AMPK and Endothelial Nitric Oxide Synthase Signaling Regulates K-Ras Plasma Membrane Interactions via Cyclic GMP-Dependent Protein Kinase 2. *Mol Cell Biol* **36**, 3086-3099, doi:10.1128/MCB.00365-16 (2016).

29 Zhou, Y. *et al.* Lipid-Sorting Specificity Encoded in K-Ras Membrane Anchor Regulates Signal Output. *Cell* **168**, 239-251 e216, doi:10.1016/j.cell.2016.11.059 (2017).

30 Villalonga, P. *et al.* Calmodulin binds to K-Ras, but not to H- or N-Ras, and modulates its downstream signaling. *Mol Cell Biol* **21**, 7345-7354, doi:10.1128/MCB.21.21.7345-7354.2001 (2001).

31 Fivaz, M. & Meyer, T. Reversible intracellular translocation of KRas but not HRas in hippocampal neurons regulated by Ca2+/calmodulin. *J Cell Biol* **170**, 429-441, doi:10.1083/jcb.200409157 (2005).

32 Wang, M. T. *et al.* K-Ras Promotes Tumorigenicity through Suppression of Non-canonical Wnt Signaling. *Cell* **163**, 1237-1251, doi:10.1016/j.cell.2015.10.041 (2015).

33 Sperlich, B., Kapoor, S., Waldmann, H., Winter, R. & Weise, K. Regulation of K-Ras4B Membrane Binding by Calmodulin. *Biophys J* **111**, 113-122, doi:10.1016/j.bpj.2016.05.042 (2016).

34 Saito, N., Mine, N., Kufe, D. W., Von Hoff, D. D. & Kawabe, T. CBP501 inhibits EGF-dependent cell migration, invasion and epithelial-to-mesenchymal transition of non-small cell lung cancer cells by blocking KRas to calmodulin binding. *Oncotarget* **8**, 74006-74018, doi:10.18632/oncotarget.18598 (2017).

35 Bosch, M., Gil, J., Bachs, O. & Agell, N. Calmodulin inhibitor W13 induces sustained activation of ERK2 and expression of p21(cip1). *J Biol Chem* **273**, 22145-22150, doi:10.1074/jbc.273.34.22145 (1998).

36 Cullen, P. J. & Lockyer, P. J. Integration of calcium and Ras signalling. *Nat Rev Mol Cell Biol* **3**, 339-348, doi:10.1038/nrm808 (2002).

37 Agell, N., Bachs, O., Rocamora, N. & Villalonga, P. Modulation of the Ras/Raf/MEK/ERK pathway by Ca(2+), and calmodulin. *Cell Signal* **14**, 649-654 (2002).

38 Lockyer, P. J., Kupzig, S. & Cullen, P. J. CAPRI regulates Ca(2+)-dependent inactivation of the Ras-MAPK pathway. *Curr Biol* **11**, 981-986 (2001).

39 Grewal, T. *et al.* Annexin A6 stimulates the membrane recruitment of p120GAP to modulate Ras and Raf-1 activity. *Oncogene* **24**, 5809-5820, doi:10.1038/sj.onc.1208743 (2005).

40 Prevarskaya, N., Skryma, R. & Shuba, Y. Ion Channels in Cancer: Are Cancer Hallmarks Oncochannelopathies? *Physiol Rev* **98**, 559-621, doi:10.1152/physrev.00044.2016 (2018).

41 Pierro, C. *et al.* Oncogenic KRAS suppresses store-operated Ca(2+) entry and ICRAC through ERK pathway-dependent remodelling of STIM expression in colorectal cancer cell lines. *Cell Calcium* **72**, 70-80, doi:10.1016/j.ceca.2018.03.002 (2018).

42 Cheung, W. Y. Cyclic 3',5'-nucleotide phosphodiesterase. Demonstration of an activator. *Biochem Biophys Res Commun* **38**, 533-538, doi:10.1016/0006-291x(70)90747-3 (1970).

43 Kakiuchi, S. & Yamazaki, R. Calcium dependent phosphodiesterase activity and its activating factor (PAF) from brain studies on cyclic 3',5'-nucleotide phosphodiesterase (3). *Biochem Biophys Res Commun* **41**, 1104-1110, doi:10.1016/0006-291x(70)90199-3 (1970).

44 O'Connell D., B. M., Marshall C.B., Ikura M., Linse S. in *Encyclopedia of metalloproteins* (ed Kretsinger R.H. Uversky V., Permyakov E.A.) (Spriner, 2013).

45 Moews, P. C. & Kretsinger, R. H. Terbium replacement of calcium in carp muscle calcium-binding parvalbumin: an x-ray crystallographic study. *J Mol Biol* **91**, 229-232, doi:10.1016/0022-2836(75)90162-x (1975).

46 Mukherjea, P., Maune, J. F. & Beckingham, K. Interlobe communication in multiple calcium-binding site mutants of Drosophila calmodulin. *Protein Sci* **5**, 468-477, doi:10.1002/pro.5560050308 (1996).

47 Zhu, T., Beckingham, K. & Ikebe, M. High affinity Ca2+ binding sites of calmodulin are critical for the regulation of myosin Ibeta motor function. *J Biol Chem* **273**, 20481-20486 (1998).

48 Yap, K. L. *et al.* Calmodulin target database. *J Struct Funct Genomics* **1**, 8-14 (2000).

49 Hoeflich, K. P. & Ikura, M. Calmodulin in action: diversity in target recognition and activation mechanisms. *Cell* **108**, 739-742 (2002).

50 Yamauchi, E., Nakatsu, T., Matsubara, M., Kato, H. & Taniguchi, H. Crystal structure of a MARCKS peptide containing the calmodulin-binding domain in complex with Ca2+-calmodulin. *Nat Struct Biol* **10**, 226-231, doi:10.1038/nsb900 (2003).

51 Lopez-Alcala, C. *et al.* Identification of essential interacting elements in K-Ras/calmodulin binding and its role in K-Ras localization. *J Biol Chem* **283**, 10621-10631, doi:10.1074/jbc.M706238200 (2008).

52 Wu, L. J., Xu, L. R., Liao, J. M., Chen, J. & Liang, Y. Both the C-terminal polylysine region and the farnesylation of K-RasB are important for its specific interaction with calmodulin. *PLoS One* **6**, e21929, doi:10.1371/journal.pone.0021929 (2011).

53 Banerjee, A., Jang, H., Nussinov, R. & Gaponenko, V. The disordered hypervariable region and the folded catalytic domain of oncogenic K-Ras4B partner in phospholipid binding. *Curr Opin Struct Biol* **36**, 10-17, doi:10.1016/j.sbi.2015.11.010 (2016).

54 Jang, H., Banerjee, A., Chavan, T., Gaponenko, V. & Nussinov, R. Flexible-body motions of calmodulin and the farnesylated hypervariable region yield a high-affinity interaction enabling K-Ras4B membrane extraction. *J Biol Chem* **292**, 12544-12559, doi:10.1074/jbc.M117.785063 (2017).

55 Agamasu, C. *et al.* KRAS Prenylation Is Required for Bivalent Binding with Calmodulin in a Nucleotide-Independent Manner. *Biophys J*, doi:10.1016/j.bpj.2019.02.004 (2019).

56 Grant, B. M. M., Marshall, C. B. & Ikura, M. Expression and Purification of Calmodulin for NMR and Other Biophysical Applications. *Methods Mol Biol* **1929**, 207-221, doi:10.1007/978-1-4939-9030-6_13 (2019).

57 Gillette, W. K. *et al.* Farnesylated and methylated KRAS4b: high yield production of protein suitable for biophysical studies of prenylated protein-lipid interactions. *Sci Rep* **5**, 15916, doi:10.1038/srep15916 (2015).

58 Gossert, A. D. & Jahnke, W. Isotope labeling in insect cells. *Adv Exp Med Biol* **992**, 179-196, doi:10.1007/978-94-007-4954-2_10 (2012).

59 Gossert, A. D. *et al.* A simple protocol for amino acid type selective isotope labeling in insect cells with improved yields and high reproducibility. *J Biomol NMR* **51**, 449-456, doi:10.1007/s10858-011-9570-9 (2011).

60 Goedhart, J. *et al.* Bright cyan fluorescent protein variants identified by fluorescence lifetime screening. *Nat Methods* **7**, 137-139, doi:10.1038/nmeth.1415 (2010).

61 Kremers, G. J., Goedhart, J., van Munster, E. B. & Gadella, T. W., Jr. Cyan and yellow super fluorescent proteins with improved brightness, protein folding, and FRET Forster radius. *Biochemistry* **45**, 6570-6580, doi:10.1021/bi0516273 (2006).

62 Guo, F., Chiang, M. Y., Wang, Y. & Zhang, Y. Z. An in vitro recombination method to convert restriction- and ligation-independent expression vectors. *Biotechnol J* **3**, 370-377, doi:10.1002/biot.200700170 (2008).

63 Fang, Z. *et al.* Inhibition of K-RAS4B by a Unique Mechanism of Action: Stabilizing Membrane-Dependent Occlusion of the Effector-Binding Site. *Cell Chem Biol* **25**, 1327-1336 e1324, doi:10.1016/j.chembiol.2018.07.009 (2018).

64 Kobashigawa, Y., Harada, K., Yoshida, N., Ogura, K. & Inagaki, F. Phosphoinositide-incorporated lipid-protein nanodiscs: A tool for studying protein-lipid interactions. *Anal Biochem* **410**, 77-83, doi:10.1016/j.ab.2010.11.021 (2011).

65 Clore, G. M. Practical Aspects of Paramagnetic Relaxation Enhancement in Biological Macromolecules. *Methods Enzymol* **564**, 485-497, doi:10.1016/bs.mie.2015.06.032 (2015).

66 Otwinowski, Z. & Minor, W. Processing of X-ray diffraction data collected in oscillation mode. *Methods Enzymol* **276**, 307-326 (1997).

67 Emsley, P., Lohkamp, B., Scott, W. G. & Cowtan, K. Features and development of Coot. *Acta Crystallogr D Biol Crystallogr* **66**, 486-501, doi:10.1107/S0907444910007493 (2010).

68 Adams, P. D. *et al.* PHENIX: a comprehensive Python-based system for macromolecular structure solution. *Acta Crystallogr D Biol Crystallogr* **66**, 213-221, doi:10.1107/S0907444909052925 (2010).

69 Schindelin, J. *et al.* Fiji: an open-source platform for biological-image analysis. *Nat Methods* **9**, 676-682, doi:10.1038/nmeth.2019 (2012).

70 Ikura, M., Kay, L. E., Krinks, M. & Bax, A. Triple-resonance multidimensional NMR study of calmodulin complexed with the binding domain of skeletal muscle myosin light-chain kinase: indication of a conformational change in the central helix. *Biochemistry* **30**, 5498-5504 (1991).

71 Martin, S. R. *et al.* Interaction of calmodulin with the phosphofructokinase target sequence. *FEBS Lett* **577**, 284-288, doi:10.1016/j.febslet.2004.10.023 (2004).

72 Liu, Z. & Vogel, H. J. Structural basis for the regulation of L-type voltage-gated calcium channels: interactions between the N-terminal cytoplasmic domain and Ca(2+)-calmodulin. *Front Mol Neurosci* **5**, 38, doi:10.3389/fnmol.2012.00038 (2012).

73 Matsubara, M., Nakatsu, T., Kato, H. & Taniguchi, H. Crystal structure of a myristoylated CAP-23/NAP-22 N-terminal domain complexed with Ca2+/calmodulin. *EMBO J* **23**, 712-718, doi:10.1038/sj.emboj.7600093 (2004).

74 Ikura, M. & Ames, J. B. Genetic polymorphism and protein conformational plasticity in the calmodulin superfamily: two ways to promote multifunctionality. *Proc Natl Acad Sci U S A* **103**, 1159-1164, doi:10.1073/pnas.0508640103 (2006).

75 Marshall, C. B., Nishikawa, T., Osawa, M., Stathopulos, P. B. & Ikura, M. Calmodulin and STIM proteins: Two major calcium sensors in the cytoplasm and endoplasmic reticulum. *Biochem Biophys Res Commun* **460**, 5-21, doi:10.1016/j.bbrc.2015.01.106 (2015).

76 Fischer, M. J. Amine coupling through EDC/NHS: a practical approach. *Methods Mol Biol* **627**, 55-73, doi:10.1007/978-1-60761-670-2_3 (2010).

77 Stoilova-McPhie, S., Grushin, K., Dalm, D. & Miller, J. Lipid nanotechnologies for structural studies of membrane-associated proteins. *Proteins* **82**, 2902-2909, doi:10.1002/prot.24631 (2014).

78 Mazhab-Jafari, M. T. *et al.* Oncogenic and RASopathy-associated K-RAS mutations relieve membrane-dependent occlusion of the effector-binding site. *Proc Natl Acad Sci U S A* **112**, 6625-6630, doi:10.1073/pnas.1419895112 (2015).

79 Pershing, N. L. *et al.* Rare codons capacitate Kras-driven de novo tumorigenesis. *J Clin Invest* **125**, 222-233, doi:10.1172/JCI77627 (2015).

80 Lampson, B. L. *et al.* Rare codons regulate KRas oncogenesis. *Curr Biol* **23**, 70-75, doi:10.1016/j.cub.2012.11.031 (2013).

81 Miyawaki, A. *et al.* Fluorescent indicators for Ca2+ based on green fluorescent proteins and calmodulin. *Nature* **388**, 882-887, doi:10.1038/42264 (1997).

82 Sidhu, R. S., Clough, R. R. & Bhullar, R. P. Ca2+/calmodulin binds and dissociates K-RasB from membrane. *Biochem Biophys Res Commun* **304**, 655-660, doi:10.1016/s0006-291x(03)00635-1 (2003).

83 Bhagatji, P., Leventis, R., Rich, R., Lin, C. J. & Silvius, J. R. Multiple cellular proteins modulate the dynamics of K-ras association with the plasma membrane. *Biophys J* **99**, 3327-3335, doi:10.1016/j.bpj.2010.10.001 (2010).

84 Garrido, E., Lazaro, J., Jaumot, M., Agell, N. & Rubio-Martinez, J. Modeling and subtleties of K-Ras and Calmodulin interaction. *PLoS Comput Biol* **14**, e1006552, doi:10.1371/journal.pcbi.1006552 (2018).

85 Emmanouilidis, L. *et al.* Allosteric modulation of peroxisomal membrane protein recognition by farnesylation of the peroxisomal import receptor PEX19. *Nat Commun* **8**, 14635, doi:10.1038/ncomms14635 (2017).

86 Lane, K. T. & Beese, L. S. Thematic review series: lipid posttranslational modifications. Structural biology of protein farnesyltransferase and geranylgeranyltransferase type I. *J Lipid Res* **47**, 681-699, doi:10.1194/jlr.R600002-JLR200 (2006).

87 Hayashi, N. *et al.* Nef of HIV-1 interacts directly with calcium-bound calmodulin. *Protein Sci* **11**, 529-537, doi:10.1110/ps.23702 (2002).

88 Hayashi, N. *et al.* Myristoylation-regulated direct interaction between calcium-bound calmodulin and N-terminal region of pp60v-src. *J Mol Biol* **338**, 169-180, doi:10.1016/j.jmb.2004.02.041 (2004).

89 Elsaraj, S. M. & Bhullar, R. P. Regulation of platelet Rac1 and Cdc42 activation through interaction with calmodulin. *Biochim Biophys Acta* **1783**, 770-778, doi:10.1016/j.bbamcr.2008.01.022 (2008).

90 Vidal-Quadras, M. *et al.* Rac1 and calmodulin interactions modulate dynamics of ARF6-dependent endocytosis. *Traffic* **12**, 1879-1896, doi:10.1111/j.1600-0854.2011.01274.x (2011).

91 Xu, B., Chelikani, P. & Bhullar, R. P. Characterization and functional analysis of the calmodulin-binding domain of Rac1 GTPase. *PLoS One* **7**, e42975, doi:10.1371/journal.pone.0042975 (2012).

92 Wang, K. L. & Roufogalis, B. D. Ca2+/calmodulin stimulates GTP binding to the ras-related protein ral-A. *J Biol Chem* **274**, 14525-14528, doi:10.1074/jbc.274.21.14525 (1999).

93 Wang, K. L., Khan, M. T. & Roufogalis, B. D. Identification and characterization of a calmodulin-binding domain in Ral-A, a Ras-related GTP-binding protein purified from human erythrocyte membrane. *J Biol Chem* **272**, 16002-16009, doi:10.1074/jbc.272.25.16002 (1997).

94 Clough, R. R., Sidhu, R. S. & Bhullar, R. P. Calmodulin binds RalA and RalB and is required for the thrombin-induced activation of Ral in human platelets. *J Biol Chem* **277**, 28972-28980, doi:10.1074/jbc.M201504200 (2002).

95 Sidhu, R. S., Elsaraj, S. M., Grujic, O. & Bhullar, R. P. Calmodulin binding to the small GTPase Ral requires isoprenylated Ral. *Biochem Biophys Res Commun* **336**, 105-109, doi:10.1016/j.bbrc.2005.08.053 (2005).

96 Rocks, O. *et al.* An acylation cycle regulates localization and activity of palmitoylated Ras isoforms. *Science* **307**, 1746-1752, doi:10.1126/science.1105654 (2005).

97 Rocks, O., Peyker, A. & Bastiaens, P. I. Spatio-temporal segregation of Ras signals: one ship, three anchors, many harbors. *Curr Opin Cell Biol* **18**, 351-357, doi:10.1016/j.ceb.2006.06.007 (2006).

98 Rocks, O. *et al.* The palmitoylation machinery is a spatially organizing system for peripheral membrane proteins. *Cell* **141**, 458-471, doi:10.1016/j.cell.2010.04.007 (2010).

99 Rodriguez-Concepcion, M., Toledo-Ortiz, G., Yalovsky, S., Caldelari, D. & Gruissem, W. Carboxyl-methylation of prenylated calmodulin CaM53 is required for efficient plasma membrane targeting of the protein. *Plant J* **24**, 775-784 (2000).

100 Bush, D. S. Calcium regulation in plant cells and its role in signaling. *Annu Rev Pant Physiol* **46**, 95-122 (1995).

101 Trewavas, A. J. & Malho, R. Signal Perception and Transduction: The Origin of the Phenotype. *Plant Cell* **9**, 1181-1195, doi:10.1105/tpc.9.7.1181 (1997).

102 Pendin, D., Greotti, E., Lefkimmiatis, K. & Pozzan, T. Exploring cells with targeted biosensors. *J Gen Physiol* **149**, 1-36, doi:10.1085/jgp.201611654 (2017).

103 Chudakov, D. M., Matz, M. V., Lukyanov, S. & Lukyanov, K. A. Fluorescent proteins and their applications in imaging living cells and tissues. *Physiol Rev* **90**, 1103-1163, doi:10.1152/physrev.00038.2009 (2010).

104 Hochreiter, B., Garcia, A. P. & Schmid, J. A. Fluorescent proteins as genetically encoded FRET biosensors in life sciences. *Sensors (Basel)* **15**, 26281-26314, doi:10.3390/s151026281 (2015).

105 Qian, Y. *et al.* A genetically encoded near-infrared fluorescent calcium ion indicator. *Nat Methods* **16**, 171-174, doi:10.1038/s41592-018-0294-6 (2019).

106 Doronin, D. A. *et al.* Genetically encoded calcium indicator with NTnC-like design and enhanced fluorescence contrast and kinetics. *BMC Biotechnol* **18**, 10, doi:10.1186/s12896-018-0417-2 (2018).

107 Perez Koldenkova, V. & Nagai, T. Genetically encoded Ca(2+) indicators: properties and evaluation. *Biochim Biophys Acta* **1833**, 1787-1797, doi:10.1016/j.bbamcr.2013.01.011 (2013).

108 Mochizuki, N. *et al.* Spatio-temporal images of growth-factor-induced activation of Ras and Rap1. *Nature* **411**, 1065-1068, doi:10.1038/35082594 (2001).

109 Bery, N. *et al.* Correction: BRET-based RAS biosensors that show a novel small molecule is an inhibitor of RAS-effector protein-protein interactions. *Elife* **7**, doi:10.7554/eLife.40515 (2018).

110 Hornbeck, P. V. *et al.* PhosphoSitePlus, 2014: mutations, PTMs and recalibrations. *Nucleic Acids Res* **43**, D512-520, doi:10.1093/nar/gku1267 (2015).

Tables

Table 1. **Inconsistent reports from the literature regarding elements involved in the KRAS4b-CaM interaction.** Coloured boxes denote reported findings in each reference. Hashed cells indicate no direct interrogation in each reference.

Reference	GTP dependent	Nucleotide independent	Farnesyl dependent	Farnesyl independent	G-domain	No G-domain	Membrane Extraction
30 (2001)							
82 (2003)							
31 (2005)							
51 (2008)							
83 (2010)							
52 (2011)							
32 (2015)							
33 (2016)							
54 (2017)							
84 (2018)							
55 (2019)							
This work							

Table 2. **Crystallographic statistics reported for deposited CaM – FCME complex structure (6OS4).** * Results from Phenix Xtriage

Values in parentheses are for the highest resolution shell

6OS4	Native FP2, SigFP2	Anomalous I(+), SigI(+), I(-), SigI(-)
Wavelength	1Å	1.77Å
Resolution range	34.78 – 1.81 (2.01 – 1.81)	34.78 – 2.05 (2.123 – 2.05)
Space group	P 61 2 2	P 61 2 2
Unit cell: a, b, c α, β, γ	40.379, 40.379, 338.137 90, 90, 120,	40.379, 40.379, 338.137 90, 90, 120
Total reflections	16289*	19319*
Unique reflections	11386 (1091)	11372 (1075)
Multiplicity		
Completeness (%)	99.91 (99.63)	99.84 (98.71)
Mean I/sigma(I)	28*	19.2*
Wilson B-factor	35.15	42.8
Reflections used in refinement	11380 (1087)	11370 (1075)
Reflections used for R-free	1139 (109)	1138 (108)
R-work	0.2024 (0.1934)	0.1912 (0.2200)
R-free	0.2418 (0.2195)	0.2253 (0.2586)
Number of non-hydrogen atoms	1194	1194
macromolecules	1107	1107
ligands	27	27
solvent	60	60
Protein residues	144	144
RMS(bonds)	0.006	0.006
RMS(angles)	0.75	0.75
Ramachandran favored (%)	98.59	98.59
Ramachandran allowed (%)	1.41	1.41
Ramachandran outliers (%)	0	0
Rotamer outliers (%)	1.83	1.83
Clashscore	0.93	0.93
Average B-factor	47.67	47.67
macromolecules	47.12	47.12
ligands	78.13	78.13
solvent	44.21	44.21

Appendices

Appendix 1. Published protocol for the expression and purification of Calmodulin in the Springer textbook *Calcium Binding Proteins of the EF-Hand Superfamily*.

Expression and Purification of Calmodulin for NMR and other biophysical applications.

Benjamin Grant[1,2], Chris Marshall[2]*, Mitsu Ikura[1,2]* (* corresponding authors)

[1] Department of Medical Biophysics, University of Toronto, Toronto, Ontario, Canada, M5G 1L7

[2] Princess Margaret Cancer Centre, University Health Network, Toronto, Ontario, Canada, M5G 1L7

Mitsu.Ikura@uhnresearch.ca, Chris.Marshall@uhnresearch.ca

i. Expression and Purification of Calmodulin

ii. Abstract

Calmodulin (CaM) is a ubiquitous calcium-sensing protein that has one of the most highly conserved sequences among eukaryotes. CaM has been a useful tool for biologists studying calcium signaling for decades. In recent years, CaM has also been implicated in numerous cancer-associated pathways, and rare CaM mutations have been identified as a cause of human cardiac arrythmias. Here, we present a collection of our most recent and effective protocols for the expression and purification of recombinant CaM from *Escherichia coli*, including various isotopic labeling schemes, primarily for nuclear magnetic resonance (NMR) spectroscopy and other biophysical applications.

iii. Key words

Calmodulin, CaM, calcium, expression, purification, NMR, isotopic labeling

This article is in memory of Dr. Claude B. Klee for her encouragement and support of MI.

1 Introduction

Calmodulin (CaM) was first discovered as an activator of cyclic AMP phosphodiesterase in the brain by Cheng (***1***) and Kakiuchi (***2***) independently. The Ca^{2+} dependency of CaM activity demonstrated by Kakiuchi opened a totally new field of calcium-dependent signaling regulators and their cellular pathways. CaM is a small, 16.7kD protein that acts as an important master regulator of Ca^{2+} signaling in cells ***(3,4)***. The CaM sequence is conserved among all vertebrates and is highly conserved throughout kingdoms animalia and plantae. CaM is highly acidic, soluble and stable, both in Ca^{2+}-free and -bound states and interacts with binding targets under both conditions ***(5)***. CaM binds Ca^{2+} through motifs called 'EF-hands', first discovered in carp parvalbumin by Kresinger et al ***(6)***. Each of 4 EF-hand motifs in CaM forms 29-amino acid helix-loop-helix structures that coordinate Ca^{2+} through side chains and backbones of five residues in a twelve-residue loop; one pair of EF-hands forms an N-terminal lobe and the other forms a C-terminal lobe. Binding of Ca^{2+} induces a structural change that opens a hydrophobic pocket in each lobe, which mediates the interaction with Ca^{2+}-dependent binding partners ***(5)***. EF-hands have been identified in 1613 protein sequences (***7***), including 221 proteins encoded in the human genome.

Due in part to its size and stability, CaM was an early target for solution protein NMR, and was used to test and develop many of the core NMR experiments employed today ***(8,9,10)***. There are currently ~200 structures of CaM in the Protein Data Bank (www.rcsb.org). In early years, CaM was purified from various tissues (e.g., heart, brain, and red blood cells) using combinations of anion exchange, gel filtration chromatography and ammonium sulfate precipitation, with many schemes taking advantage of the high stability of CaM through

precipitation of undesired proteins by heating ***(11)*** and trichloroacetic acid (TCA), followed by hydrophobic column chromatography (***12***).

With the development of recombinant DNA technology, researchers moved to over-expression of CaM in bacterial cells in order to obtain large quantities of protein, as well as to produce mutants to probe structure/function relationships. In the 1990's, *Drosophila* CaM was cloned into a heat-inducible pAS system for expression in *E. coli* to allow incorporation of isotopic labels ***(13)***. This construct did not contain any affinity tags and was purified through a multi-step process involving TCA precipitation of unwanted proteins (3 % TCA), followed by TCA precipitation of CaM (6 % TCA), Ca^{2+}-dependent binding of resuspended CaM to phenyl Sepharose, and elution with ethylenediaminetetraacetic acid (EDTA) after extensive washing. The *Drosophila melanogaster* CaM sequence has three amino acid substitutions relative to vertebrate CaM, thus many studies adopted recombinant expression of *Xenopus laevis* CaM, which has an amino acid sequence that is identical to that of all known vertebrates. However, it should be noted that recombinant CaM differs from endogenous CaM in that the initiating Met residue is not removed, and it lacks acetylation of the N-terminus and trimethylation of Lys115.

Recent implications of CaM in cancer-associated pathways have renewed and expanded interest in this protein for *in vitro* biophysical and biochemical characterization. Here we present our laboratory's most recent and effective protocols for the expression and purification of recombinant CaM from *E. coli* and include techniques for various isotopic amino acid labeling schemes for NMR. We use a T7-inducible promotor system to express a hexa-histidine tagged CaM protein, which we purify through a two-step process: Nickel-nitrilotriacetic acid (Ni-NTA) affinity chromatography followed by size exclusion liquid chromatography (Figure 1). The entire

protocol can be performed within a week and yields approximately 30mg/L of highly pure, functional protein.

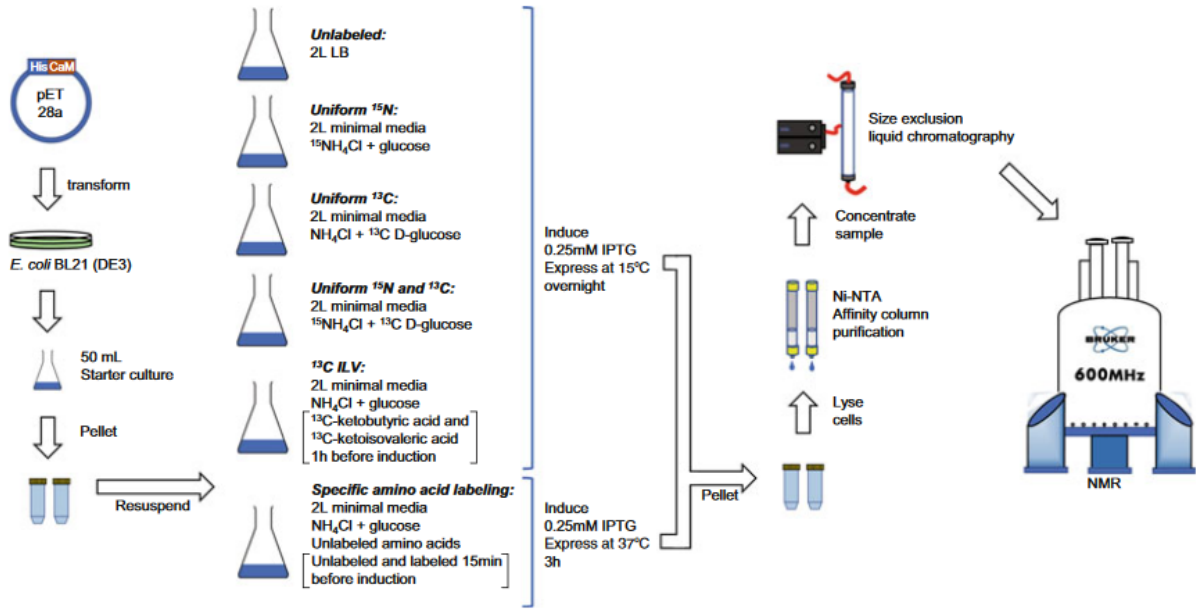

Fig. 1 Schematic flow of calmodulin expression and purification protocol

2 Materials

2.1 CaM in pET28 vector

CaM construct: CaM has been engineered with an N-terminal hexa-histidine (His) tag and linker containing a specific cleavage motif that is recognized by thrombin. This construct was cloned into the pET28a vector with its stop codon using the NdeI and BamHI restriction endonuclease sites. This encodes a reversibly His-tagged CaM protein under the control of a T7 promoter such that expression can be induced by isopropyl β-D-1-thiogalactopyranoside (IPTG) in DE3^{+} *E. coli* strains, with selection through kanamycin resistance. Following cleavage of the His tag by thrombin, three extra residues (Gly-Ser-His) remain at the N-terminus.

2.2 Competent cells

The construct is expressed in *E. coli* BL21 ($DE3^{+}$) which is compatible with the T7 expression system employed by pET vectors. Strains with additional copies of specific tRNA genes that are rare in the *E. coli* genome (e.g., Codon + or Rosetta) can improve yields, but are not necessary. These strains carry an additional antibiotic resistance marker (e.g., chloramphenicol).

2.3 Stock solutions

1. LB broth: Dissolve in water 10 g/L tryptone, 5 g/L yeast extract and 10 g/L NaCl, or purchase premixed broth powder and follow instructions.

2. M9 Media (10x stock): Dissolve in water Na_2HPO_4, 6 g/L, KH_2PO_4, 3 g/L and NaCl, 0.5 g/L.

3. Trace elements (1000x): Add 5 mL of 0.5 M EDTA, pH 8.0, to 80 mL of water. Add trace elements one at a time in the following order, with stirring, waiting at least 10 minutes between the addition of each compound: Ferric chloride ($FeCl_3.6H_2O$) 833 mg, zinc chloride ($ZnCl_2$) 50 mg, cupric chloride ($CuCl_2.2H_2O$) 12.6 mg, cobalt chloride ($CoCl_3.6H_2O$) 10 mg, boric acid (H_3BO_3) 10 mg, manganese chloride ($MnCl_2.4H_2O$) 2500 mg. Do not readjust pH or there will be precipitation. Top up to 100 mL and filter (0.22 μm).

4. Kanamycin (1000x): Prepare 50 mg/mL stock in water, store in aliquots at -20^{O}C

5. Chloramphenicol (1000x): Prepare 30 mg/mL solution in ethanol, store at -20^{O}C.

6. Biotin (1000x): Prepare a 1 mg/mL solution in 50 % ethanol, ideally stored at 4^{O}C.

7. Thiamine (1000x): 1mg/mL in water.

8. Magnesium Sulphate ($MgSO_4$) (1000x): 1M solution in water.

9. Ammonium chloride (NH_4Cl) and/or ^{15}N ammonium chloride (for uniform ^{15}N labeling).

10. 20% (w/v) glucose in water or ^{13}C D-glucose (for uniform ^{13}C labeling).

11. ^{13}C-ketobutyric acid (for methyl labeling of Ile) and ^{13}C-ketoisovaleric acid (for methyl labeling of Leu and Val).

12. ^{15}N and/or ^{13}C amino acids (for labeling of specific amino acids).

13. Minimal media: Add 200 mL of 10x M9 to 1800 mL of water in a 6 L Erlenmeyer flask and autoclave. After media has cooled, add 1 mL/L of kanamycin, [chloramphenicol for Codon +], biotin, thiamine, magnesium sulphate and trace elements (1000x stocks), as well as 0.3 mL/L of 1 M $CaCl_2$. Calcium and metals in the trace elements solution will form a visible precipitate with the phosphate in M9, which is not a cause for concern. The remaining components of the minimal media are dependent on isotopic labeling schemes which are covered in *Methods*.

14. Lysis buffer: Tris pH 8.0, 50 mM, NaCl, 150 mM, NP-40 (detergent), 0.1 % v/v, glycerol, 10 % v/v, imidazole, 10mM. Make 1 L and store. Before use, take 50 mL in a Falcon tube and add β-mercaptoethanol, 10 mM (pure liquid β-mercaptoethanol is 14.3 M), lysozyme (egg white), DNase I (both enzymes can be added by scooping a small amount of powder with a pipette tip) and phenylmethylsulfonyl fluoride (PMSF), 1 mM (TOXIC) (*see* **Note 1)**.

15. His wash buffer 1: Tris pH 8.0, 50 mM, NaCl, 500 mM, glycerol, 10% v/v, imidazole, 10 mM. Make 1L and store. Before use, aliquot 100 mL and add β-mercaptoethanol, 10 mM.

16. His wash buffer 2: Tris pH 8.0, 50 mM, NaCl, 150 mM, glycerol, 10 % v/v, imidazole, 10 mM. Make 1 L and store. Before use, aliquot 100 mL and add β-mercaptoethanol, 10 mM.

17. His elution buffer: Tris pH 8.0, 50 mM, NaCl, 150 mM, glycerol, 10 % v/v, imidazole, 250 mM. Make 1 L and store. Before use, aliquot 50 mL and add β-mercaptoethanol, 10 mM.

18. General dialysis buffer: Tris pH 8.0, 50 mM, NaCl, 150 mM, glycerol, 20 % v/v, DTT, 1 mM. Make 4 L in a beaker and store short term at 4^{O}C

19. Gel filtration buffer: 4-(2-hydroxyethyl)-1-piperazineethanesulfonic acid (HEPES) pH 7.4, 20 mM, NaCl, 100 mM, tris(2-carboxyethyl)phosphine (TCEP), 2 mM. TCEP is a reducing agent available as a highly acidic hydrochloride salt (TCEP-HCl), thus the pH of TCEP-containing buffers must be adjusted before topping up to final volume. Filter (0.22 μm) and degas 20 minutes. Store at 4^{O}C.

20. Chelation buffer: HEPES pH 7.4, 20 mM, NaCl, 100 mM, EDTA, 20 mM, TCEP, 2 mM. Prepare in smaller batches as needed.

3 Methods

3.1 Transformation

1. Thaw 50 μL *E. coli* BL21 (DE3^{+}) [Codon + optional] competent cells on ice.

2. Add 50-200 ng of plasmid to cells, mixing gently. Store on ice for 30 minutes.

3. Heat shock at 42^{O}C for 1 minute. Return to ice for 5 minutes.

4. Add 450 μL of LB to tube and incubate at 37^{O}C for 1 hour.

5. Plate 100 μL on kanamycin LB plate [add chloramphenicol for Codon +] and incubate at 37^{O}C overnight.

(*see* **Note 2**)

3.2 Expression

1. Prepare a starter culture: pick one colony of transformed cells with a sterile loop and inoculate 50 mL of LB containing 1x kanamycin (50 μg/L) [add 30 μg/L chloramphenicol for Codon +]. Shake at 37^{O}C overnight. (*see* **Note 3**)

2. Prepare media based on desired isotopic labeling scheme.

i. unlabeled CaM: LB broth is used for preparation of unlabeled protein. Autoclave 2 L of LB in a 6L Erlenmeyer flask prior to inoculation. The volume and number of flasks can be adjusted for the desired protein yield, however for efficient aeration, the flasks should not be filled beyond ~1/3.

ii. uniform ^{15}N-labeling: For preparation of isotopically labeled CaM, minimal M9 media is used to control available isotopes. In this case, $^{15}NH_4Cl$ is the only source of nitrogen present in the media and will therefore be incorporated in newly synthesized amino acids and proteins. Prepare up to 2 L of minimal media, as described in *Materials*. For uniform ^{15}N labeling, add 10 mL/L glucose (0.2 % w/v) and 1 g/L $^{15}NH_4Cl$.

iii. Uniform ^{13}C-labeling: Prepare minimal media as described and add 1 g/L unlabeled NH_4Cl and 2 g/L ^{13}C D-glucose. As glucose is the principle carbon source in the media, ^{13}C will be incorporated in all newly synthesized amino acids and proteins.

iv. Uniform ^{15}N- and ^{13}C-labeling: Prepare minimal media as outlined above using both isotopically labeled $^{15}NH_4Cl$, 1 g/L, and ^{13}C D-glucose, 2 g/L.

v. Specific methyl labeling--ILV: For specific methyl labeling, prepare minimal media with unlabeled NH_4Cl (1 g/L) and glucose (0.2% w/v). Isotopic labeling of Ile, Leu, Val

(ILV) methyl groups is achieved by adding isotopically labeled metabolic precursors of these amino acids. ^{13}C-ketobutyric acid (for Ile – 50 mg/L) and ^{13}C-ketoisovaleric acid (for Leu and Val – 100 mg/L) are added 1 hour prior to the anticipated induction of CaM expression, i.e., when the OD_{600} is approximately 0.5.

vi. Specific amino acid labeling: For specific labeling of amino acids, prepare minimal media with unlabeled NH_4Cl (1 g/L) and glucose (0.2% w/v) and 100 mg/L of each amino acid not to be isotopically labeled. Isotopic labeling of specific amino acids is achieved by supplying a source of the labeled amino acid(s) at a crucial time to ensure incorporation in proteins and minimize isotopic scramble to other amino acids due to metabolic processes. Immediately prior to the anticipated induction of CaM expression, i.e., when the OD_{600} is approximately 0.6-0.8, add 500 mg/L addition unlabelled amino acids and 100 mg/L of desired specific labeled amino acid(s). Wait 15 minutes and induce. Gly, Ala and Ser labeling is inefficient due to rapid interconversion with metabolites, and Gln, Glu, Asn and Asp will readily scramble.

An example of a specific isotopic labeling scheme for CaM (methyl labeling of ILVM residues) using these techniques is shown below (Appendix 6).

3. Set aside 1 mL of media for use as a spectrophotometer blank later on. Transfer the starter culture to two 50 mL Falcon tubes and centrifuge at 2300 × g for 10 minutes. Resuspend pellets in 5-10 mL of new media and inoculate the large flask.

4. Shake flask at 37^{O}C and 180 rpm (*see* **Note 4**). Measure OD_{600} of cultures roughly every hour, using the blank set aside in step 3. Cell cultures grow much more slowly in M9 media than in LB. When OD_{600} reaches roughly 0.4, lower the temperature to 15^{O}C. It takes

some time to cool the shaker, and significantly longer for the culture to equilibrate to this temperature, during which the cells will continue to grow. The goal is to cool the culture to 15^{O}C when the OD_{600} reaches between 0.6-0.8, to optimize the yield of soluble protein yield. At this time, induce protein expression by adding 0.25 mL/L 1 M IPTG, and continue shaking at 15^{O}C overnight. (*see* **Notes 5** and **6**)**.** For specific amino acid labeling, overnight expression promotes isotopic scrambling. In this case, induce expression at 37^{O}C and express protein for 3 hours.

5. The following morning, harvest cells by centrifugation in 1 L centrifuge bottles at 8500 × g for 20 minutes. Discard supernatant and transfer cell pellets into 50 mL Falcon tubes. These cell pellets can be used for protein purification immediately, or frozen at -80^{O}C for later use. (*see* **Notes 7** and **8**)

3.3 Purification

1. Add DNase I, lysozyme, PMSF (*see* **Note 1**) and β-mercaptoethanol to 50 mL lysis buffer. Add fresh lysis buffer to cell pellets, frozen or fresh, leaving 5-10 mL in the Falcon tube for air. Rock or rotate the tube at 4^{O}C to resuspend the pellet for at least 30 minutes but no more than 2 hours. Lysis efficiency is improved when the DNase I and lysozyme have time to work. Before continuing, ensure the remaining cell pellet is fully resuspended by pipetting until homogenous.

2. Lyse cells by sonication on ice using intermittent pulses (e.g., 0.5 seconds on and 2.0 seconds off) to prevent heating of the lysate. (*see* **Notes 9** and **10**)**.** Sonication can be performed twice to ensure complete lysis.

3. Transfer lysate to 35 mL ultracentrifuge bottles and spin at 45,000 × g for 40 minutes. (*see* **Note 11**)**.** Samples can be collected from the pellet and supernatant to check for effective lysis. (*see* **Note 12**)**.**

4. Wash 5-10 mL of Ni-NTA resin by pouring the resin slurry (in 20% ethanol storage solution) into a 50 mL Falcon tube and pelleting gently at 200 × g for 3 minutes. Pour off the ethanol, rinse with water and repeat centrifugation. Resuspend Ni-NTA resin with the lysate supernatant and stir at 4^{O}C for 1 hour.

5. Pour lysate-resin slurry into a gravity flow column and collect flow-through as Ni-NTA resin settles. Resin should not be allowed to run dry. Samples can be collected throughout purification for subsequent analysis by sodium dodecyl sulfate–polyacrylamide gel electrophoresis (SDS-PAGE).

6. Wash Ni-NTA resin with His Wash 1 (high salt). Slowly pipette wash buffer down the side of the column to prevent disruption of the resin bed. (*see* **Note 13**)**.** Wash with approximately 10-20 column volumes (volume of resin bed) of His Wash 1 until clean. (*see* **Note 14**)**.**

7. Wash Ni-NTA resin with His Wash 2 (low salt) for 10 column volumes.

8. Elute CaM from Ni-NTA resin by slowly adding His Elution buffer, 2 column volumes at a time. Monitor protein levels (*see* **Note 14**) until no more protein is liberated. Elution volume is generally around 40 mL. (*see* **Note 15** and **16**)**.**

9. Add 10 U thrombin (bovine thrombin is commercially available at low cost) to elution fraction for cleavage of His tag *during* dialysis. Collect samples for SDS-PAGE before addition

of thrombin, and after dialysis, to confirm complete cleavage of the His tag. If downstream applications require immobilization through the His tag, perform dialysis without thrombin to remove imidazole.

10. Prepare 4 L general dialysis buffer (stored at 4^{O}C). Measure a sufficient length of 10,000 molecular weight cut-off (MWCO) dialysis membrane to accommodate the sample with space for clamps. Wet the dialysis membrane in dialysis buffer and fill with elution fraction after clamping one end (*see* **Note 17**). Clamp other side and affix a buoyant object to keep the dialysis membrane clear of the magnetic stir rod. Dialyze over night.

11. Carefully empty dialysis bag into a beaker on ice. At this point, check pre/post cleavage samples by SDS-PAGE before continuing. Concentrate sample to less than 10 mL using 50 mL 10,000 MWCO centrifugal concentrators. (*see* **Note 18**) Centrifuge at 2300 × g for 10 minutes at a time, pausing between spins to thoroughly mix the sample to prevent aggregation, and to add more protein. Before discarding the flow-through, check for protein by testing with Bradford dye, to ensure the membrane has not ruptured. As the protein becomes more concentrated the flow rate will decrease. The protein solution may also become visibly viscous or appear faint yellow, which are not causes of concern, however it should not become cloudy.

12. Prepare, filter and degas gel filtration buffer (this can be performed in advance) and equilibrate size exclusion (also known as gel filtration) chromatography column such as Superdex 75 26/60 run on an AKTA (GE Healthcare Life Sciences), or similar fast protein liquid chromatography (FPLC) (*see* **Note 19**). Filter the sample (0.22 μm), load into a 10 mL loop and run 1.2 column volumes (~350 mL) of buffer at < 2 mL/minute. CaM should elute at a volume of ~200 mL.

13. Collect elution fractions and concentrate once more to a working concentration of CaM for the given purpose. CaM is stable for NMR at concentrations above 1 mM, though 100-200 μM is sufficient for most experiments (*see* **Note 20**). Samples can be aliquoted, flash frozen in liquid nitrogen or ethanol/dry ice bath and stored at -80^{O}C indefinitely.

Preparation methods:

1. CaM from *E. coli* will be purified bound partially to Mg^{2+}. If Ca^{2+}-bound CaM is required, add 10 mM $CaCl_2$ to sample before use. Binding is fast and will displace other cations that may be present in the sample. An example of a ^{1}H-^{15}N heteronuclear single quantum correlation (HSQC) spectrum of Ca^{2+} loaded, uniformly ^{15}N labeled CaM is included (Appendix 5). If apo CaM is required, a buffer exchange must first be performed, either on a single sample or with a batch, into chelation buffer. Use 10,000 MWCO centrifugal concentrators for buffer exchange (available in 15 mL, 4 mL or 500 μL sizes). Add chelation buffer until it makes up at least 50% of the volume before switching back to gel filtration buffer. Thoroughly exchange buffer back into gel filtration buffer to remove the EDTA. An example of a ^{1}H-^{15}N HSQC of uniformly ^{15}N labeled apo CaM is shown below (Appendix 4). (*see* **Note 21**).

2. For formation of a CaM-peptide complex, mix Ca^{2+}-bound or apo CaM and peptide at low concentrations, then co-concentrate the mixture in a 3,000 MWCO centrifugal concentrator to the working concentration. Mixing at low concentrations reduces the risk of precipitation.

3. Lyophilisation allows long-term storage of CaM preparations. First, exchange apo CaM (Ca^{2+}-containing buffers are not amenable to this technique) into a buffer of 25 mM ammonium bicarbonate. Ammonium bicarbonate provides sufficient buffering capacity but is volatile and

thus dissipates during lyophilization. Following freeze-drying, pure apo CaM powder can be stored at -20^{O}C for very long periods. To resuspend, place a drop of buffer beside the CaM powder and allow the powder to be slowly ‘drawn in’. Adding buffer too quickly produces clumps that are difficult to dissolve.

4 Notes

1. PMSF is a protease inhibitor and is extremely toxic. Make a stock solution in ethanol to reduce routine exposure to the powder, and always wear PPE. It is rapidly degraded in water, thus must be added to lysis buffer immediately before use. There are also commercially available protease inhibitor cocktails that contain PMSF and are easier to handle.

2. This is a very flexible protocol that can be adjusted according to time constraints. Initial incubation on ice should be at least 15 minutes. The heat shock is the most critical step and should be performed at 42^{O}C for 1 minute before returning the tube to ice, but the post-heat shock incubation on ice can be reduced to as little as 2 minutes. After addition of LB, shaking at 37^{O}C should be longer than 15 minutes but less than 1.5 hours. Resuspension and plating volumes can be adjusted to optimize colony density. The plate can be incubated at room temperature over a weekend in place of overnight incubation at 37^{O}C.

3. Expression can be expedited by resuspending the entire plate, rather than a single colony, with 1-2 mL of media and inoculating the 50 mL LB starter culture. Shake at 37^{O}C for approximately 3 hours (rather than overnight) to reach an appropriate cell density to pellet and proceed.

4. Alternatively, aeration and mixing of the E. coli culture can be achieved by bubbling compressed air in a system such as a LEX Bioreactor (Epiphyte Three).

5. Due to slow growth in M9 media, the one-day expression method described (*see* **Note 3**) can take as long as 12 hours to achieve the O.D. required for induction.

6. The expression system used is highly efficient and can produce very large quantities of recombinant protein, which can form insoluble inclusion bodies. Often the overall yield of soluble protein can be improved by reducing the IPTG concentration and lowering the induction temperature. If a refrigerated incubator is not available or time is an issue, the induction of expression can also be performed at 37°C for 3-4 hours. Because CaM is highly soluble, this produces acceptable protein yields.

7. Freezing the cell pellets at -80°C has no adverse impact on protein yield or quality and promotes cell lysis.

8. It is important, especially when unfamiliar with the protocol, to monitor every stage of the expression and purification by SDS-PAGE. Several samples should be collected during expression and purification. The first is to test that induction of protein expression occurred. A useful trick is to save a cuvette used to measure OD_{600} pre-induction until the following morning, so that samples of the culture both pre- and post-induction have similar cell densities. Take 100 μL of each sample and centrifuge in Eppendorf tubes at max speed for 1 minute. Discard supernatant and resuspend pellets in 50 μL of 1x SDS-PAGE sample buffer. When run on a gel, these samples should have similar background protein levels and a single strong band in the post-induction sample around 16 kD corresponding to CaM.

9. Heat generated by the sonication process will melt the ice around the sample beaker. Periodically check that the beaker is supported and that the tip of the sonicator remains ~1cm from the bottom. A plastic beaker is preferable to glass, which may break.

10. Alternative lysis methods such as a French press are suitable.

11. Lipids can be loosely pelleted and contaminate the supernatant. To avoid clogging columns and filters, decant supernatant carefully and immediately following centrifugation.

12. Similar to monitoring expression as outlined above (*see* **note 8)** it is important to check the proportion of protein found in the supernatant. For this to be reliable, the pellet and supernatant fractions need to be normalized: before centrifugation, take 50 μL of lysate and centrifuge separately in an Eppendorf tube, max speed for 1 minute. Separate supernatant from pellet and solubilize both in SDS-PAGE sample buffer, to the same volume. As a highly soluble protein, CaM should only be present in the supernatant. If a large amount of CaM is found in the pellet, next time try slower expression (lower IPTG induction concentration) and/or more thorough lysis.

13. The resin bed is easily disrupted by the flow of buffer, which can create voids in the resin bed, allowing the buffer to channel rather than flowing evenly through the resin. If this happens, it is best to let the resin settle before continuing.

14. Bradford dye can be used to monitor the washing or elution progress. Make 10 mL of fresh Bradford dye before beginning column purification, and aliquot 400 μL into Eppendorf tubes. Collect one drop from the gravity flow column in a tube to qualitatively assess protein levels and decide when washing or elution is complete. When protein is present, Bradford dye turns blue.

15. The most efficient method to elute protein is to let 1 column volume elute at a time, with brief incubations in between to allow for protein dissociation from the resin. As the protein becomes more dilute, extend the wait period. Elution is complete when these flow samples do not react with Bradford dye.

16. The Ni-NTA purification step can be automated using a pre-packed Ni-NTA column on an FPLC system, such as AKTA (GE Healthcare Life Sciences).

17. Wet the dialysis membrane in dialysis buffer and tease one side between fingers until it opens. Pipette buffer through the open membrane, making sure that it can pass freely through the entire length before clamping and adding sample. To monitor thrombin cleavage, run samples taken before and after dialysis on SDS-PAGE. Cleaved CaM runs with an approximate molecular weight just below 15 kD on SDS-PAGE due to its high negative charge.

18. Samples may be concentrated by alternative means to centrifugal concentrators

19. Size exclusion chromatography can be performed without an FPLC system, using a pump (e.g., peristaltic) and a column manually packed with size exclusion resin. The UV absorbance of each fraction can be measured manually to detect protein.

20. We use two methods to determine the concentrations of CaM, which are generally consistent: UV absorbance at 280 nm and Bradford. CaM lacks tryptophan, thus its UV absorbance is relatively low, with predicted extinctions coefficient at 280 nm of 2980 $M^{-1}cm^{-1}$. For Bradford reagent, the concentration can be determined using a standard curve (e.g., Abs = 0.0447[concentration (mg/mL)] – 0.0597).

21. For sensitive analysis of apo CaM, it is important to decalcify all buffers. Ca^{2+} contamination can be present even in highly purified water and high-grade reagents. Buffers can be passed through a Chelex® 100 Resin (Bio-Rad) column to remove residual cations. This is not required for all purposes, however, the affinity of CaM for Ca^{2+} is enhanced in the presence of high affinity Ca^{2+}-dependent target peptides, thus traces of Ca^{2+} contamination may be sufficient to support Ca^{2+}-dependent interactions.

Acknowledgement

This work was supported by grants from Canadian Institutes of Health Research, Natural Sciences and Engineering Research Council of Canada, and Heart and Stroke Foundation of Canada. M.I. holds the Canada Research Chair in Cancer Structural Biology. The NMR facility at UHN is supported by Canada Foundation for Innovation and the Princess Margaret Foundation.

5 References

1. Cheung W.Y., *Cyclic 3'-5'-nucleotide phosphodiesterase. Demonstation of an activator.* Biochem. Biophys. Res. Commun., 1970. **38**(3): p. 533-8.

2. Kakiuchi S., Yamazaki R. *Calcium dependent phosphodiesterase activity and its activating factor (PAF) from brain studies on cyclic 3',5'-nucleotide phosphodiesterase (3)*. Biochem. Biophys. Res. Commun., 1970. **41**(5): p. 1104-10.

3. Cohen P., Klee C.B. (eds). *Calmodulin.* Molecular Aspects of Cellular Regulation. Volume 5, Elsevier.

4. Marshall, C.B., et al. *Calmodulin and STIM proteins: Two major calcium sensors in the cytoplasm and endoplastic reticulum*. Biochem Biophys Res Commun, 2015. **460**(1): p. 5-21.

5. O'Connell D., B.M., Marshall C.B., Ikura M., Linse S., *Calmodulin,* in *Encyclopedia of metalloproteins,* K.R.H. Uversky V., Permyakov E.A., Editor. 2013, Spriner.

6. Moews P.C., Kretsinger R.H. *Terbium replacement of calcium in carp muscle calcium-binding parvalbumin: an x-ray crystallographic study*. J. Mol. Bio, 1975. **91**(2): p. 229-32.

7. Kawasaki H., Kretsinger R.H. *Structural and functional diversity of EF-hand proteins: Evolutionary perspectives.* Protein Sci., 2017.

8. Ikura M., Kay L.E., Bax A. *Novel approach for sequential assignment of 1H, 13C, 15N spectra of proteins: heteronuclear triple-resonance three-dimensional NMR spectroscopy. Application to calmodulin*. Biochemistry, 1990. **29**(19): p. 4659-67.

9. Ikura M., Kay L.E., Bax A. *Improved three-dimensional 1H-13C-1H correlation spectroscopy of a 13C-labeled protein using constant-time evolution*. J Biomol NMR, 1991. **1**(3): p. 299-304.

10. Ikura M., Spera S., Barbato G., Kay L.E., Krinks M., Bax A. *Secondary structure and side-chain 1H and 13C resonance assignments of calmodulin in solution by heteronuclear multidimensional NMR spectroscopy*. Biochemistry, 1991. **30**(38): p. 9216-28.

11. Muallem S., Karlish S.J. *A simple, rapid and efficient procedure for purification of calmodulin from human red blood cells*. FEBS lett., 1979. **107**(1): p. 209-12.

12. Yoshida M., Minowa O., Yagi K. *Divalent cation binding to wheat germ calmodulin*. J. Biochem., 1983. **94**(6): p. 1925-33.

13. Ikura M., Marion D., Kay L.E., Shih H., Krinks M., Klee C.B., Bax A. *Heteronuclear 3D NMR and isotopic labeling of calmodulin. Towards the complete assignment of the 1H NMR spectrum*. Biochem Pharmacol., 1990. **40**(1): p. 153-60.

Appendix 2. Primer sequences used for plasmid construction.

Target gene	Primer sequences* (5' to 3')
Codon-optimized KRAS4b	F: CGCG**GGATCC**ACCGAGTACAAGCTGGTGG
	R: ATAAGAAT**GCGGCCGC**TTACATAATCACACATTTGGTC
Codon-optimized KRAS4b-C185Astop	F: CGCG**GGATCC**ACCGAGTACAAGCTGGTGG
	R: ATAAGAAT**GCGGCCGC**TTAGGCTTTGGTCTTGG
CaM	F: CGCG**GGATCC**ACCATGGCTGACCAACTGACAGAAGAGC
	R: CGCG**GGATCC**TCCGCCGCTGCCTCCGCCGCTGCCTCCGCCCTTTGCTGTCATCATTTGTAC
CaM1234Q	F: CTACCG**GGTACC**GCTGACCAACTGACAGAAGAGCAG
	R: CTACCG**ACTAGT**TCCGCCGCTGCCTCCGCCCTTTGCTGTC
mTurquoise2	F: CTACCG**GCATGC**ACCATGGTGAGCAAGGGCGAGGAGCTG
	R: CTACCG**GGTACC**TCCGCCGCTGCCTCCGCCGCTGCCTCCGCCCTTGTACAGCTCGTCCATGCCG
FLAG-mTurquoise2	F: CTACCG**GCATGC**ACCATGACGGACTACAAGGATGACGATGACAAGGTGAGCAAGGGCGAGGAGCTG
	R: CTACCG**GGTACC**TCCGCCGCTGCCTCCGCCGCTGCCTCCGCCCTTGTACAGCTCGTCCATGCCG
SYFP2	F: CTACCG**ACTAGT**GGCGGAGGCAGCGTGAGCAAGGGCGAGGAGCTGTTCACC
	R: CTACCG**GGATCC**TCCGCCGCTGCCTCCGCCGCTGCCTCCGCCCTTGTACAGCTCGTCCATGCCGAGAGTG
Insertion for mTurquoise2	F: CTGCAGTGCTGCGGTACCGCTGACCAACTGACAGAAG
	R: GCCGCATGCACTTCGAAAGGTCGACTGAATTGGTTCC
Insertion for SYFP2	F: GGCGGAACTAGTGGCGGAGGCAGCGGCGGA
	R: GCTGCCTCCGCCCTTTGCTGTCATCATTTGTACAAACTCTTCGTAGTTTACTTGGCCG

*F and R denotes forward and reverse primers, respectively. Bold letters indicate restriction enzyme sites.

Appendix 3. CaMeRAS^{WT} chimeric FRET construct – nucleotide and primary amino acid sequences showing domain structure. The positions of mTurquise2 (mTq2), CaM, SYFP2 and KRAS4b are indicated by cyan, orange, yellow and pink boxes below the sequences [56].

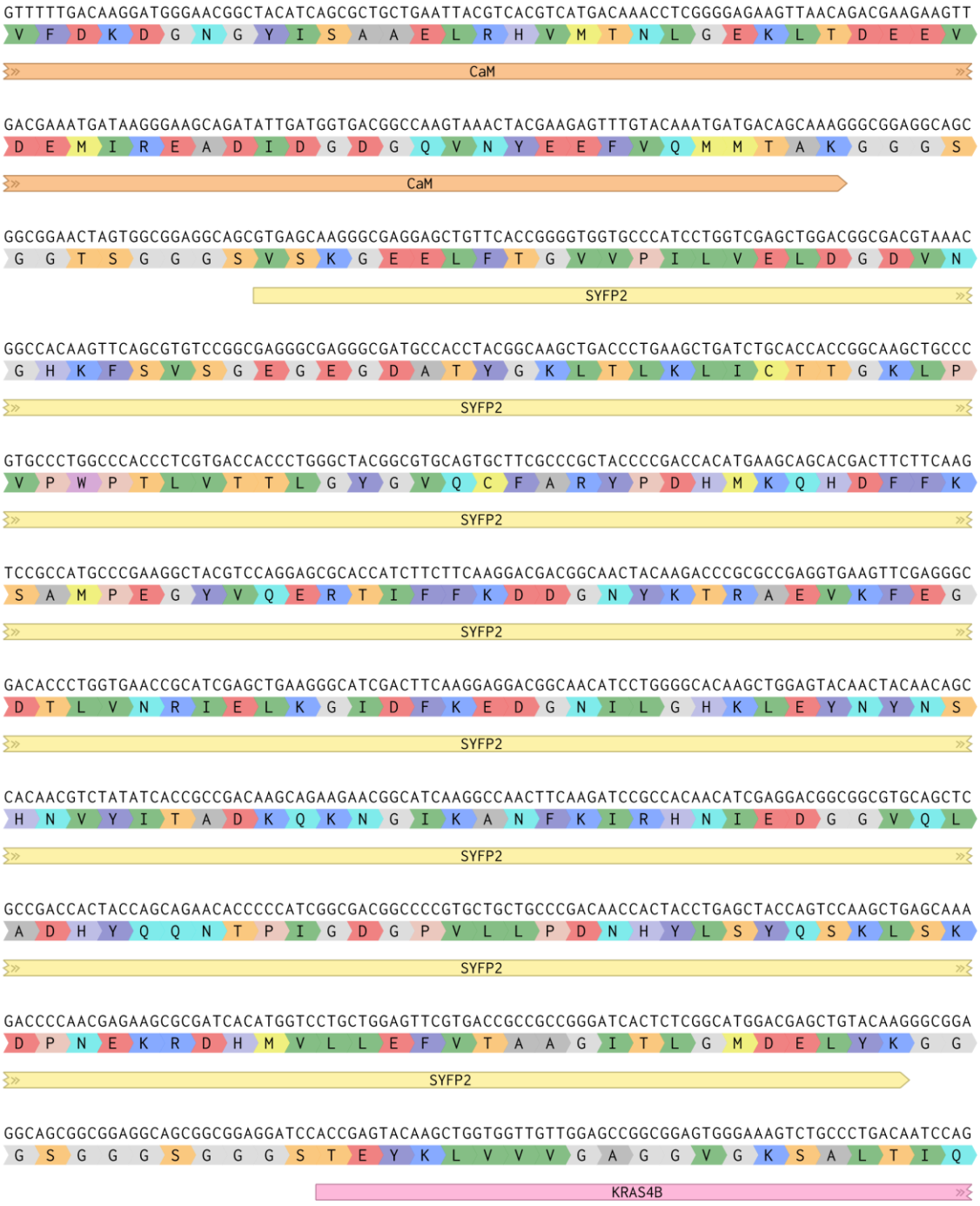
GTTTTTGACAAGGATGGGAACGGCTACATCAGCGCTGCTGAATTACGTCACGTCATGACAAACCTCGGGGAGAAGTTAACAGACGAAGAAGTT
V F D K D G N G Y I S A A E L R H V M T N L G E K L T D E E V
CaM
GACGAAATGATAAGGGAAGCAGATATTGATGGTGACGGCCAAGTAAACTACGAAGAGTTTGTACAAATGATGACAGCAAAGGGCGGAGGCAGC
D E M I R E A D I D G D G Q V N Y E E F V Q M M T A K G G G S
CaM
GGCGGAACTAGTGGCGGAGGCAGCGTGAGCAAGGGCGAGGAGCTGTTCACCGGGGTGGTGCCCATCCTGGTCGAGCTGGACGGCGACGTAAAC
G G T S G G G S V S K G E E L F T G V V P I L V E L D G D V N
SYFP2
GGCCACAAGTTCAGCGTGTCCGGCGAGGGCGAGGGCGATGCCACCTACGGCAAGCTGACCCTGAAGCTGATCTGCACCACCGGCAAGCTGCCC
G H K F S V S G E G E G D A T Y G K L T L K L I C T T G K L P
SYFP2
GTGCCCTGGCCCACCCTCGTGACCACCCTGGGCTACGGCGTGCAGTGCTTCGCCCGCTACCCCGACCACATGAAGCAGCACGACTTCTTCAAG
V P W P T L V T T L G Y G V Q C F A R Y P D H M K Q H D F F K
SYFP2
TCCGCCATGCCCGAAGGCTACGTCCAGGAGCGCACCATCTTCTTCAAGGACGACGGCAACTACAAGACCCGCGCCGAGGTGAAGTTCGAGGGC
S A M P E G Y V Q E R T I F F K D D G N Y K T R A E V K F E G
SYFP2
GACACCCTGGTGAACCGCATCGAGCTGAAGGGCATCGACTTCAAGGAGGACGGCAACATCCTGGGGCACAAGCTGGAGTACAACTACAACAGC
D T L V N R I E L K G I D F K E D G N I L G H K L E Y N Y N S
SYFP2
CACAACGTCTATATCACCGCCGACAAGCAGAAGAACGGCATCAAGGCCAACTTCAAGATCCGCCACAACATCGAGGACGGCGGCGTGCAGCTC
H N V Y I T A D K Q K N G I K A N F K I R H N I E D G G V Q L
SYFP2
GCCGACCACTACCAGCAGAACACCCCCATCGGCGACGGCCCCGTGCTGCTGCCCGACAACCACTACCTGAGCTACCAGTCCAAGCTGAGCAAA
A D H Y Q Q N T P I G D G P V L L P D N H Y L S Y Q S K L S K
SYFP2
GACCCCAACGAGAAGCGCGATCACATGGTCCTGCTGGAGTTCGTGACCGCCGCCGGGATCACTCTCGGCATGGACGAGCTGTACAAGGGCGGA
D P N E K R D H M V L L E F V T A A G I T L G M D E L Y K G G
SYFP2
GGCAGCGGCGGAGGCAGCGGCGGAGGATCCACCGAGTACAAGCTGGTGGTTGTTGGAGCCGGCGGAGTGGGAAAGTCTGCCCTGACAATCCAG
G S G G G S G G G S T E Y K L V V V G A G G V G K S A L T I Q
KRAS4B

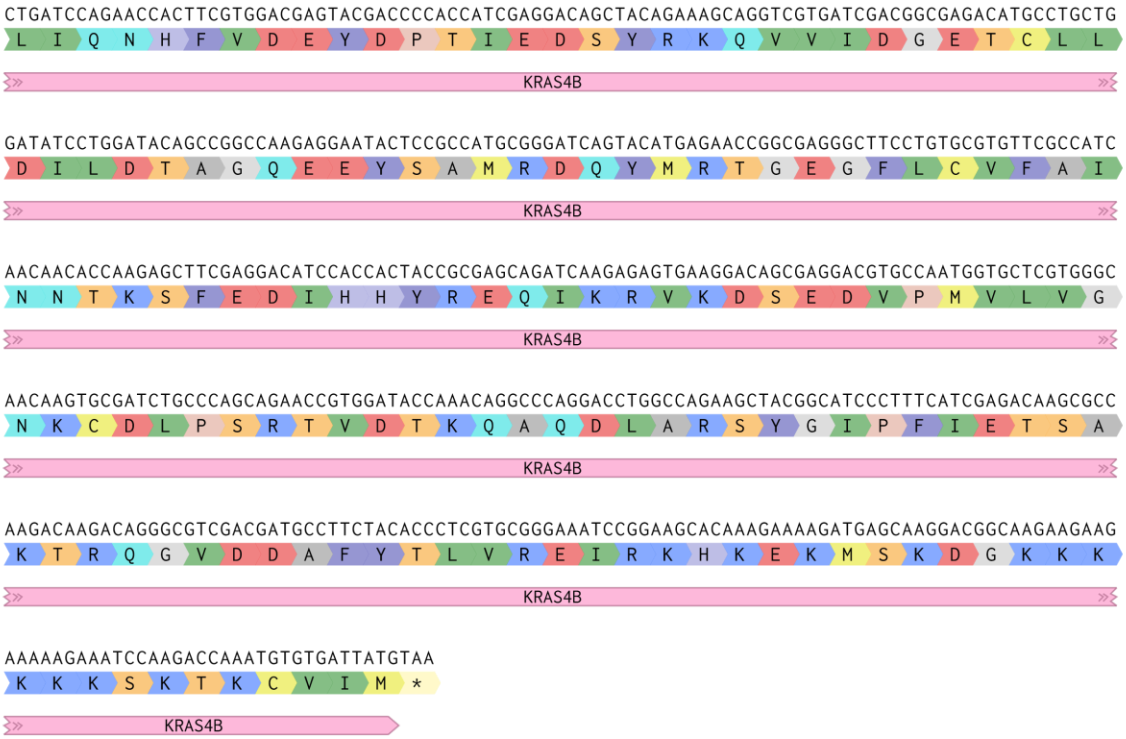
CTGATCCAGAACCACTTCGTGGACGAGTACGACCCCACCATCGAGGACAGCTACAGAAAGCAGGTCGTGATCGACGGCGAGACATGCCTGCTG
L I Q N H F V D E Y D P T I E D S Y R K Q V V I D G E T C L L
KRAS4B
GATATCCTGGATACAGCCGGCCAAGAGGAATACTCCGCCATGCGGGATCAGTACATGAGAACCGGCGAGGGCTTCCTGTGCGTGTTCGCCATC
D I L D T A G Q E E Y S A M R D Q Y M R T G E G F L C V F A I
KRAS4B
AACAACACCAAGAGCTTCGAGGACATCCACCACTACCGCGAGCAGATCAAGAGAGTGAAGGACAGCGAGGACGTGCCAATGGTGCTCGTGGGC
N N T K S F E D I H H Y R E Q I K R V K D S E D V P M V L V G
KRAS4B
AACAAGTGCGATCTGCCCAGCAGAACCGTGGATACCAAACAGGCCCAGGACCTGGCCAGAAGCTACGGCATCCCTTTCATCGAGACAAGCGCC
N K C D L P S R T V D T K Q A Q D L A R S Y G I P F I E T S A
KRAS4B
AAGACAAGACAGGGCGTCGACGATGCCTTCTACACCCTCGTGCGGGAAATCCGGAAGCACAAAGAAAAGATGAGCAAGGACGGCAAGAAGAAG
K T R Q G V D D A F Y T L V R E I R K H K E K M S K D G K K K
KRAS4B
AAAAAGAAATCCAAGACCAAATGTGTGATTATGTAA
K K K S K T K C V I M *
KRAS4B

Appendix 4. ^{1}H-^{15}N HSQC of uniformly ^{15}N-labeled Ca^{2+}-free calmodulin. Sample contains 0.5 mM calmodulin in gel filtration buffer (20 mM HEPES 7.4, 100 mM NaCl, 1 mM TCEP). HSQC collected at 25°C with 8 scans [56].

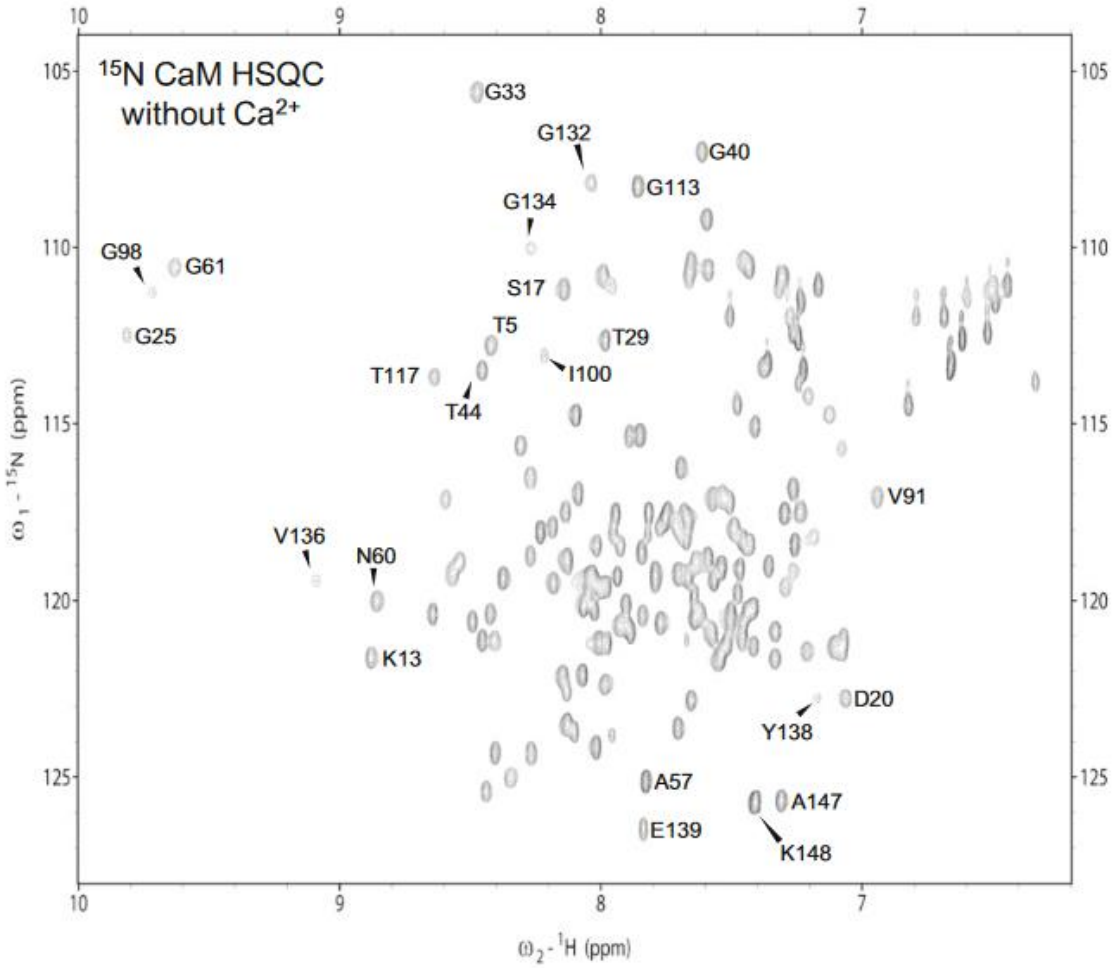

Appendix 5. ^{1}H-^{15}N HSQC of uniformly ^{15}N-labeled calmodulin bound to Ca^{2+}. Sample contains 0.75 mM calmodulin in gel filtration buffer (20 mM HEPES 7.4, 100 mM NaCl, 1 mM TCEP) with 10 mM $CaCl_2$. HSQC collected at 25°C with 4 scans [56].

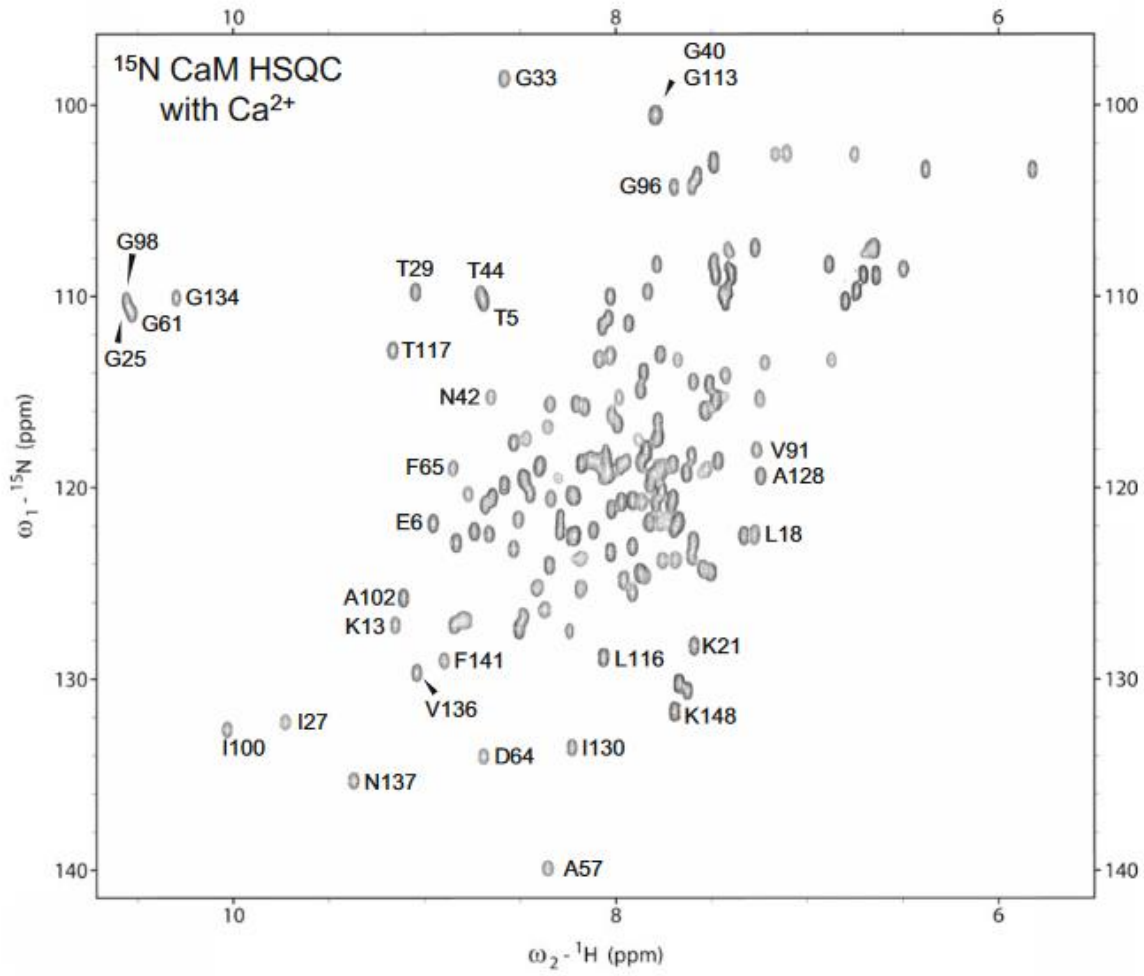

Appendix 6. ^{1}H-^{13}C HSQC of specifically labeled ^{13}C-methyls of Ile, Leu, Val, Met in calmodulin bound to Ca^{2+}. Sample contains 0.75 mM calmodulin in gel filtration buffer (20 mM HEPES 7.4, 100 mM NaCl, 1 mM TCEP) with 10 mM $CaCl_2$. HSQC collected at 25°C.